

Power Electronics-Based Safety Enhancement Technologies for Lithium-Ion Batteries: An Overview From Battery Management Perspective

Zhaoyang Zhao ¹, Member, IEEE, Haitao Hu ², Senior Member, IEEE, Zhengyou He ³, Senior Member, IEEE, Herbert Ho-Ching Iu ⁴, Senior Member, IEEE, Pooya Davari ⁵, Senior Member, IEEE, and Frede Blaabjerg ⁶, Fellow, IEEE

Abstract—Safety enhancement for lithium-ion batteries (LIBs) has received a lot of attention from academic and industrial fields. However, there is a lack of overview from the perspective of the application power electronics (PEs) in the systems. This article gives an overview of PE-based safety enhancement technologies for LIBs, mainly focusing on battery management. It introduces the latest advances in battery protection, balancing, monitoring, and lifetime improvement, all based on PE technologies. Detailed discussion and future research opportunities are given. This article aims to provide a reference for PE researchers who want to make some efforts in LIB safety.

Index Terms—Balancing, battery management, lifetime improvement, lithium-ion batteries (LIBs), monitoring, power electronics (PEs), protection, safety enhancement.

NOMENCLATURE

ADI	Analog devices, Inc.	BIM	Broadband impedance measurement.
ANFIS	Adaptive neural fuzzy inference system.	BMC	Battery monitoring and control.
APC	Alternating pulsed current.	BMS	Battery management system.
ASD	Adjustable speed drive.	C2ASU	Cell to auxiliary storage unit.
ASRC	Alternating sinusoidal-ripple current.	C2L	Cell to load.
BB	Battery balancing.	CC-CV	Constant current-constant voltage.
BBU	Battery balancing unit.	CCT	Cross-correlation technique.
		CIDAB	Capacitively isolated dual active bridge.
		CPE	Constant phase element.
		CSC	Conventional switched capacitor.
		CSN	Cell selection network.
		CT-CV	Constant temperature-constant voltage.
		DAB	Dual active bridge.
		DFT	Discrete Fourier transform.
		DIBS	Discrete-interval binary sequence.
		DLIA	Digital lock-in amplifier.
		EIS	Electrochemical spectroscopy impedance.
		EMI	Electromagnetic interference.
		ESPSs	Energy storage power stations.
		EVs	Electric vehicles.
		FB-PS-ZVS	Full-bridge-phase shift-zero-voltage switching.
		FC	Fuel cell.
		FET	Field-effect transistor.
		FFT	Fast Fourier transform.
		FLC	Fuzzy logic control.
		ICBCs	Integrated cascaded bidirectional converters.
		ICs	Integrated circuits.
		LDO	Low dropout.
		LIBs	Lithium-ion batteries.
		LSC	Logical switching control.
		LSRA	Least-square regression analysis.
		MG	Microgrid.
		MOSFET	Metal-oxide-semiconductor field-effect transistor.
		MPC	Model predictive control.
		MT	Multiwinding transformer.
		NPC	Negative pulsed current.
		OLC	Open-loop control.
		PC	Pulse current.
		PCCC	Pulsed current-constant current.
		PEs	Power electronics.

Manuscript received 19 December 2022; revised 7 March 2023; accepted 3 April 2023. Date of publication 6 April 2023; date of current version 19 May 2023. This work was supported in part by the National Natural Science Foundation of China under Grant 52027810, in part by the Sichuan Science and Technology Program under Grant 2022NSFSC0001, in part by the Reliable Power Electronics-Based Power Systems (REPEPS) Project from The VELUX Foundations through the Villum Investigator Program under Award 00016591, in part by the Natural Science Foundation of Sichuan Province under Grant 2023NSFSC0814, and in part by the Central University Science and Technology Innovation Project under Grants 2682022ZTPY070, 2682022KJ029, and 2682023CX004. Recommended for publication by Associate Editor G. Grandi. (Corresponding author: Haitao Hu.)

Zhaoyang Zhao, Haitao Hu, and Zhengyou He are with the Institute of Smart City and Intelligent Transportation, Southwest Jiaotong University, Chengdu 610031, China (e-mail: zhaoyang.zhao@swjtu.edu.cn; hht@swjtu.edu.cn; hezy@swjtu.edu.cn).

Herbert Ho-Ching Iu is with the School of Electrical, Electronics and Computer Engineering, University of Western Australia, Crawley, WA 6009, Australia (e-mail: herbert.iu@uwa.edu.au).

Pooya Davari and Frede Blaabjerg are with the AAU Energy, Aalborg University, 9220 Aalborg, Denmark (e-mail: pda@energy.aau.dk; fbl@energy.aau.dk).

Color versions of one or more figures in this article are available at <https://doi.org/10.1109/TPEL.2023.3265278>.

Digital Object Identifier 10.1109/TPEL.2023.3265278

PI	Proportional integral.
PIC	Perturbation injection converter.
PRBS	Pseudorandom binary sequence.
PRS	Pseudorandom sequence.
PS-SCCs	Phase-shift switched capacitor converters.
QRZCS	Quasi-resonant zero-current switching.
QSMC	Quasi-sliding mode control.
RMS	Root mean square.
SC	Switched capacitor.
SF	Single frequency.
SI	Switched inductor.
SIC	Supercapacitor interface converter.
SOC	State of charge of batteries.
SOH	State of health of batteries.
SOS	State of safety of batteries.
SOT	State of temperature of batteries.
SPDT	Single-pole double-throw switches.
SRC	Sinusoidal ripple current.
SuperC	Supercapacitor.
TI-RVMs	Tapped inductor resonant voltage multipliers.
TIs	Texas Instruments.
TSEP	Thermal-sensitive electric parameter.
VM	Voltage multiplier.
WN	White noise.
ZVS	Zero-voltage switching.

I. INTRODUCTION

LIBs have been widely used for energy storage in various applications, such as consumer electronics, EVs, and ES-PSs [1], [2]. However, LIB is sensitive to thermal and electrical stresses. Its safety declines over time due to internal physical and chemical changes, such as lithium dendrite and heat production [3], [4], [5], [6], [7]. A lot of safety accidents caused by batteries have been reported in recent years [8], [9].

In the last two decades, many efforts have been made to investigate the failure mechanisms and safety enhancement techniques of LIBs. Some of the latest results and state-of-the-art techniques have been reviewed in the published overview papers. Feng et al. [10] systematically reviewed the thermal runaway mechanisms of LIBs. In [11] and [12], the critical progress in materials design to enhance LIB's safety has been summarized. In [13] and [14], the advanced thermal management techniques to improve battery safety have been reviewed, including air/liquid cooling and their configurations, etc. Furthermore, the safety enhancement strategies, including materials modification, electrothermal management, etc., have been thoroughly reviewed in [15], [16], [17], [18], and [19].

Generally, researchers in the fields of electronic and electrical engineering would pay more attention to monitoring and management techniques of LIBs, instead of materials design. In [20], [21], [22], [23], [24], and [25], the SOC estimation [20], [21], SOH estimation [22], [23], and lifetime prediction [24], [25] of LIBs have been reviewed. Hu et al. [26] and Wang et al. [27] further methodically reviewed state estimation techniques of LIBs, including SOC, SOH, SOT, and SOS estimation. In [28]

and [29], LIB systems' fault types and diagnosis techniques have been summarized. Considering that a BMS usually integrates the function of state estimation, operation control, fault diagnosis, etc., the state-of-the-art BMS techniques have been systematically summarized in [31], [32], and [33].

Focusing on the safety enhancement of LIBs, these overviews provide comprehensive summaries of the latest techniques from the design to application phases. However, there is a lack of summarizing the feasible solutions from the PEs perspective, which plays an essential role in battery management [34]. It is important to review PE-based techniques for the following purposes [35].

- 1) Summarize the existing PE-based safety enhancement techniques and provide a reference for PE researchers who want to make some efforts in LIB safety.
- 2) Benchmark existing solutions and identify their advantages and limitations, in order to provide new suggestions for industrial application.
- 3) Analyze the existing challenges and explore future research opportunities.

Recently, some overview papers have glanced at PE-based safety enhancement techniques for LIBs. Considering that BB can reduce the safety risks caused by cell/module inconsistencies, Turksoy et al. [36] and Ghaeminezhad et al. [37] reviewed BB techniques. It is known that EIS can reflect some health status information of LIBs, Varnosfaderani and Strickland [38] reviewed the online EIS estimation techniques, including interface converter and balancing circuit-based schemes. Although these review papers give an analysis of some PE-based safety enhancement methods, there are the following limitations.

- 1) The published papers do not give a comprehensive design procedure for some critical techniques, such as online EIS estimation and BB, which is essential for industry application and academic research.
- 2) Besides online EIS estimation and BB, there are some other safety enhancement schemes. Unfortunately, there is a lack of systematic summarization of PE-based solutions.

Therefore, the main goal of this article is to provide a better understanding of both industry and academic research on PE-based safety enhancement techniques of LIBs. The main contributions are given as follows.

- 1) Provides an overview of PE-based safety enhancement solutions of LIBs from the perspective of battery management.
- 2) Summarizes the implementation principles for some critical techniques, such as BB and EIS measurement. Then, the various possible schemes are derived.
- 3) Discusses and compares existing schemes, including specific commercial and industrial solutions. Based on this, gives suggested solutions for industrial applications.
- 4) Existing challenges and future research opportunities are summarized, which can provide a reference for PE researchers who want to make some efforts in LIB safety.

The rest of this article is organized as follows. Section II reviews the safety enhancement techniques. Then, the protection, balancing, online monitoring, and lifetime improvement

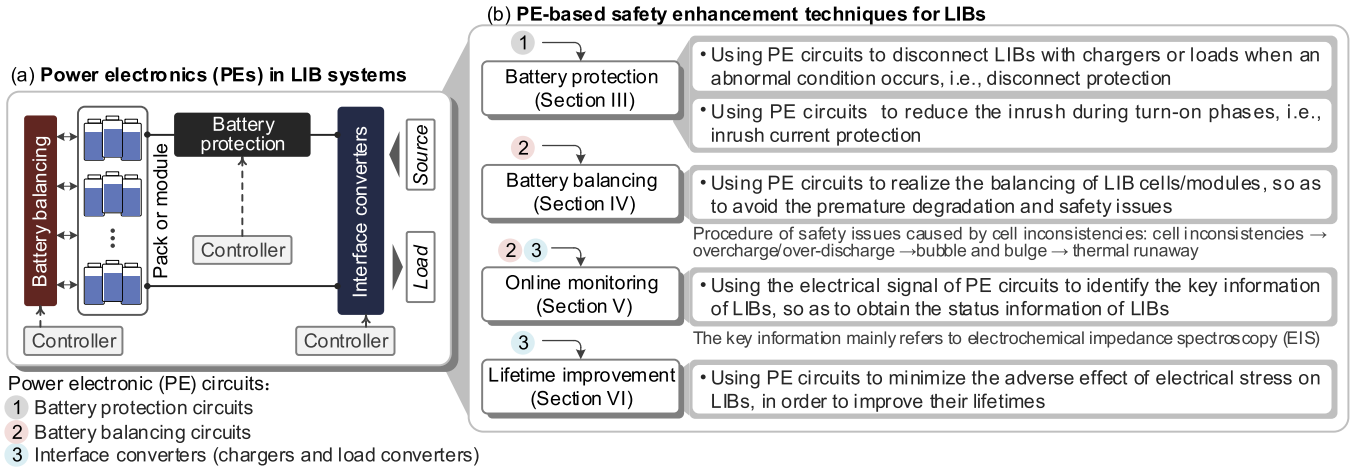


Fig. 1. PEs in LIB systems and the PE-based safety enhancement techniques.

for LIBs are discussed in Sections III–VI, respectively. Finally, Section VII concludes this article.

II. PEs FOR SAFETY ENHANCEMENT OF LIBS

Fig. 1(a) shows typical PE applications in LIB systems. According to the function of PE devices, there are three main categories of circuits, i.e., battery protection circuits, BB circuits, and interface converters (including chargers and load converters). From the perspective of battery safety, four categories of PE-based techniques are usually used to enhance the safety of LIBs, i.e., battery protection, BB, online monitoring, and lifetime improvement, as shown in Fig. 1(b).

Battery protection refers to using PE circuits to realize the protection function of LIB systems. It mainly includes disconnect protection and load inrush current protection, which are discussed in Section III.

BB means using PE circuits to realize the balancing of LIB cells or modules, in order to avoid premature degradation and safety issues. A simple procedure of safety issues caused by cell inconsistencies is shown in Fig. 1(b). A detailed discussion of the state-of-the-art balancing techniques is given in Section IV.

Online monitoring refers to using electrical signals of PE circuits to identify the critical information of LIBs, in order to realize the health state estimation. It is different from the widely used state estimation methods in [26] and [27]. Notice that the critical information discussed here mainly refers to the EIS of LIBs, which is discussed in Section V.

Lifetime improvement means using interface converters to reduce the damage of electrical stress on LIBs, which is discussed in Section VI.

III. BATTERY PROTECTION TECHNIQUES

A. Basics of Battery Protection Techniques

Generally, battery protection techniques have been well studied and commercially applied [39], [40], where disconnected protection and load inrush current/precharge protection are basic techniques.

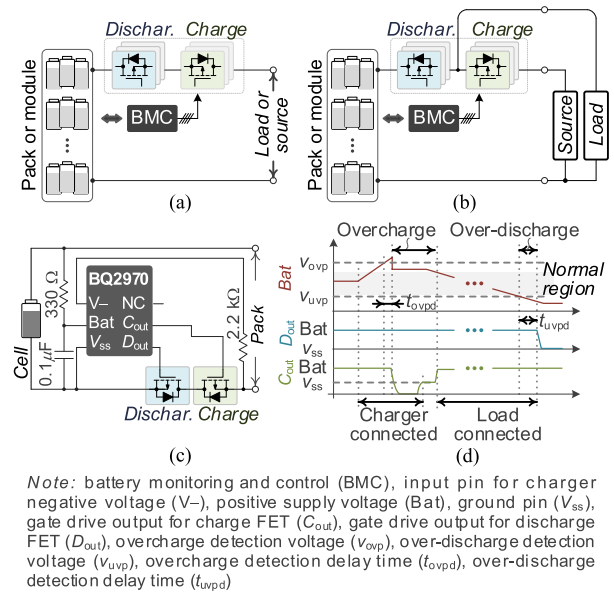


Fig. 2. Typical battery protection circuits [39], [42]. (a) Series-switches type disconnect protection. (b) Separate-port type disconnect protection. (c) Simplified schematic of TI's IC BQ2970. (d) Timing charts of BQ2970.

Nowadays, some state-of-the-art BMS ICs have been designed. Fig. 2(a) and (b) show the typical topologies of disconnect protection, i.e., series-switches and separate-port types, respectively. Referring to Fig. 2(a), two metal-oxide-semiconductor field-effect transistors (MOSFETs) are connected in series to form a bidirectional switch [41]. The charging and discharging paths are disconnected when the BMC unit detects an abnormal condition, e.g., overcharge, undercharge, and short circuit. Unlike that in Fig. 2(a), the charging and discharging paths are separately controlled in Fig. 2(b). Similarly, load inrush current protection can be implemented using MOSFETs and resistors, which are discussed in detail in [39].

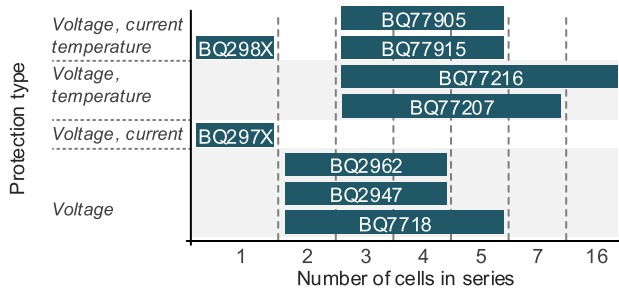


Fig. 3. Typical battery protection ICs released by TI [43].

B. Typical Commercial and Industrial Solutions for Battery Protection

Taking a battery protection IC BQ2970 as an example, Fig. 2(c) and (d) show its simplified schematic and timing charts, respectively [42]. It can be seen that the cell voltage can be limited to a specific region (i.e., normal operation area) based on the setting of overcharge detection voltage (v_{ovp}) and overdischarge detection voltage (v_{uvp}). For BQ2970, typical values of v_{ovp} and v_{uvp} are designed as 4.275 and 2.9 V, respectively. Besides BQ2970, other BMS ICs have been released for battery protection. Taking TI as an example, Fig. 3 shows the available products [43]. Generally, the principles of these ICs are similar to that of BQ2970. However, the cell counts and protection types (e.g., voltage protection, current protection, temperature protection) are different. Notice that the current protection functions (including overcurrent and short circuit protection) are not shown in the example. A detailed discussion can be found in the datasheets, such as BQ298X and BQ79731 [43].

Moreover, some similar products have been released by ADI. Typical products include DS2762 (for one cell) [44] and DS277x (for two cells) [45]. The operation principle is similar to that of TI's BQ series. However, the fuel gauge function has been integrated into ADI's DS series. A capacity estimation function is provided.

In summary, battery protection techniques have been deployed in large-scale commercial applications. Most of the products have been released by TI, ADI, etc. However, few latest patents focus on this field.

C. Stability Enhancement and EMI Suppression Techniques

Although a protection circuit can limit the voltage of a battery cell or module/pack in a given range, the battery voltage may fluctuate sharply under harsh operation conditions with frequent load fluctuations, such as in EV applications. It may impact the system performance and cause the instability of interface converters, increasing the safety risks of systems. Fortunately, some advanced methods have been presented to address this issue [46].

Taking an EV system as an example, Fig. 4(a) shows the typical power-train structure. Generally, three types of solutions are used to stabilize the dc-link voltage to enhance the stability of systems. One is optimal the control strategies of traction

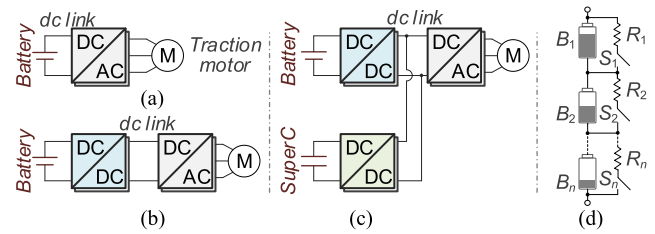


Fig. 4. Example of battery-fed converter systems and passive balancing circuits [46], [56]. (a) Typical power-train architecture. (b) Two-stage power-train architecture. (c) Additional power buffers for the power-train system. (d) Passive balancing circuits.

inverter (i.e., Type I), such as traction machine torque control [47]. Another is to add a dc/dc converter between the battery and inverter (i.e., Type II), as shown in Fig. 4(b). Nowadays, some advanced control strategies have been presented to improve the input and/or output transient performances of battery-driven converters, such as optimized state feedback [48], geometric control [49], and virtual direct power control [50]. Moreover, additional power buffers are also considered to stabilize the dc-link voltage (i.e., Type III), as shown in Fig. 4(c). Here, additional SuperC are connected in parallel with the battery to suppress the transient fluctuations [51], [52]. Notice that Fig. 4 just shows an example of stability enhancement of battery-fed converter systems, detailed discussion can be found in [46].

Besides stability issues, EMI is also needed to be suppressed in battery systems, in order to enhance safety [53]. Some widely used methods can be considered, such as common mode noise filtering, differential mode noise filtering, chip/passive EMI suppression filters, and electromagnetic shielding, which are discussed in detail in [54].

IV. BB TECHNIQUES

BB techniques have already received widespread attention in recent years. This section presents the principle of designing a balancing circuit, and the feasible schemes are derived. Then, the existing schemes are discussed. Based on this, we present suggested solutions.

A. Basics of BB

Usually, the terminal voltage of a single LIB cell is relatively low (e.g., 2–4.2 V). A large number of battery cells are widely connected in series to meet the higher voltage demand of practical applications. However, there exist slight differences in voltages, internal resistances, and/or SOCs of fresh cells due to manufacturing inconsistencies. These slight differences will be enlarged with the aging of batteries, which results in the overcharge or overdischarge of cells and even leads to premature degradation and safety issues of cells, such as explosion, fire, and thermal runaway [55]. Therefore, it is essential to design BB circuits to reduce the difference between cells, in order to enhance the lifetime and safety of battery systems.

Fig. 4(d) shows a typical BB circuit, which utilizes a parallel resistor to dissipate the energy of higher SOC/voltage cells, also known as dissipative balancing or passive balancing [56]. The control of the passive balancing scheme is simple and easily implemented. However, energy dissipation will reduce the system efficiency and may cause heat problems, reducing the safety of systems [57]. To overcome these drawbacks, PE-based active balancing schemes, including switched-capacitor circuits, switched-inductor circuits, dc/dc power converters, etc., have been presented to transfer the excess energy from the cells with the higher SOC (or voltage) to the lower ones, which are detailed discussed in the following.

B. Derivation of Active Balancing Topologies

According to the path of energy transfer, four basic categories of principles are generally used to realize BB, as shown in the first column of Table I. The first one is to realize the energy transfer between adjacent battery cells, i.e., adjacent cell–cell type (Principle I). The second one is to design PE circuits to realize the energy transfer between arbitrary cells in packs, i.e., arbitrary cell–cell type (Principle II). The third one is to realize the energy transfer between cells and a battery pack, i.e., cell–pack type (Principle III). The fourth one is to adjust energy transfer between individual cells and source/load, i.e., cell–bus type (Principle IV).

Furthermore, from the perspective of energy transfer elements, three types of circuits can be used for BB, i.e., capacitor-based type (Type A), magnetic element-based type (Type B), and converter-based type (Type C). Notice that the converter-based type mainly refers to the schemes that utilize conventional dc/dc converters, such as a buck–boost and Cuk. Here, the multiport converters consisting of a multiwinding transformer are considered to belong to the magnetic element-based type, i.e., Type B.

The possible BB topologies can be derived based on the four categories of energy transfer principles and three types of circuits. Referring to Table I, there exist 11 available schemes, which are discussed in the following.

1) *Derived Schemes Based on Principle I*: Assuming that the SOCs (or voltages) of cells B_1 and B_n are highest and lowest, respectively, and the SOCs (or voltages) of other cells are equalized, the energy transfer path and general structure of Principle I are shown in the first row and first column of Table I. Here, E_1-E_{n-1} represents the transferred energy that moves from one cell to its adjacent one. From the perspective of energy transfer elements, three derived schemes are based on Principle I, i.e., schemes 1A, 1B, and 1C.

Scheme 1A utilizes capacitors to realize the energy transfer between adjacent cells. Table I(a) shows a simple implementation example of scheme 1A, also known as the CSC scheme [58]. Here, the energy is transferred from a cell to its adjacent cell through the capacitor, and the transfer path is controlled by single-pole double-throw switches. Similarly, the inductors and dc/dc converters can be used to realize the energy transfer. Simple examples of schemes 1B and 1C are given in Table I(b) and (c), respectively [59], [60].

Notice that the examples in Table I are simple to illustrate the implementation of schemes 1A, 1B, and 1C. Detailed application cases will be discussed in Section IV-C.

2) *Derived Schemes Based on Principle II*: The second row and first column of Table I show the energy transfer path and general structure of Principle II. Here, the energy interaction is implemented between arbitrary battery cells. There exist three derived schemes based on Principle II, i.e., schemes 2A, 2B, and 2C.

A simple implementation example of scheme 2A is shown in Table I(d), also known as the flying capacitor scheme [61]. Here, the excess energy of the highest cell is stored in the flying capacitor. Then, it is selectively discharged to the lowest cell by the selection switches.

Scheme 2B utilizes magnetic elements (including the multiwinding transformers and inductors) to realize the energy transfer between battery cells. It is well known that the multiwinding transformer has multiport features, which is suitable for cell strings. Here, scheme 2B mainly refers to the multiwinding transformer-based schemes. Table I(e) [62] shows a typical implementation example, where battery cells are coupled connected by a multiwinding transformer. When the MOSFETs of higher SOC (or voltage) cells turn ON, the excess energy will go into the transformer. Then, the energy flows into the lower SOC (or voltage) cells from the transformer winding due to their voltages being lower than that on the winding sides.

Scheme 2C usually consists of a selection network and a dc/dc converter. A typical implementation example is shown in Table I(f) [63]. Here, a resonant converter is used to realize the energy transfer between battery cells. Other types of bidirectional converters can be used.

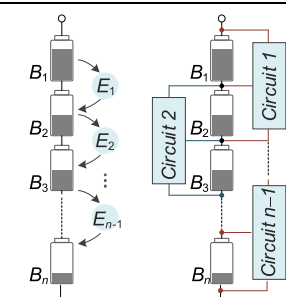
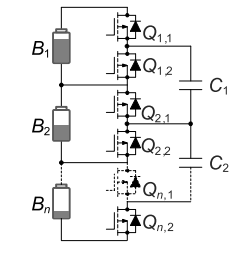
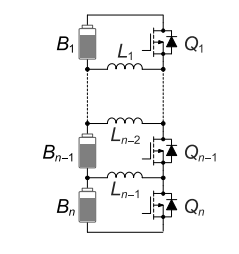
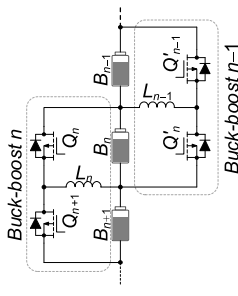
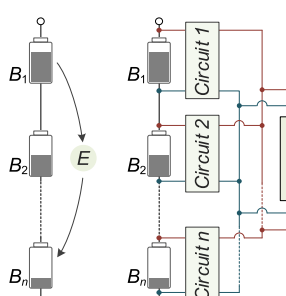
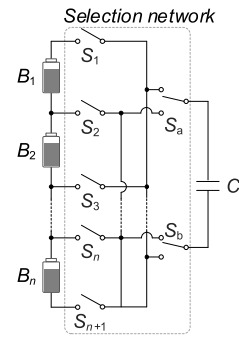
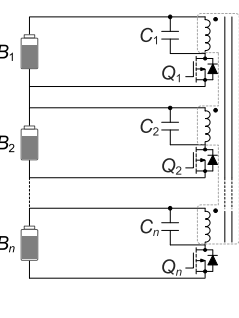
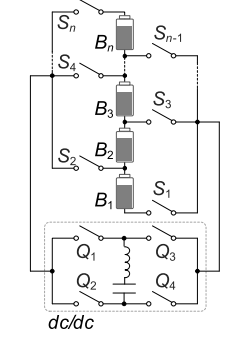
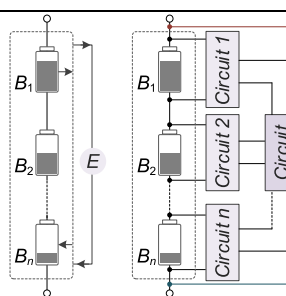
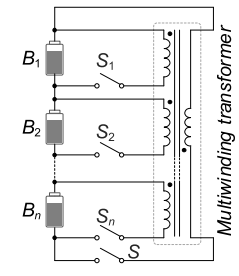
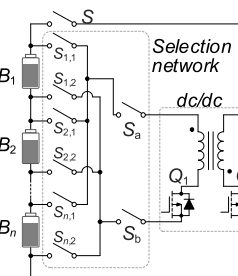
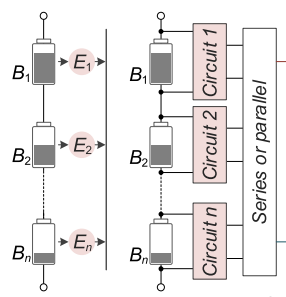
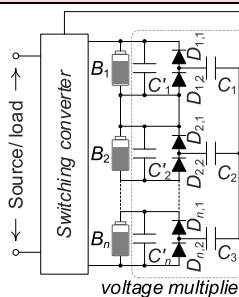
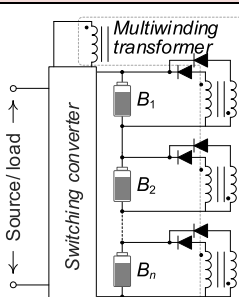
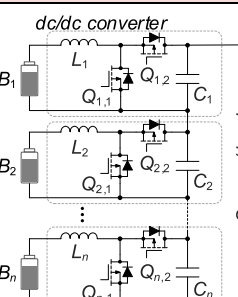
3) *Derived Schemes Based on Principle III*: The third row and first column of Table I show the energy transfer path and general structure of Principle III. Here, the energy of higher SOC (or voltage) cells can be transferred to the battery packs, and energy from the whole pack can also be delivered to the lower SOC (or voltage) cells. Generally, the capacitor-based circuit is difficult to realize the energy transfer between cells and pack, which is not considered in Principle III. There exist two derived schemes based on Principle III, i.e., schemes 3B and 3C.

Similar to scheme 2B, a multiwinding transformer is widely used in scheme 3B. Unlike scheme 2B, one winding is connected to the whole battery pack to realize the energy transfer between the cells and pack. A typical implementation example is shown in Table I(g) [64]. Here, the balancing principle is based on a flyback converter.

Similarly, scheme 3C resembles to scheme 2C. Usually, a selection network is used to select the equalized cells, and a bidirectional converter is utilized to realize the energy transfer. A typical implementation example is also given in Table I(h) [65]. Here, a bidirectional flyback converter is used, other types of bidirectional converters are also feasible.

4) *Derived Schemes Based on Principle IV*: The fourth row and first column of Table I show the energy transfer path and general structure of Principle IV. Here, the energy in the cells is obtained or released using the charger or discharger. Usually,

TABLE I
DERIVATION OF BB TOPOLOGIES AND TYPICAL EXAMPLES

	Type A: Capacitor-based scheme	Type B: Magnetic element-based scheme	Type C: Converter-based scheme (excluding multiwinding transformer-based converters)
 <p>Principle I: Energy transfers between adjacent cells</p>	 <p>(a) Example of scheme 1A [58]</p>	 <p>(b) Example of scheme 1B [59]</p>	 <p>(c) Example of scheme 1C [60]</p>
 <p>Principle II: Energy transfers between arbitrary cells</p>	 <p>(d) Example of scheme 2A [61]</p>	 <p>(e) Example of scheme 2B [62]</p>	 <p>(f) Example of scheme 2C [63]</p>
 <p>Principle III: Energy transfers between pack and cells</p>	<p>N/A</p>	 <p>(g) Example of scheme 3B [64]</p>	 <p>(h) Example of scheme 3C [65]</p>
 <p>Principle IV: Energy transfers between cells and source/load</p>	 <p>(i) Example of scheme 4A [66]</p>	 <p>(j) Example of scheme 4B [67]</p>	 <p>(k) Example of scheme 4C [68]</p>

the capacitor-based circuit (e.g., SC circuit) has not been used in scheme 4A. The VM-based schemes can be considered to belong to scheme 4A. Referring to the implementation example in Table I(i) [66], a VM consisting of capacitors and diodes

is integrated into the discharger or charger. And the square-wave voltage generated at the switching node of the PWM converters is utilized to drive the VM. The voltages of capacitors C_1-C_n are automatically unified when an ac current/voltage is

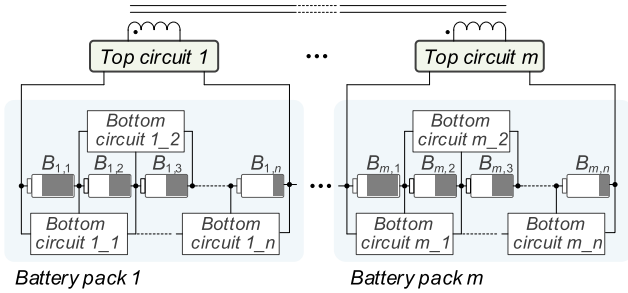


Fig. 5. Implementation example of hybrid scheme [69].

applied to the VM, which results in the paralleled cells being balanced.

An implementation example of scheme 4B is shown in Table I(j) [67]. A multiwinding transformer is used, where one winding is integrated into a charger or discharger. The balancing energy is obtained from the charger or discharger by magnetic coupling, and it is distributed to cells depending on their terminal voltages.

Scheme 4C usually controls the energy flow of each battery using multiple converters or multiple-input converters, which are used as chargers or dischargers. Taking the multiple-input converter as an example, the implementation example is shown in Table I(k) [68]. Here, the energy of each cell is controlled by a buck/boost converter. It should be noted that other types of converters used for charging or discharging are also available.

5) *Hybrid Schemes*: Notice that Table I shows 11 basic schemes for BB. Generally, they can be combined in practical application, in order to improve the balancing performance (e.g., reducing the balancing time).

Fig. 5 shows an implementation example of a hybrid scheme, where schemes 1C and 2B are utilized [69]. Here, the series-connected battery string is grouped into different packs and the equalizer is designed as two layers. The top layer is connected to the packs, and scheme 2B (multiwinding transformer) is used to realize the energy transfer between one pack to any other pack bidirectionally. The bottom layer utilizes scheme 1C (buck–boost converter) to realize the energy transfer between adjacent cells in packs.

C. Applications of Balancing Techniques

Based on the derived schemes, various balancing techniques have been proposed in [70], [71], [72], [73], [74], [75], [76], [77], [78], [79], [80], [81], [82], [83], [84], [85], [86], [87], [88], [89], [90], [91], [92], [93], [94], [95], [96], [97], [98], [99], [100], [101], [102], [103], [104], [105], [106], [107], [108], [109], [110], [111], [112], [113], [114], [115], [116], [117], [118], [119], [120], [121], [122], [123], [124], [125], [126], [127], [128], [129], [130], [131], [132], [133], [134], [135], [136], [137], [138], [139], [140], [141], [142], [143], [144], [145], [146], [147], [148], [149], [150], [151], [152], [153], [154], [155], [156], [157], [158], [159], [160], [161], [162], [163], [164], and [165], the detailed discussions are given in the following.

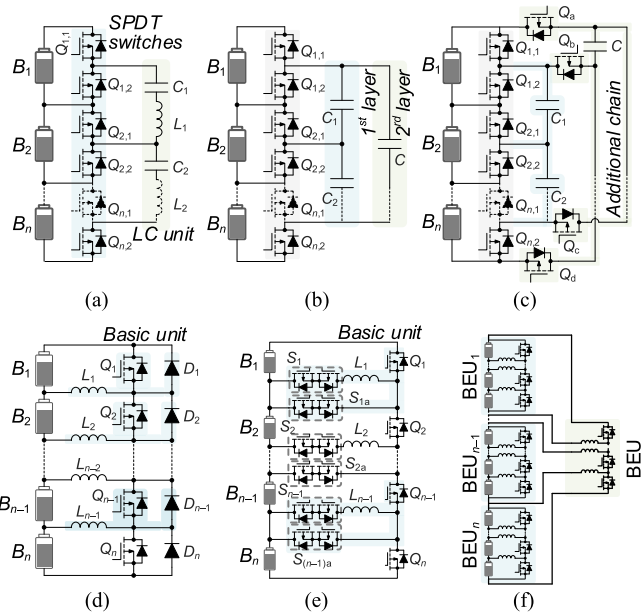


Fig. 6. Application of schemes 1A and 1B. (a) Resonant SC scheme [70]. (b) Double-layer SC scheme [71]. (c) Chain-structure SC scheme [72]. (d) Improved SI scheme with diodes [74]. (e) Improved SI scheme with bidirectional switches [75]. (f) Multilayer SI structure [76].

1) Implementation of BB Based on Principle I:

a) *Based on scheme 1A*: Table I(a) shows the basic SC topology for BB. Although it has the advantages of small size and low cost, the main disadvantage of this structure is that the switching loss is relatively high due to the hard switching. Considering this issue, Ye et al. [70] used resonant SC tanks to replace conventional switched capacitors, which can realize zero-current switching, as shown in Fig. 6(a).

On the other hand, the energy is transferred from one cell to its adjacent cell in the conventional SC topology. The balancing speed is generally slow when the number of cells is high. Baughman and Ferdowsi [71] proposed a double SC structure to overcome this limitation, as shown in Fig. 6(b). Here, an additional capacitor C is added to bridge connect the capacitors in the first tier, in order to add an energy path (i.e., the second-tier bridging capacitors). To further improve the balancing speed, Kim et al. [72] proposed a chain structure for the SC scheme, as shown in Fig. 6(c). Here, a pseudoconnection is made between the top and bottom cells, enabling direct energy transfer between them. Moreover, the energy transfer path between cells has been reduced by half, which improves the balancing speed.

b) *Based on scheme 1B*: The basic switched-inductor (SI) based balancing topology is reported in [59] and [73], as shown in Table I(b). Here, a power switch and an inductor are connected to each cell, transferring energy from one cell to its adjacent one. Similar to the conventional SC topology, the energy transfer path is relatively long when the number of cells is high. To improve the balancing speed, Zheng et al. [74] proposed a balancing circuit including a MOSFET and a freewheeling diode for each cell, as shown in Fig. 6(d). Here, diodes are used to add energy transfer paths. When a cell needs to be discharged, its corresponding MOSFET turns ON, and energy is stored in its

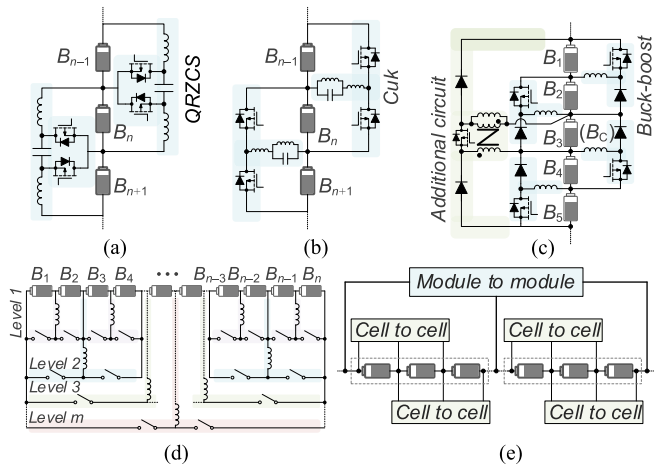


Fig. 7. Application of scheme 1C. (a) QRZCS buck-boost scheme [77]. (b) Cuk converter scheme [78], [79], [80]. (c) Additional buck-boost scheme [81]. (d) Multilayer buck-boost scheme [82]. (e) Modularized buck-boost scheme [83], [84], [85].

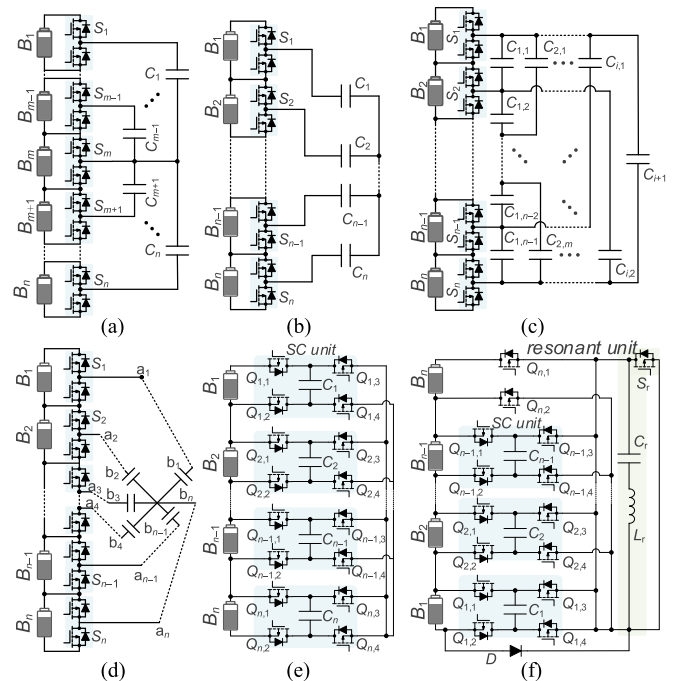
corresponding inductor. Then, the switch turns OFF, and the energy is transferred to other inductors through diodes simultaneously, which can improve the energy transfer speed. Moreover, multiple cells can be equalized simultaneously, which is another advantage of this scheme.

Similarly, an improved inductor-based scheme has been proposed in [75], as shown in Fig. 6(e). Compared with the basic SI scheme reported in [59] and [73], bidirectional switches $S_{1-}S_{n-1}$ and $S_{1a-}S_{(n-1)a}$ are added to provide more flexible balancing paths. By controlling these bidirectional switches and the MOSFETs Q_1-Q_n , the energy transfer can be realized between adjacent and arbitrary cells, significantly improving the balancing speed.

On the other hand, a multilayer structure can be constructed to speed up the balancing process. Based on the basic SI circuit, Cao et al. [76] proposed a two-layer structure, as shown in Fig. 6(f). Here, several cells are considered as a module and the first-layer BBU is used to realize the balancing of cells in modules. Furthermore, the second-layer BBU is controlled to realize the balancing of modules. Generally, the multilayer structure can realize the balancing of cells and modules, which can shorten the energy-transfer path and the balancing process.

c) *Based on scheme 1C*: A simple application example of scheme 1C is shown in Table I(c), i.e., the bidirectional buck-boost scheme [60]. Based on it, Lee et al. [77] presented a QRZCS dc/dc converter to reduce the MOSFET switching loss and increase the efficiency of BB circuits, as shown in Fig. 7(a). Similarly, other types of dc/dc converter can be used, such as modified Cuk converter [78], [79], [80], as shown in Fig. 7(b).

Although the schemes mentioned above are simple, the balancing speed reduces as the number of batteries increases because the energy is only transferred from a cell to its adjacent one. Considering this issue, Kim et al. [81] proposed an improvement scheme, as shown in Fig. 7(c). Here, an additional circuit consisting of diodes, MOSFETs, and a coupled inductor is designed to realize the energy transfer between adjacent cells, the center cell (B_C), and other cells.



Note: S_n represents two MOSFETs connected in series

Fig. 8. Application of scheme 2A. (a) Multilayer structure [86]. (b) Basic star structure [86]. (c) Delta structure [87]. (d) Improved star structure [88]. (e) Basic series-parallel structure [91]. (f) Improved series-parallel structure [92].

Moreover, the basic dc/dc converter can be connected in a hierarchical structure to improve the balancing speed. Taking the buck-boost converter as a basic balancing unit, Peng et al. [82] presented a multilayer structure, as shown in Fig. 7(d). Furthermore, the concept of modularized can be considered, as shown in Fig. 7(e). Here, a battery pack is divided into several modules, each containing several cells [83], [84], [85]. The basic dc/dc converters (e.g., buck-boost) are used to realize the balancing between adjacent modules and adjacent cells.

2) Implementation of BB Based on Principle II:

a) *Based on scheme 2A*: A simple application example of scheme 2A is shown in Table I(d), i.e., single-capacitor scheme [61]. Although its implementation is simple, only one cell can be balanced simultaneously. Therefore, many improved SC schemes have been presented to realize the balancing between any cells, in order to improve the balancing speed.

A straightforward design idea is to add or change energy-transfer paths based on the basic SC scheme [cf., Table I(d)]. Ye et al. [86] proposed a series of SC schemes, including the multilayer structure and basic star structure, as shown in Fig. 8(a) and (b), respectively. Furthermore, Shang et al. presented a series of improved schemes, including delta structure [87], improved star structure [88], mesh structure [89], coupling-capacitor structure [90], etc.

The delta scheme and improved star scheme are shown in Fig. 8(c) and (d), respectively. The mesh structure is similar to the improved star scheme. However, additional capacitors are connected between points a_n and b_n . The coupling-capacitor scheme is similar to that of the basic star structure. The difference

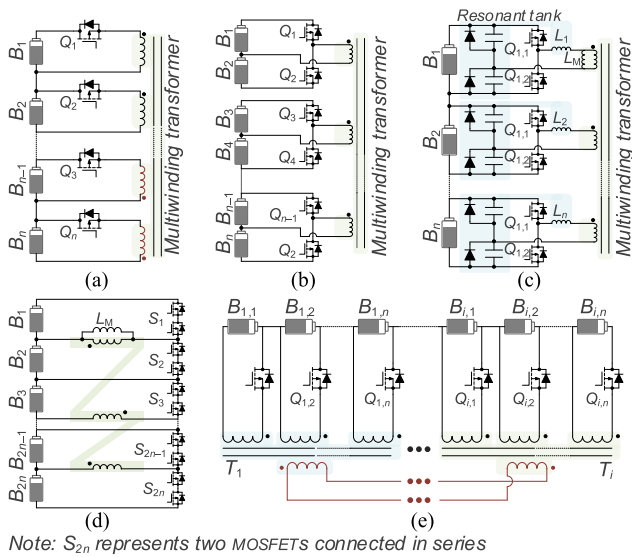


Fig. 9. Application of scheme 2B. (a) Forward–flyback scheme [96]. (b) Half-bridge scheme [97]. (c) Half-bridge LLC scheme [98]. (d) Odd–even structure [99]. (e) MT-based modularization scheme [100].

is that a coupling capacitor consisting of one big plate and several small plates are used.

Another idea for improving the balancing speed is to design a series–parallel structure [91], as shown in Fig. 8(e). Here, SC units consisting of four MOSFETs and one capacitor are designed to realize the energy transfer between each cell. First, all capacitors are connected in parallel with cells and they are charged or discharged from battery cells. Second, all capacitors are being connected in parallel, which results in the charges of capacitors being balanced automatically. Based on it, Zhou et al. [92] proposed an improved structure, as shown in Fig. 8(f). Here, capacitors C_1 – C_{n-1} and B_n are controlled to realize a similar function of [91]. Besides, an additional resonant unit is used to realize the energy transfer between arbitrary cells, which improves the balancing performance.

Notice that most of the SC schemes mentioned above operate under hard switching. Considering this issue, the authors in [93] and [94] replaced the capacitors in Fig. 8(a) and (e) as LC circuits, which can improve the balancing efficiency.

b) Based on scheme 2B: A simple application example of scheme 2B is shown in Table I(e) (i.e., forward type), which illustrates that multiwinding transformer can be used for balancing [62]. However, additional capacitors are required to form demagnetizing circuits, so as to reset the energy stored in transformers. In order to avoid additional demagnetizing circuits, Shang et al. [95] and Chen et al. [96] proposed an improved scheme (i.e., forward–flyback type), as shown in Fig. 9(a). Here, the transformer windings are divided into two groups with opposite polarities. It can realize the demagnetization for the transformer by the flyback conversion. In order to reduce the number of transformer windings, Shang et al. [97] further proposed a half-bridge scheme. Here, two cells are connected to one winding, as shown in Fig. 9(b). Moreover, considering the relatively low efficiency of hard switching, Zou et al. [98] proposed a similar half-bridge LLC scheme, as shown in Fig. 9(c).

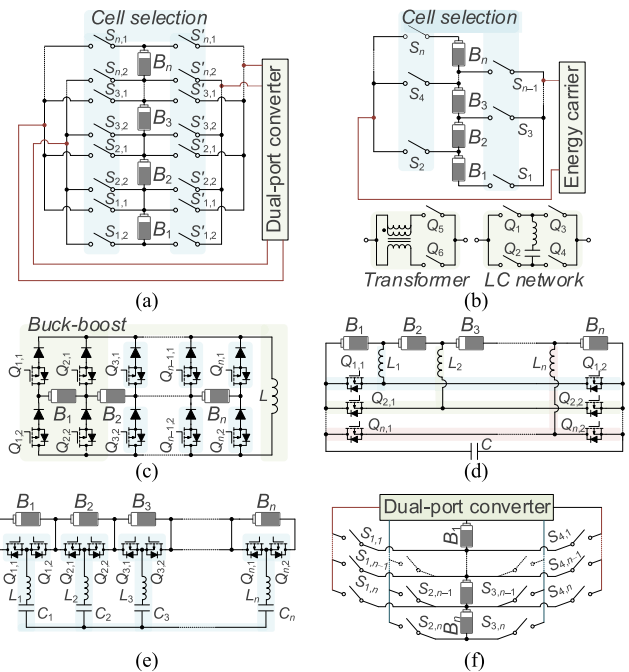


Fig. 10. Application of scheme 2C. (a) Dual-port converter scheme [101], [102], [103]. (b) Single-port energy carrier scheme [105], [106], [107]. (c) Central inductor-based converter [108], [109]. (d) Multiphase interleaved converter [110]. (e) Half-bridge converter-based scheme [111]. (f) Matrix LC converter-based scheme [112].

Besides the schemes mentioned above, other multiwinding transformer-based structures can also be used for BB. In [99], an odd–even structure was presented, as shown in Fig. 8(d). Here, the cell-to-cell energy transfer can be realized by selecting buck–boost, flyback, or both switching patterns. Moreover, similar to the modularization SC schemes, the multiwinding transformer-based schemes also can be modularized to improve the balancing speed, as shown in Fig. 8(e) [100].

c) Based on scheme 2C: Fig. 10(a) shows a typical implementation example of scheme 2C, which includes a CSN and a dual-port converter. The dc/dc converter is utilized for energy transfer. Some basic dc/dc converters can be considered, such as flyback converters [101], LLC converters [102], boost and quasi-resonant LC cascaded converters [103]. The CSN consisting of switches (MOSFETs or relays) is used to select the unbalanced cells in modules. Considering that the switches count in Fig. 10(a) is relatively high, Dam and John [104] presented a low-frequency CSN to reduce the selection switch count. And a capacitively level-shifted Cuk converter is used.

Fig. 10(b) shows another widely used scheme based on scheme 2C. Here, a single-port energy carrier converter is used for energy transfer, and the switch count is less than that in Fig. 10(a). Generally, the transformer network [105], [106], bridge LC network [63], and bridge inductor network [107] can be designed as energy carriers, as shown in Fig. 10(b). Notice that the bridge inductor network is similar to that of the bridge LC network. The only difference is that an LC circuit is used instead of an inductor. Besides that, inductors also can be used as energy carriers, as shown in Fig. 10(c) [108], [109] and Fig. 10(d) [110]. Here, the energy storage element and selection switches

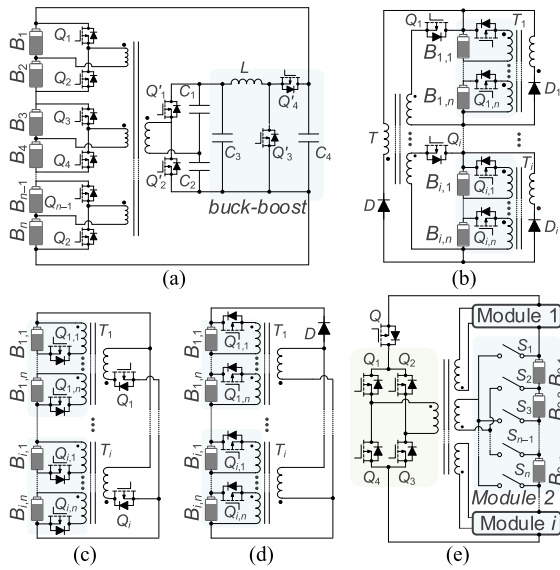


Fig. 11. Application of scheme 3B. (a) MHB scheme [114]. (b) Basic modulation scheme based on MT [115]. (c) Forward–flyback conversions-based scheme [116]. (d) Forward conversion-based scheme [117]. (e) MT with CSNs [120].

are formed as dc/dc converters to realize the energy transfer, which is different from that in [63], [105], [106], and [107].

The aforementioned schemes usually transfer energy between single cells. In order to realize the energy transfer between multicell, Dam and John [111] proposed a half-bridge converter-based scheme, which provides a direct energy transfer path from multicell, as shown in Fig. 10(e). Besides that, Shang et al. [112] proposed a matrix LC converter-based scheme to add energy transfer paths, as shown in Fig. 10(f). Moreover, Uno and Yoshino [113] presented a dual phase-shift-controlled CIDAB converter-based scheme. The implementation scheme is similar to that in Fig. 10(a). However, CIDAB converters are connected with two groups (including several cells). The selection network selects cells in different groups to realize energy transfer.

3) Implementation of BB Based on Principle III:

a) Based on scheme 3B: Generally, scheme 3B is mainly based on multiwinding transformers. Table I(g) shows a simple application example, where one transformer winding is required for each cell [64]. In order to reduce the number of transformer windings, Shang et al. [114] proposed a multiport half-bridge (MHB) structure, as shown in Fig. 11(a). Here, one winding is connected with two cells. Also, a buck–boost converter is connected to the MHB converter and battery pack to improve the balancing speed.

Considering the feature of multiport, multiwinding transformers are suitable for modularization schemes. Park et al. [115] proposed a simple modularization scheme, as shown in Fig. 11(b). However, it is just a two-layer structure of the basic scheme in [61], and the number of windings is relatively high. Based on multiwinding transformers, various improved schemes have been reported in [116], [117], and [118]. Li et al. [116] proposed a forward–flyback conversion-based scheme, as shown in Fig. 11(c). The forward and flyback converter balances the battery cells (in one module) and modules, respectively. Similarly,

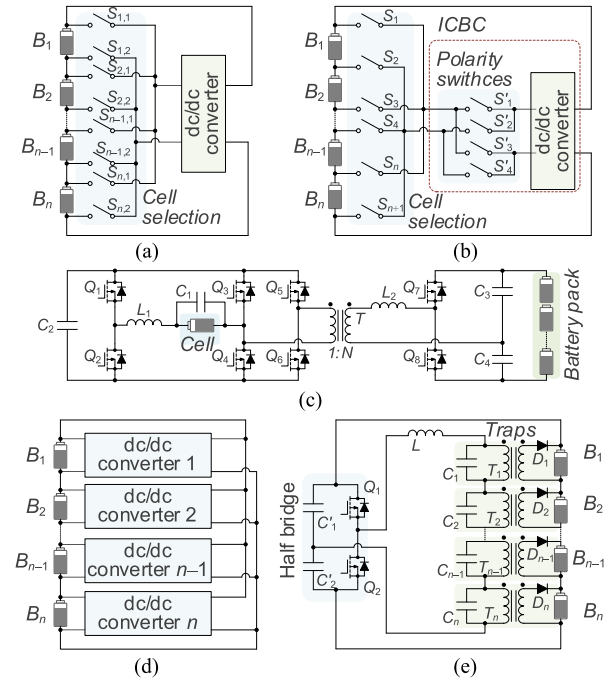


Fig. 12. Application of scheme 3C. (a) Nonpolarity adjusted CSN scheme [121]–[130]. (b) Polarity-adjusted CSN scheme [132], [133]. (c) Integrated cascade converter scheme [134]. (d) Multiconverter scheme [139], [140]. (e) Wave-trap concept-based scheme [141].

a forward conversion-based scheme has been presented in [117] and [118], as shown in Fig. 11(d). Here, the battery modules and cells are equalized based on forwarding conversion. Moreover, a dual-frequency converter-based modularization structure was presented in [119], which comprises an MHz miniaturized common-mode class-D-based cell-level equalizer and a kHz multiactive-bridge-based module-level equalizer. The cell-level and module-level equalizers are both based on multiwinding transformers.

Furthermore, multiwinding transformers with CSNs can also be used for BB, as shown in Fig. 11(e) [120]. Here, a CSN is used to select target cells. An H-bridge section is utilized to adjust the polarity of the input voltage of the transformer. Notice that the aforementioned schemes can realize the energy transfer between cells and packs. The energy transfer between cells also can be realized based on the multiwinding transformers.

b) Based on scheme 3C: Fig. 12(a) shows a typical architecture of scheme 3C, which includes a CSN and a dc/dc converter. Generally, the CSN is used to select the targeted cells, and the converter is utilized to realize the energy interaction between cells and the pack.

Usually, various kinds of dc/dc converters can be employed, such as flyback converter [121], [122], [123], bidirectional flyback converter [124], [125], [126], [127], LLC converter [128], LC series resonant circuit [129], bidirectional L2C3 resonant converter [130], and buck and resonant LC cascaded converter [131]. Notice that the circuit structure in [131] is similar to that in Fig. 12(a). However, the energy of a battery module is delivered to the cell in its adjacent module to improve the balancing current and efficiency.

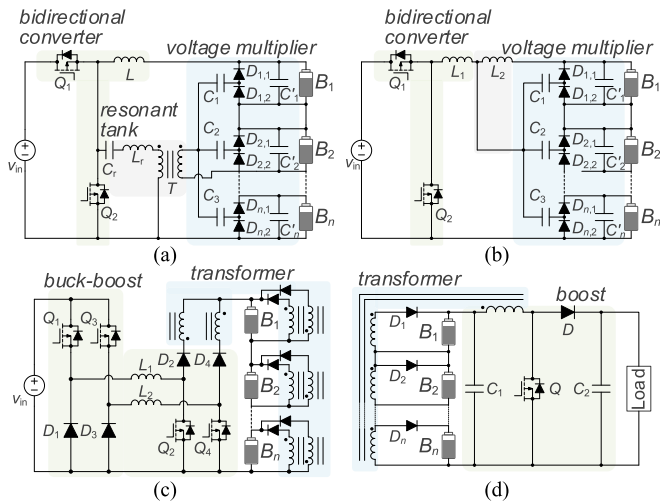


Fig. 13. Application of schemes 4A and 4B. (a) Buck converter with a VM [142]. (b) Tapped-inductor-driven VM scheme [143]. (c) MT-integrated noninverting buck-boost converter [67]. (d) Magnetic-integrated boost converter [146], [147].

Assuming that there exist n cells, the CSN in Fig. 12(a) generally contains $2n$ bidirectional switches. In order to reduce the switch counts, a polarity-adjusted architecture has been presented, as shown in Fig. 12(b) [132], [133]. Here, the voltage polarity of targeted cells is adjusted via the polarity switches. $n+1$ bidirectional switches and four polarity switches are required in this architecture. In order to further reduce the switch count and improve the integration, Qi et al. proposed a series of ICBCs to combine the polarity switches and traditional dc/dc converters [134], [135], [136], and [137]. A typical example is shown in Fig. 12(c) [134]. Considering that only one cell can be equalized at a time in the schemes mentioned above, the same authors further proposed a multiport ICBC scheme in [138], which is similar to those in [134], [135], [136], and [137].

Besides the schemes in Fig. 12(a) and (b), other structures can also be considered. Dong et al. [139] and McCurlie et al. [140] presented a multiconverter scheme, as shown in Fig. 12(d). Each battery cell is connected to the pack via a bidirectional flyback transformer-based buck-boost converter. Moreover, Arias et al. [141] used the wave-trap concept to select the cell that is going to be charged, which can reduce the switch counts, as shown in Fig. 12(e). Each trap consists of a battery cell, a transformer, and a diode. The energies on the battery pack are distributed to unbalanced cells via the control of the switching frequency and duty cycle of a half-bridge converter.

4) Implementation of BB Based on Principle IV:

a) *Based on schemes 4A and 4B:* Table I(i) shows the typical structure of scheme 4A, i.e., the VM-based schemes. Generally, ac voltage/current exists in any type of a dc/dc converter, which can be used to drive a VM. Based on this, Uno et al. and Yang et al. proposed a series of VM schemes, such as boost converter-based scheme [142], transformer-based scheme [66], [143], tapped-inductor-scheme [144], [145]. Two typical examples are shown in Fig. 13(a) and (b). Here, the square-wave

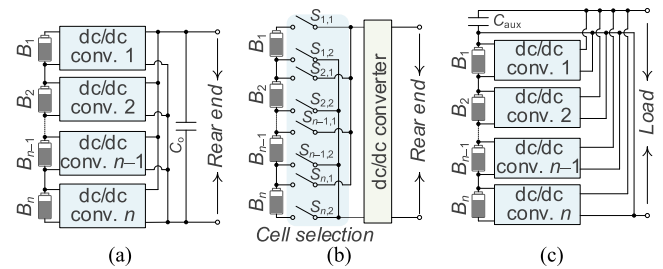


Fig. 14. Application of scheme 4C. (a) Multiconverter parallel structure [148]. (b) Selection switches-based scheme [154], [155], [156], [157], [158]. (c) Series-connected energy storage scheme [160], [161].

voltage generated at the switching node is introduced to drive the VM and realize cell balancing.

Utilizing the magnetic coupling characteristics of multiwinding transformers, Hsieh et al. proposed a series of BB topologies based on scheme 4B. A basic structure of scheme 4B is also shown in Table I(j). A typical implementation example is shown in Fig. 13(c). The equalizer obtains the energy from the buck-boost converter by magnetic coupling. And the energy is distributed to each battery cell based on its terminal voltage. Besides this, other connection structures (e.g., multiswitch-based structure and single secondary winding-based structure) and converters (e.g., CLL converter, noninverting buck-boost converter) can be used, which are discussed in [67]. Similarly, Liu et al. [146], [147] proposed an improved scheme, as shown in Fig. 13(d). Here, the magnetic element of dc/dc converters is integrated with the transformer used for BB, which can reduce the volume of the converters.

c) *Based on scheme 4C:* Unlike all the above schemes, scheme 4C utilizes the charger or discharge converter to realize cell balancing. Generally, there exist three typical structures, i.e., multiconverter parallel type, multiconverter series type, and selection switches type.

Fig. 14(a) shows the diagram of the multiconverter parallel structure. Here, each battery cell is connected to a dc/dc converter, and the voltage/charge of each cell is adjusted by its corresponding converter. Generally, various topologies can be considered, such as DAB converter [148] and bidirectional flyback converter [149], [150]. The multiconverter series structure is similar to that in Fig. 14(a). However, the right ends of each converter are connected in series. Theoretically, all kinds of converters can be used, such as the Cuk converter [151] and full-bridge inverter [152], [153]. Although the balancing function can be integrated into chargers, the majority of the aforementioned schemes are designed for discharge converters.

Similar to the cell selection schemes in Fig. 12, the CSN can also be used in scheme 4C. In [154], [155], [156], [157], and [158], a series of selection switch-based schemes were presented, which have a similar structure, as shown in Fig. 14(b). Here, a cell is selected by the switching network and it is controlled to be charged or discharged via a central dc/dc converter. In [154], [155], [156], [157], and [158], the structure of the switching network is the same as those in Fig. 12(a) and (b), respectively. In order to reduce the switch counts, Riczu and Bauman [159] proposed an improved scheme with an odd and

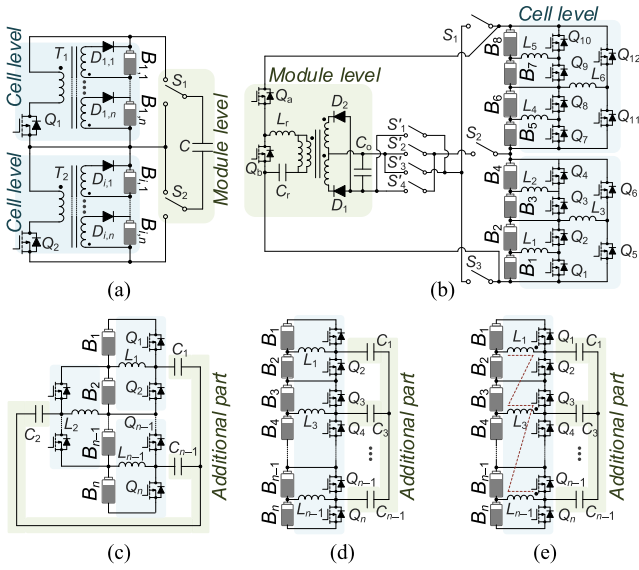


Fig. 15. Application of scheme 5. (a) MT- and SC-based hybrid scheme [115]. (b) Adjacent buck-boost and central converter-based hybrid scheme [160]. (c) Adjacent buck-boost and SC-based scheme I [165]. (d) Adjacent buck-boost and SC-based scheme II [165]. (e) Adjacent buck-boost and SC-based scheme III [165].

even cell control strategy, which can avoid using the polarity switches in Fig. 12(b).

Generally, most of the aforementioned schemes directly transfer the excess energy of cells to the rear end via dc/dc converters. In [160] and [161], the authors proposed a novelty scheme in which cells' energy is first to be transferred to an auxiliary capacitor C_{aux} via dc/dc converters. Then, the whole pack, including C_{aux} , is used to feed the load, as shown in Fig. 14(c).

5) *Implementation of BB Based on Hybrid Schemes*: In order to improve the balancing performance, the derived 11 schemes can be combined in practical applications. Generally, there exist two main solutions. One is modularization schemes, in which a battery pack is divided into several modules, and a module consists of several cells. Module-level and cell-level balancing are designed for modules and cells, respectively. The same or different balancing schemes can be used for modules and cells. Another is the nonmodularization scheme. Usually, the basic schemes (e.g., switched-capacitor scheme, switched-inductor scheme) are combined to overcome the limitation of a single scheme.

a) *Modularization hybrid schemes*: Recently, various modularized balancing schemes have been reported. One is to use the same scheme for module-level and cell-level balancing, such as the schemes in [76], [83], [84], [85], [100], [115]–[119], and [131], which is discussed in Sections IV-C1–IV-C4.

Another is to use different schemes for modules and cells, which is discussed in the following. In [115], a hybrid scheme consisting of multiwinding transformers and switched capacitors was also presented, as shown in Fig. 15(a). Here, schemes 3B and 1A are used for cell-level and module-level balancing, respectively. Peng et al. [162] proposed a hybrid scheme based on schemes 1C and 3C, as shown in Fig. 15(b). The

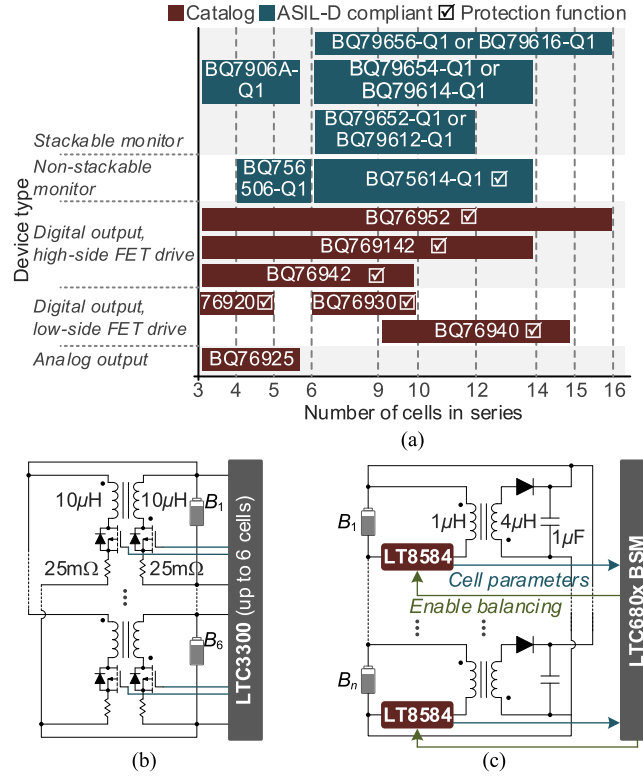


Fig. 16. Typical commercial BB ICs released by TIs and ADIs. (a) TIs' battery monitors and balancers [166]. (b) Typical application of ADI LTC3300 [169]. (c) Typical application of ADI LT8584 [170].

two-level buck-boost scheme and a centralized dc/dc converter are used for cell-level and module-level balancing, respectively. Similarly, Uno et al. [163], [164] presented a hybrid scheme consisting of TI-RVMs and PS-SCCs. The TI-RVMs and PS-SCCs are employed for cell-level and module-level balancing, respectively.

b) *Nonmodularization schemes*: Besides the hybrid modularization schemes, basic balancing schemes can be combined to optimize the performance. Liu et al. [165] proposed a series of hybrid schemes based on SC converters and buck-boost converters. Referring to Fig. 15(c), an interleaved BB converter and an SC converter are integrated, which results in the energy transfer between adjacent cells and any cells. Similarly, a sequential buck-boost converter and coupled buck-boost converter can be combined with an SC converter, as shown in Fig. 15(d) and (e).

D. Typical Commercial and Industrial Solutions for BB

Nowadays, some commercial BMS ICs have integrated the function of BB. Taking TIs' BQ series as an example, Fig. 16(a) shows the available products [166]. Usually, they are mainly designed for voltage, current, and/or temperature monitoring for batteries, called battery monitors and balancers. In some ICs, the protection function has also been intergraded (e.g., BQ76940). Generally, a passive balancing scheme [cf., Fig. 4(d)] is employed in these ICs, and balance FETs for each cell are integrated into ICs. As discussed in Section IV-A, the drawback

TABLE II
TYPICAL PATENTS ABOUT BB

Scheme	Description	Applicant
Passive scheme	device with integrated balancing switches	Marelli Corporation [171], Samsung SDI [172]
	passive balancing for cells	LG Energy Solution [173]
1A	switched capacitors (similar to scheme 1A in Table I)	Qingdao Anjie Energy [174]
1B, 1C	switched inductor and buck–boost (similar to schemes 1B and 1C in Table I)	The University of Toledo [175]
1C	bypass circuit with energy storage components [similar to Fig. 7(b)]	TIs [176]
2A	switched capacitor/inductor (similar to scheme 2A in Table I)	Huawei Technologies Co. [177]
2C	selection network (similar to scheme 2C in Table I)	LG CHEM [178]
3B	multiwinding transformer (similar to 3B in Table I)	IFP Energies Nouvelles [179], Wenzhou University [180]
	multiwinding transformer and dc/dc converter [similar to Fig. 11(a)]	Intersil Americas LLC [181]
3C	selection network and a central converter [similar to Fig. 12(a)]	SK Innovation [182], 24M Technologies [183]
4C	selection network and a central converter [similar to Fig. 14(b)]	ITRI, TW [184]

of passive balancing is heat generation. A tradeoff between balancing speed and heat generated should be considered.

Similar to TIs' BQ series, ADI and NXP semiconductors release some BMS ICs with battery monitoring and balancing functions. Typical products include ADI's MAX17843/MAX1785x [167] and NXP's MC3377x series [168]. Although some valuable functions have been integrated, such as Coulomb counting (for SOC estimation) and battery temperature measurements, passive balancing is used. Besides, ADI released special ICs for BB, such as LTC3300 and LT8584 [169], [170]. Referring to the typical applications in Fig. 16(b) and (c), it is found that active balancing [i.e., scheme 3C, cf., Fig. 12(d)] is considered. Notice that the operation principles of these two types of ICs are different. Although LTC3300 integrates the monitoring function, an additional battery stack monitor IC (LTC680x series) is needed.

Besides commercial products, some patents have been granted or submitted in recent years [171], [172], [173], [174], [175], [176], [177], [178], [179], [180], [181], [182], [183], [184]. Table II summarizes the typical patent schemes. It can be seen that passive balancing still attracts the attention of some enterprises. And some improved strategies based on Principles I–IV have been presented. The implementations of these patent solutions comply with the derivation principles in Table I, similar schemes are labeled in Table II.

E. Discussions of Balancing Schemes

1) *Comparison and Remarks:* In [185] and [186], mathematical models and simulation analysis are given to compare the main balancing structures, where the balancing speed is mainly in focus. Considering the number of circuit components, balancing speed, balancing circuit efficiency, and control strategy are important performance indexes, Tables III and IV give a comprehensive comparison of them. Notice that patent solutions are not considered in Tables III and IV due to a lack

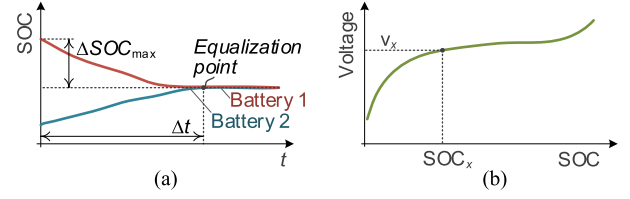


Fig. 17. Calculation of balancing speed. (a) Example of SOC balancing for two batteries. (b) Example of the relationship between SOC and battery voltage.

of detailed data. Here, the balancing speed α is calculated using the maximum variation of SOC (ΔSOC_{\max}) and the balancing time Δt , as shown in Fig. 17(a), i.e.,

$$\alpha = \Delta\text{SOC}_{\max} / \Delta t. \quad (1)$$

Considering that SOC's variations are not given in some literature, ΔSOC_{\max} is derived from the relationship between SOC and battery voltage [187], [188], [189], as shown in Fig. 17(b). Notice that α is just used to conduct benchmarking, there is no actual physical meaning and units. Referring to Tables III and IV, some remarks are given as follows.

- 1) The passive balancing scheme in Fig. 4(d) has the advantage of low cost, low control complexity, and excellent modularization. It is widely used in commercial and industrial applications. However, energy dissipation will reduce the efficiency and it may cause safety issues.
- 2) The derived schemes based on scheme 1A have the advantage of low control complexity. However, the number of energy transfer paths is relatively low, which results in the balancing speed being relatively low. The derived schemes based on scheme 2A are usually improved schemes of scheme 1A, which can increase the energy transfer path counts and balancing speed. However, the corresponding component counts are increased, especially the number of capacitors and MOSFETs. Moreover, the modularization capabilities of SC-based schemes (based on schemes 1A and 2A) are relatively poor. They are not suitable for large-scale LIB systems.
- 3) The derived schemes of schemes 1B, 2B, and 3B are mainly based on switched inductors and multiwinding transformers. Usually, the balancing speed and modularization capabilities are better than those of SC-based schemes (based on schemes 1A and 2A). And the complexity of control strategies is similar to that of SC-based schemes. However, the volumes of inductors and transformers are relatively large, which reduces their applicability in high power density applications.
- 4) The derived schemes of schemes 1C, 2C, and 3C are mainly based on dc/dc converters, which have received extensive attention. The schemes in [77], [78], and [80] (based on scheme 1C) are basic methods. However, their balancing speeds are relatively low due to the relatively low energy transfer path counts. This limitation can be breakout by using multilayer structures [82], modularized structures [83], [84], [85], and additional energy transfer paths [81]. However, a larger amount of

TABLE III
 SUMMARY OF BALANCING SCHEMES BASED ON DERIVED METHODS 1A–2C

	Description	Number of components					Reported max. speed α (n, m)	Eff. (%)	Control strategy	
		MOS, RE	T (N_T)	L	C	D				
1 A	SC between adjacent cells (basic SC) [58]	$2n, 0$	0	0	$n-1$	0	-	-	OLC with given PWM	
	Quasi-resonant LC between adjacent cells [70]	$2n, 0$	0	$n-1$	$n-1$	0	0.9×10^{-6} (2,0)	98.2		
	Double-tiered SC [71]	$2n, 0$	0	0	$2n-3$	0	-	-		
	Chain structure of SC [72]	$2n+4, 0$	0	0	n	0	1.0×10^{-6} (8,0)	>97		
1 B	SI between adjacent cells (basic SI) [59], [73]	$n, 0$	0	n	0	0	-	<90	PI adjusts Δv_{adj}	
	Evolved structure based on basic SI [74]	$n, 0$	0	$n-1$	0	n	6.7×10^{-5} (4,0)	91.2	-	
	SI-based multiple buck–boost converters [75]	$5n-4, 0$	0	$n-1$	0	0	4.8×10^{-5} (6,0)	<91.3	OLC with given PWM	
1 C	Basic SIs are used for cells and modules [76]	$n+m$	0	$n+m$	0	0	8.3×10^{-5} (16,4)	-	LSC with calculated d	
	Buck–boost between adjacent cells [60]	$2n-2, 0$	0	$n-1$	0	0	-	-	-	
	Soft-switching buck–boost converter [77]	$2n-2, 0$	0	$2n-2$	$n-1$	$2n-2$	-	<85.6	OLC with given PWM	
	Modified bidirectional Cuk converter [78], [79], [80]	$2n-2, 0$	0	$2n-2$	$n-1$	0	- ^[78]	-	ANFIS for each conv.	
							8.7×10^{-5} (2,0) ^[79]	-	FLC for each conv.	
	A parallel buck–boost converter is connected with buck–boost-based battery strings [81]	$n+2, 0$	1	$n-1$	0	$n+2$	2.6×10^{-5} (8,0)	82.5	LSC enables/disables each converter	
							-	<90	control variables calculation for each layer	
	Multilayer buck–boost converter [82]	$2n-2, 0$	0	$n-1$	0	0	1.9×10^{-5} (4,0)	<90	FLC for each conv.	
	Buck–boost converters [83] and Cuk converters [84], [85] are used for cells and modules	$2n+2m-4, 0$	0	$n+m-2$	0 ^[83]	0 ^{[84], [85]}	-	-	hierarchical cell equalizing control [31]	
	2 A	CSN with a single capacitor [61]	$2n+6, 0$	0	0	1	0	1.7×10^{-6} (2,0)	-	OLC with given PWM
Basic star structures of SC [86]		$2n, 0$	0	0	$n-1$	0	-(SuperC)	-		
Delta structure of SC [87]		$2n, 0$	0	0	$\sum_{i=1}^{n-1} (n-i)$	0	3.9×10^{-5} (4,0)	<94.5		
Improved star structure of SC [88]		$2n, 0$	0	0	$n-1$	0	3.1×10^{-5} (4,0)	<93.1		
Mesh-structure of SC [89]		$2n, 0$	0	0	$2n-2$	0	5.5×10^{-5} (4,0)	<91.7		
Switched-coupling-capacitor [90]		$n, 0$	0	0	n (CC)	0	2.7×10^{-5} (4,0)	<92.7		
Series–parallel SC [91]		$4n, 0$	0	0	n	0	-(SuperC)	-		
Additional LC resonant unit connects with series–parallel SC [92]		$4n-1, 0$	0	1	n	0	-(SuperC)	>88.5	LSC	
Multilayer switched-LC circuit [93]		$2n, 0$	0	0	$n-1$	0	-(SuperC)	-	OLC with given PWM	
Series-parallel switched-LC circuit [94]	$4n, 0$	0	$4n$	$4n$	0	3.9×10^{-5} (4,0)	95.2	-		
2 B	Direct balance circuit based on MT [62]	$n, 0$	1 (n)	0	n	0	-	-	OLC with given PWM	
	MT based forward–flyback scheme [95]	$n, 0$	1 (n)	0	0	0	3.9×10^{-5} (8,2)	<90		
	Grouped MT based forward–flyback [96]	$2n, 0$	1 ($2n$)	0	0	0	8.8×10^{-5} (6,0)	80.7		
	MT-based half-bridge converter [97]	$n, 0$	1 ($n/2$)	0	0	0	7.8×10^{-5} (4,0)	<95		
	MT-based half-bridge LLC converter [98]	$2n, 0$	1 (n)	n	$2n$	$2n$	4.5×10^{-5} (7,0)	<90		
	MT-based odd–even structure [99]	$2n, 0$	1 ($n/2$)	0	0	0	8.1×10^{-6} (6,0)	-		
	MT-based modular structure [100]	$n, 0$	$m(n+m)$	0	0	0	1.7×10^{-5} (8,2)	<95		
2 C	CSN with an LC resonant network [63]	$2n+10, 0$	0	1	1	0	2.8×10^{-5} (12,0)	<96	LSC for CSN and transformer network, special controllers for converters	
	CSN with a flyback converter [101]	1, $2n$	1 (2)	0	2	1	-(SuperC)	59.4		
	CSN with an LLC converter [102]	$4n+4, 2$	1 (3)	1	3	2	3.8×10^{-5} (12,0)	<94.5		
	CSN with quasi-resonant LC and boost [103]	5, $2n$	0	2	2	5	1.4×10^{-5} (8,0)	98		
	Low-frequency CSN with a central bidirectional converter [104]	$4n+12, n+4$	0	2	2	0	-	<92.9		
	CSN with a transformer network [105]	$2n+6, 0$	1 (2)	0	0	8	-(SuperC)	-		
	CSN with a bridge transformer network [106]	$2n+6, 0$	1 (2)	0	0	0	3.88×10^{-6} (12, 0)	80.4		
	CSN with an inductor network [107]	$2n+4, 0$	0	1	0	0	1.96×10^{-6} (16, 0) 5.70×10^{-6} (16, 4)	79.4		
	Central inductor-based converter [108], [109]	$2n, 0$ ^[54]	0	1	0	$2n$	-	-		LSC
	Multiphase interleaved converter [110]	$2n, 0$	0	$2n$	1	0	3.47×10^{-5} (8, 0)	<95		OLC with given PWM
	Common bussing half-bridge converter [111]	$2n, 0$	0	n	n	0	2.43×10^{-4} (4, 0)	90.8		converter control
Matrix CSN with an LC resonant converter [112]	4, $4n$	0	1	1	0	6.06×10^{-5} (8, 0)	<90	LSC for CSN		
Modularized CSN with CIDABs [113]	4 <i>m</i> , <i>m</i> (<i>n</i> +12)	0	4 <i>m</i> -1	2(2 <i>m</i> -1)	0	5.15×10^{-6} (12, 0) 2.14×10^{-6} (0, 2)	84	LSC for CSN		

Notes: MOSFET (MOS), relay (RE), transformer (T), the number of winding in transformers (N_T), inductor (L), capacitor (C), diode (D), the number of battery cells (n), the number of battery modules (m), switched capacitor (SC), switched inductor (SI), cell selection network (CSN), multiwinding transformer (MT), capacitively isolated dual active bridge (CIDAB), supercapacitor (SuperC), open loop control (OLC), proportional integral (PI), voltage difference between adjacent cells (Δv_{adj}), logical switching control (LSC), duty cycle (d), adaptive neural fuzzy inference system (ANFIS), fuzzy logic control (FLC), state of charge (SOC), and quasi-sliding mode control (QSMC).

TABLE IV
SUMMARY OF BALANCING SCHEMES BASED ON DERIVED METHODS 3B–5

	Description	Number of components					Reported max. speed $\alpha(n, m)$	Eff. (%)	Control strategy
		MOS, RE	$T(N_T)$	L	C	D			
3 B	Basic MT based structure [64]	$n+1, 0$	$1(n+1)$	0	0	0	-	90	LSC
	MT-based multiport half-bridge [114]	$n+4, 0$	$n/2+1$	1	2	0	3.4×10^{-4} (12,0)	88	OLC with given PWM
	Basic modularized MT scheme [115]	$2m+1, 0$	$m+1(n+2m+1)$	0	0	$n+m$	-	-	OLC with given PWM
	Forward–flyback conversion based on modularized MT [116], [117], [118]	$n, 0^{[116]}$	$m(n+2)$	0	0	1	1.4×10^{-5} (8,2)	<97	OLC with given [116], [117] PWM, adjusted PWM [118]
	MT-based dual frequency converter [119]	$2n+2m, 0$	$2m$	$2n+m$	$2m$	0	6.1×10^{-3} (16,4)	<93	power flow control
3 C	CSN with an H-bridge and a modularized MT [120]	$2n+2m+5, 0$	$1(m+1)$	0	0	0	5.6×10^{-5} (4,2)	89.5	LSC for CSN and H-bridge
	CSN with a two-level flyback converter [121]	$4n+4, 0$	$2(4)$	0	2	2	1.2×10^{-3} (88,11)	>75	LSC for CSN, and special controllers for converters
	CSN with a bidirectional flyback converter [122]	$4n+2, 0$	$1(2)$	0	2	2	-	-	
	CSN with a time-shared flyback converter [123]	$n+1, 0$	$1(2)$	0	0	$2n-1$	4.3×10^{-5} (4,0)	<88	
	CSN with bidirectional flyback converters [124], [125], [126], [127]	$4n+2, 0^{[124]}$ $2n+2, 0^{[127]}$	$2(4)$ $2(4)$	0 1	2 1	2 $2n+2$	2.2×10^{-5} (88,11) 1.7×10^{-3} (4,0)	81.6 -	
	CSN with an LLC converter [128]	$2, 2n$	$1(3)$	1	2	2	7.2×10^{-5} (4,0)	<88.1	
	CSN with an LC series resonant circuit [129]	$4n, 0$	0	1	1	3	-(SuperC)	-	
	CSN with an L2C3 resonant circuit [130]	$2n+4, 0$	$1(2)$	1	3	0	2.6×10^{-3} (4,0)	<90.1	
	CSN with a buck–LLC cascaded converter [131]	$2.5n, n$	0	$0.25n$	$0.25n$	0	2.9×10^{-5} (8,2)	<90	
	Adjusted CSN with a full-bridge converter [132]	$2n+14, 0$	$1(2)$	1	2	0	-	-	
	Adjusted CSN with a ZVS dc–dc converter [133]	$2n+10, 0$	$1(2)$	1	3	0	3×10^{-5} (13,0)	<84.2	
	CSN with integrated cascade bidirectional converters [134], [135], [136], [137], [138]	$2n+10, 0^{[134]}$	$1(2)$	2	4	0	4.6×10^{-3} (13,0)	<85.1	
		$2n+8, 0^{[135]}$	$1(2)$	1	3	0	5.2×10^{-3} (13,0)	<85.2	
		$2n+8, 0^{[136]}$	$1(2)$	2	6	0	5.2×10^{-3} (13,0)	<86.8	
		$2n+10, 0^{[137]}$	$1(2)$	2	5	0	7.1×10^{-5} (13,0)	<87.7	
$2n+6m+2, 0^{[138]}$		$1(m)$	$m+1$	$m+4$	0	8.7×10^{-5} (12,2)	<91.1		
Multiple bidirectional flyback converter [139], [140]	$2n, 0^{[140]}$	$n(2n)$	0	0	0	1.8×10^{-4} (6,1)	90 [140]	star search algorithm [139], fast MPC [140]	
Wave-trap units with half-bridge converter [141]	$2, 0$	0	n	n	n	-(Cap)	-	OLC for half-bridge	
4 A	Buck converter [66], boost converter [142], BB converter [143] with a VM	$1, 0^{[142]}$	0	1	n	$2n$	3.3×10^{-5} (3, 0)	<90	There is no need of controller for balancing circuits. Special controllers are required for interface converters.
	tapped-inductor-based VM [144], [145]	$2, 0^{[144]}$	0	2	n	$2n$	-(SuperC)	<93	
4 B	MT-integrated CLL converter [67]	$2, 0$	$2(n+2,3)$	1	1	$2n+2$	-	-	
	MT-integrated interleaved BB converter [67]	$4, 0$	$1(n+2)$	2	0	$2n+4$	-	-	
	MT-integrated noninverting BB converter [67]	$2, 0$	$1(n+1)$	1	0	$2n+2$	-	-	
Magnetic -integrated boost converter [146], [147]	$1, 0$	$1(n+1)$	0	1	1	6.3×10^{-5} (4, 0)	94.1		
4 C	C2L using multi parallel DAB [148] and bidirectional flyback converters [149], [150]	$8n, 0^{[148]}$ $2n, 0^{[150]}$	$n(2n)$ $n(2n)$	n 0	$4n$ $2n$	0 0	4×10^{-3} (21, 0) 4.2×10^{-3} (3,0)	93 <85	There is no need of additional balancing circuits. Special controllers are required for interface converters.
	C2L using multi series Cuk [151]	$2n, 0$	0	$n+1$	$n+1$	0	-	-	
	C2L using full-bridge inverter [152], [153]	$4n, 0$	0	0	0	0	-	-	
	C2L using CSN and a buck converter [154], an isolated dc/dc [155], and an LC circuit [156]	$4n+2, 0^{[154]}$ $4n+1, 0^{[156]}$	0 0	1 1	1 0	0 0	- 1×10^{-4} (3,0)	90 96.1	
	C2ASU using CSN and a bidirectional four-switch converter [157], forward converter [158], flyback converter [159]	$4n+4, 0^{[157]}$	0	1	1	0	1.4×10^{-4} (6,0)	93	
		$2n+14, 0^{[158]}$	$1(2)$	1	2	0	-	-	
		$2n+2m+2, 0^{[159]}$	$m(2m)$	0	$2m$	0	-	<71.9	
	A series-connected auxiliary energy storage unit is used to adjust energy [160], [161]	$4n+4, 0^{[160]}$	$n(2n)$	n	$4n+1$	0	-	<93.4	
5	Two-level buck–boost and a dc/dc converter are used for cell- and module-level balancing [162]	$6m+2, 0$	0	$3m$	2	2	1.64×10^{-5} (8,2)	<94	LSC for CSN, and special controllers for converters
	TI-RVMs and PS-SCCs are used for cell-level and module-level balancing [163], [164]	$2m, 0$ $2m, 0$	0 $m(2)$	$2m$ m	$m+2$ $m+3$	$2mn$ $2mn$	-(SuperC) -(SuperC)	90 <85.6	OLC with given PWM for module layer, and there is no need of controller for cell layers.
	Hybrid scheme based on SC and buck–boost [165]	$n, 0$	$n/2$	0	$n/2$	0	2.5×10^{-4} (6,0)	96	OLC with given PWM

Notes: MOSFET (MOS), relay (RE), transformer (T), the number of winding in transformers (N_T), inductor (L), capacitor (C), diode (D), the number of battery cells (n), the number of battery modules (m), multiwinding transformer (MT), cell selection network (CSN), zero-voltage switching (ZVS), voltage multiplier (VM), cell to load (C2L), cell to auxiliary storage units (C2ASU), tapped inductor resonant voltage multipliers (TI-RVMs), phase-shift switched capacitor converters (PS-SCCs), switched capacitor (SC), logical switching control (LSC), open loop control (OLC), model predictive control (MPC).

circuit components is required. Similarly, the components count of 2C and 3C-derived schemes is also relatively high, in order to obtain a better balancing speed. Notice that the scalability of converter-based schemes (based on schemes 1C, 2C, and 3C) is usually better than those of

capacitor-based schemes (based on schemes 1A and 2A) and magnetic element-based schemes (based on schemes 1B, 2B, and 3B), due to the design of capacitor matrices and multiwinding transformers is usually dependent on the battery cell counts.

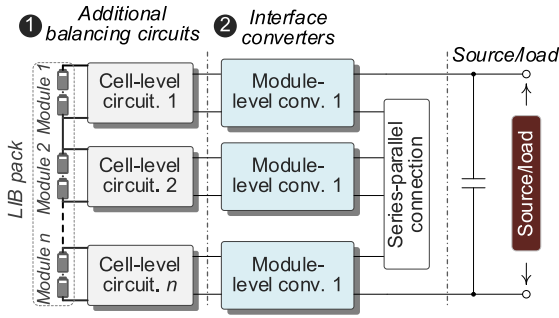


Fig. 18. Suggested balancing solution for LIB systems in EVs and ESPSs.

5) 4A and 4B-based schemes mainly refer to the VMs and magnetic-integrated schemes. The schemes in [142] and [143] (based on scheme 4A) utilize VM to realize the balancing, which does not need an additional controller for VM. However, the conversion efficiency is relatively high due to diodes. Similarly, the integrated magnetic schemes (based on scheme 4B) in [67], [146], and [147] do not need additional controllers for balancing circuits. However, the number of converters will be large if a converter is designed for each cell.

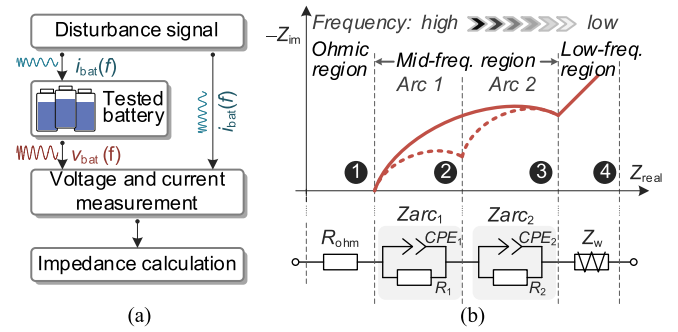
6) The hybrid scheme mainly includes modularization and nonmodularization schemes. Although nonmodularization schemes can overcome some limitations of conventional schemes, it is not suitable for large-scale energy storage applications. The hybrid scheme can overcome the limitation of one type of scheme, which has good prospects.

2) *Suggested Feasible Solutions*: The key goal of employing a BB scheme in industrial applications is to obtain the performance of high speed, high efficiency, low cost, and low complexity. From the authors' point of view, the passive scheme and Principle I-based schemes (1A, 1B, and 1C) are suitable for small-scale energy storage applications, such as consumer electronics. For large-scale energy storage applications, such as EVs and ESPSs, modularization schemes are recommended.

Fig. 18 shows the suggested solution for LIB systems in EVs and ESPSs, which mainly includes two layers. Assuming that a LIB pack is derived into several modules, the first layer uses additional circuits to realize the balancing of cells (i.e., cell-level balancing). The balancing schemes without complex circuits and control strategies are recommended, such as the coupling-capacitor scheme [90], and the multiwinding transformer-based scheme [77], [78]. The second layer is used to realize the balancing of different modules (i.e., module-level balancing). In order to reduce the complexity and cost, existing interface converters are recommended to be utilized (i.e., 4C-based scheme), such as chargers and load converters.

V. ONLINE MONITORING TECHNIQUES

PE-based online monitoring techniques mainly refer to impedance measurement techniques for LIBs. In this section, the basics of LIB impedance are introduced. Then, the existing



Regions	Typical freq.	Typical physical/chemical meanings
Ohmic	>1000 Hz	• The resistance of current collectors, active material, electrolyte and separator
Mid-freq.	0.1–1000 Hz	• Associate with SEI, double layer capacity, and charge-transfer processes
Low-freq.	<0.1 Hz	• Diffusion processes at two electrodes

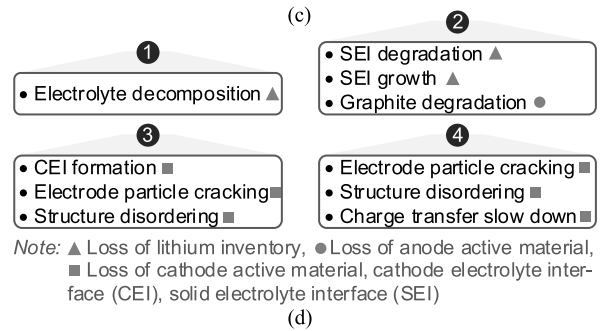


Fig. 19. Measurement method, typical spectrum, equivalent circuit, and degradation phenomena revealed from EIS. (a) Typical measurement method. (b) Typical EIS spectrum and equivalent circuit. (c) Typical physical and chemical meanings in EIS spectrum. (d) Typical degradation phenomena revealed in EIS.

PE-based schemes are discussed. Based on this, we give suggested solutions for industrial applications.

A. Basics of LIB Impedance

1) *Basic Principles*: Generally, the impedance is related to the internal physical and chemical processes of batteries, which can provide the condition information of batteries, such as SOH, SOC, and fault [190]. Fig. 19(a) shows a typical measurement scheme of a battery impedance [191].

Usually, a low-amplitude excitation signal $i_{bat}(f)$, including sinusoidal signal [192], square wave signal [193], PRS [194], etc., is injected into a battery, and the impedance $z(f)$ at a given frequency f is calculated as

$$z(f) = v_{bat}(f)/i_{bat}(f) \quad (2)$$

where $v_{bat}(f)$ represents the response signal at f .

An EIS of batteries can be obtained by measuring the impedance at different frequencies (i.e., broadband impedance). A typical EIS of LIBs is shown at the top of Fig. 19(b), where Z_{real} and Z_{im} , respectively, represent the real part and imaginary part of $z(f)$ in the complex domain, i.e.,

$$z(f) = Z_{real}(f) + j \cdot Z_{im}(f). \quad (3)$$

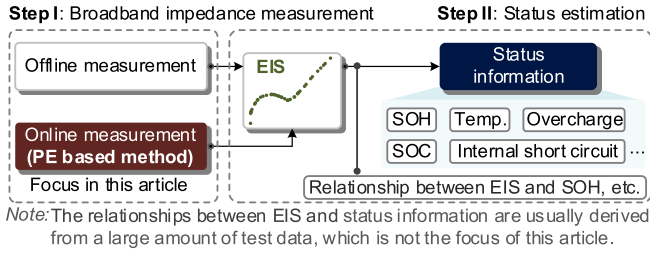


Fig. 20. State estimation procedure of LIBs.

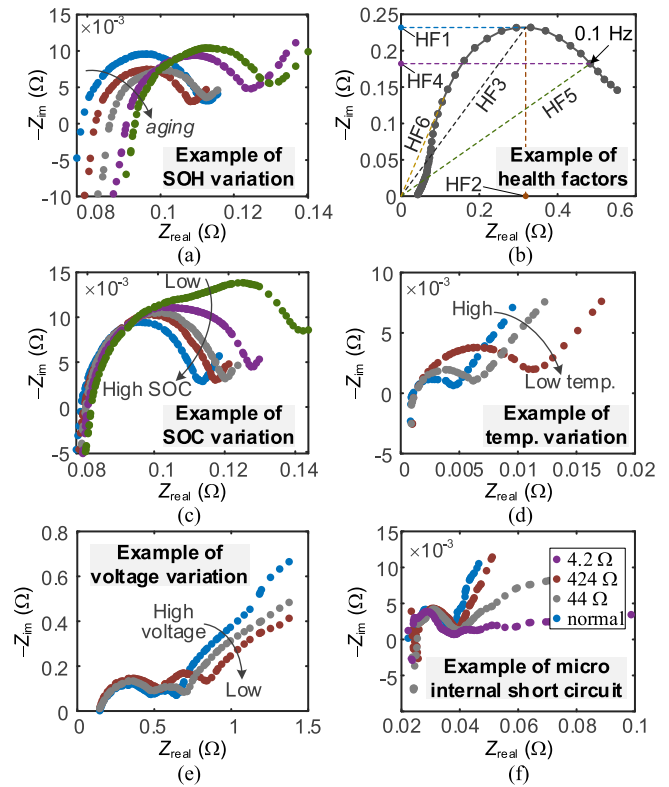
Generally, the EIS can be divided into three regions, i.e., ohmic region, midfrequency region, and low-frequency region. The corresponding frequency range and typical physical/chemical meanings are summarized in Fig. 19(c). It should be noted that the high-frequency inductive behavior usually does not provide useful information of batteries, which is ignored in Fig. 19(b). Moreover, considering different chemistries and aging mechanisms, the midfrequency region can be indicated as a singular arc or two arcs, as shown in the top of Fig. 19(b) [195], [196].

Furthermore, the bottom of Fig. 19(b) shows a typical equivalent circuit of batteries, composed of an ohmic resistance R_{ohm} , two ZARC elements Z_{arc1} and Z_{arc2} , and a Warburg element Z_w . Here, a ZARC element is composed of resistance and a CPE connected in parallel. The EIS can be used to characterize the degradation phenomena of Li-ion batteries. Typical degradation phenomena revealed in different frequency regions are summarized in Fig. 19(d).

2) *EIS-Based State Estimation*: Due to the EIS being related to the internal physical and chemical processes of batteries, it can be used to analyze the status information of batteries, such as SOH and SOC. Fig. 20 shows the typical state estimation procedure of batteries. It mainly includes two steps, i.e., BIM (Step I) and status estimation (Step II).

Step I mainly includes two categories. One is the offline measurement method, which depends on industrial instruments, including electrochemical workstations, spectrum analyzers, impedance analyzers, etc. Although the measurement accuracy of offline methods is relatively high, the tested battery must be dismantled from applications. It cannot realize the real-time BIM of batteries. Another is the online measurement method, which has attracted great attention. It utilizes the existing PE devices in applications to realize the BIM (i.e., PE-based method), which does not need additional expensive measurement devices. Moreover, it can realize real-time measurement facilitates for the application in practice, which will be detailed discussed in the next part.

Based on the measured EIS, some important status information of batteries can be estimated (i.e., Step II), such as SOH, SOC, temperature, and overcharge [197], [198], [199], [200], [201]. Fig. 21(a) shows an example of EIS variation with the degradation of an LIB. Generally, the health factors (HFs) of batteries can be extracted from EIS, as shown in the example in Fig. 21(b). Similarly, the EIS is changed when the SOC, temperature, etc. are charged. Fig. 21(c)–(f) show the effect of



Note: the peak value of the imaginary part (HF1), the real part at the peak of the imaginary part (HF2), the amplitude at the peak of the imaginary part (HF3), the imaginary part (HF4) and the amplitude (HF5) at 0.1 Hz, the phase peak value (HF6)

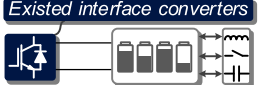

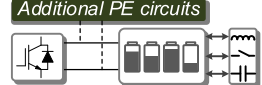
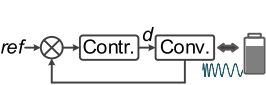
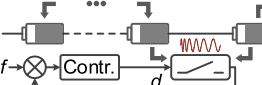
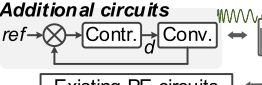

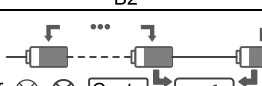
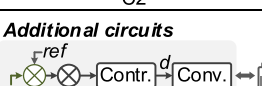
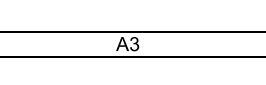
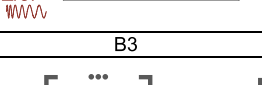
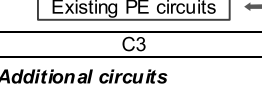
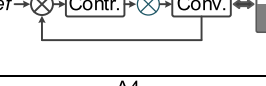
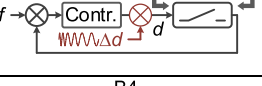
Fig. 21. Example of EIS based status estimation of LIBs. (a) Example of SOH variation [197]. (b) Example of HFs [198]. (c) Example of SOC variation [197]. (d) Example of temperature variation [199]. (e) Example of voltage variation [200]. (f) Example of micro internal short circuit [201].

SOC, temperature, overcharge, and internal micro short circuit on EIS. Moreover, the EIS can also be used to identify the degradation patterns and internal materials of batteries. Notice that the relationships between EIS and state information (e.g., SOH, SOC, temperature, etc.) of batteries vary with different kinds of batteries. There are no unit criteria to judge the status of batteries. Usually, a large amount of test data (e.g., open-access dataset—Panasonic 18650PF Li-ion battery data [202], [203]) and some state-of-the-art algorithms (e.g., machine learning algorithms [204], [205]) are used to obtain the relationship between EIS and battery status, which is not in the focus of this article.

B. Derivation of PE-Based BIM Methods

Referring to Fig. 19(a), the key to online BIM is to obtain excitation signals and measure the response of batteries at different frequencies. In PE-based schemes, the wideband excitation signals are generated by PE components or systems instead of industrial instruments, which can be implemented real-online or quasi-online (monitoring under special conditions, such as shutdown). From implementation perspective, the PE-based methods can be divided into three types. One is to realize the BIM using the existing interface converters (Type A), such as battery

TABLE V
 DERIVATION OF PE-BASED BIM METHODS

	Type A	Type B	Type C
			
Principle I Existed broadband signal during normal operation	A1 	B1 	C1 
Principle II Reference point perturbation during normal operation	A2 	B2 	C2 
Principle III Duty cycle perturbation during normal operation	A3 	B3 	C3 
Principle IV Excitation signal generated outside of normal operation	A4 	B4 	C4 Not suitable

d—duty cycle, *ref*—reference voltage and/or current, Δd —duty cycle perturbation, Δref —reference point perturbation

chargers, and load converters. Another is to use the existing cell balancing circuits (Type B). Moreover, additional PE circuits can be designed to realize the BIM (Type C).

Furthermore, four main categories of principles are generally used to generate the excitation signals for BIM. One is based on self-generated multifrequency signals of PE circuits during normal operation periods, such as ripples and harmonics (Principle I). Another is to add perturbation signals on reference points (Principle II) and duty cycles (Principle III) when converters normally operate, in order to generate broadband excitation voltage/current on batteries. Moreover, it is also feasible to control the existing PE circuits used as an excitation source (Principle IV). Here, the PE circuits are out of normal operation.

Based on the three types of circuits and four categories of signal generation principles, the PE-Based BIM methods can be derived, as shown in Table V. There exist 11 derived methods.

1) *Derived Methods Based on Type A*: The methods A1–A4 are based on the existing interface circuits, which are illustrated using the examples in Figs. 22(a)–(d).

Method A1 uses an existing multifrequency signal in systems to estimate BIM, a typical implementation example is shown in Fig. 22(a) [206]. Here, a battery pack is used to feed an ASD system, which is common in EV drive systems. Generally, the main traction current i_{bat} was frequently variation due to driver or controller response, which causes the battery voltage v_{bat} fluctuates. Referring to (2), the battery impedance at different frequencies can be calculated using the time–frequency analysis algorithms, such as FFT, then to obtain the EIS.

Different from method A1 which utilizes the existing signal characteristics, methods A2 and A3 generate the excitation signals by adding perturbation to the control of power converters. Fig. 22(b) shows an implementation example of method A2 [207]. Here, a small ac perturbation signal $V_{ref, ac}$ is added to the steady-state reference point $V_{ref, dc}$, which results in generating a perturbation superimposed over the battery voltage v_{bat} and battery current i_{bat} . Similarly, the broadband excitation signal on v_{bat} and i_{bat} can be generated by adding a perturbation to the steady-state duty cycle (method A3), as shown in the example in Fig. 22(c) [208]. Notice that the types of perturbation signals in Fig. 22(b) and (c) are different. Generally, the sinusoidal, square wave, and PRS signals are feasible. Moreover, the perturbation signal is added to the voltage reference in Fig. 22(b), it can also be added to the current reference.

Methods A1–A3 generate the excitation signal during the normal operation period of interface converters. Besides, the converters can be designed as a special excitation source, which operates out of normal operation (A4). Fig. 22(d) shows an implementation example of method A4 [209]. Here, a DAB converter is designed to operate in an ac mode to generate ac disturbance on batteries, which is different from its normal operation status (dc mode).

2) *Derived Methods Based on Type B*: Methods B1–B4 are based on the existing cell balance circuits, which are derived from Principles I to IV, respectively.

Method B1 utilizes the self-generated excitation signal of cell balancing circuits to realize the BIM. Fig. 22(e) shows an

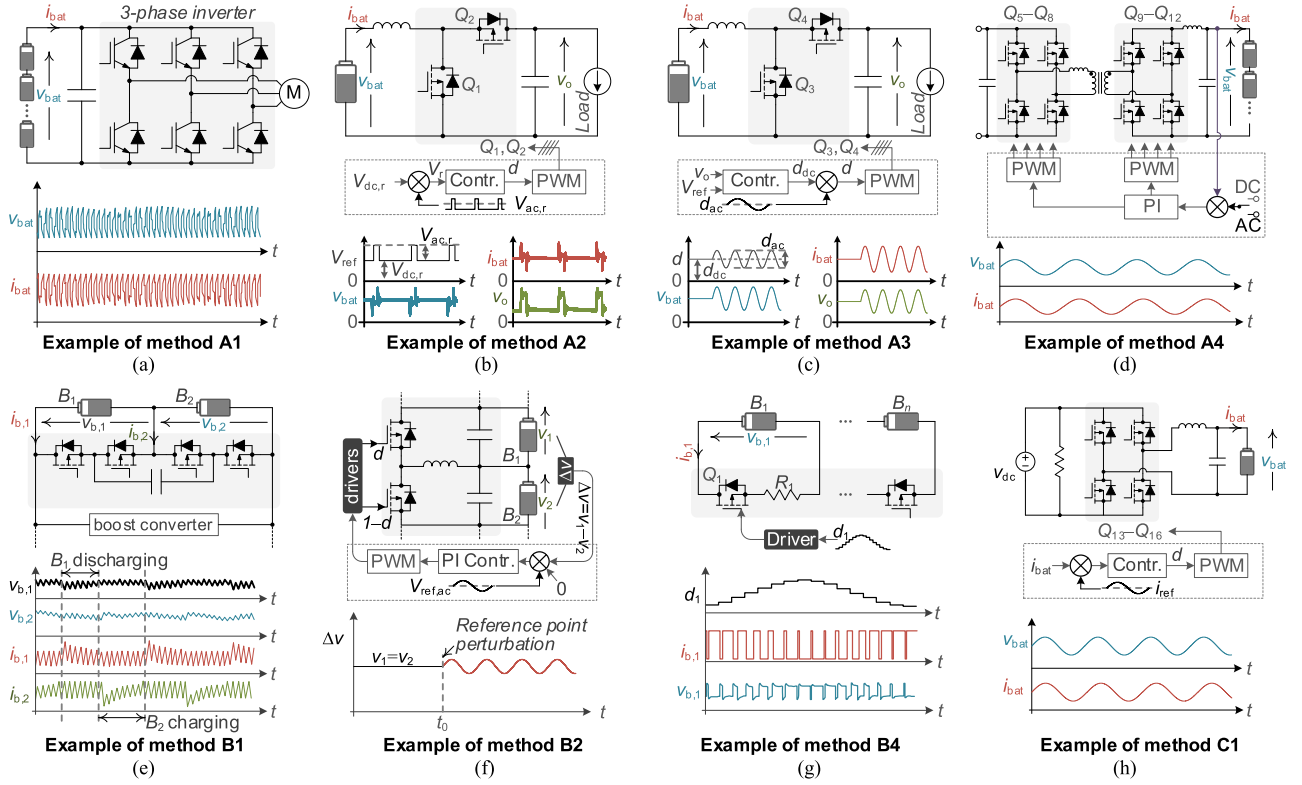


Fig. 22. Implementation examples of derived methods. (a) Example of method A1 [206]. (b) Example of method A2 [207]. (c) Example of method A3 [208]. (d) Example of method A4 [209]. (e) Example of method B1 [210]. (f) Example of method B2 [211]. (g) Example of method B4 [213]. (h) Example of method C1 [214].

implementation example of method B1 [210]. Here, a switched capacitor balancing circuit is used to realize the cell balancing and the perturbation signal generation. Usually, the perturbation signal on batteries is generated due to the charging or discharging of unbalanced batteries, as shown at the bottom of Fig. 22(e).

Similar to methods A2 and A3, methods B2 and B3 generate the excitation signals by adding a perturbation to the control of balancing circuits. Fig. 22(f) shows an implementation example of method B2 [211]. Here, a switched inductor ladder converter is used, and the voltage difference Δv is chosen as a control variable to realize the voltage balancing of different cells. Usually, Δv is controlled as 0 in a nominal balancing mode. Also, an ac perturbation is added to the reference point in BIM mode to generate the excitation on batteries. Similarly, the implementation method B3 [212] is similar to those in B2 and A3, which are not shown in Fig. 22.

Fig. 22(g) shows the implementation example of method B4 [213]. Here, the balancing function is not enabled. A perturbation signal is added to the control of balancing circuits, in order to generate the broadband elicitation signals on batteries.

3) *Derived Methods Based on Type C*: Referring to Table V, there exist three derived methods based on additional circuits. Here, the PE circuits are specifically designed for BIM. Fig. 22(h) shows an implementation example of method C1 [214]. Here, an inverter is used to generate the excitation on batteries. Besides, additional circuits can also generate broadband perturbation through control (i.e., methods C2 and C3), which are similar to methods A2, A3, B2, and B3.

C. Application of PE-Based BIM Methods

1) Implementation of BIM Based on Interface Converters:

a) *Based on method A1*: As discussed in Fig. 22(a), the multifrequency signal in ASD can be used to realize the BIM of batteries [206], which is based on method A1. Similarly, the same method is used to measure the broadband impedance of fuel cells [215]. It should be noted that the PE circuits connected with batteries in [206] and [215] are voltage-source inverters. Usually, there exist multifrequency band signals on voltage and current (e.g., fundamental, harmonic, and ripples), which can be used to analyze the battery impedance at different frequencies. Different from that, Bayati et al. [216] proposed a battery charger based on SRC charging–discharging methods, as shown in Fig. 23(a). Here, the dc stage consists of two parts. The left one generates dc current i_{dc} , which reference is $i_{dc,r} = I_0$. The right one generates ac current, whose reference is $i_{ac,r} = I_1 \cos(2\pi f_c t)$. I_0 and I_1 are constant amplitudes, and f_c represents the frequency of ac current. Notice that the voltage loop of dc stage is not shown in Fig. 23(a). The dc and ac parts work act as independent current sources until the battery reaches maximum voltage. Then, one part works as a voltage source, and the other one is turned OFF.

b) *Based on methods A2*: Fig. 22(b) shows an implementation example of method A2 [207]. Here, a pulse waveform perturbation $V_{ac,r}$ is added to the voltage reference $V_{dc,r}$ of an interface converter, i.e., buck–boost converter, which results in perturbations appearing on the battery voltage and current.

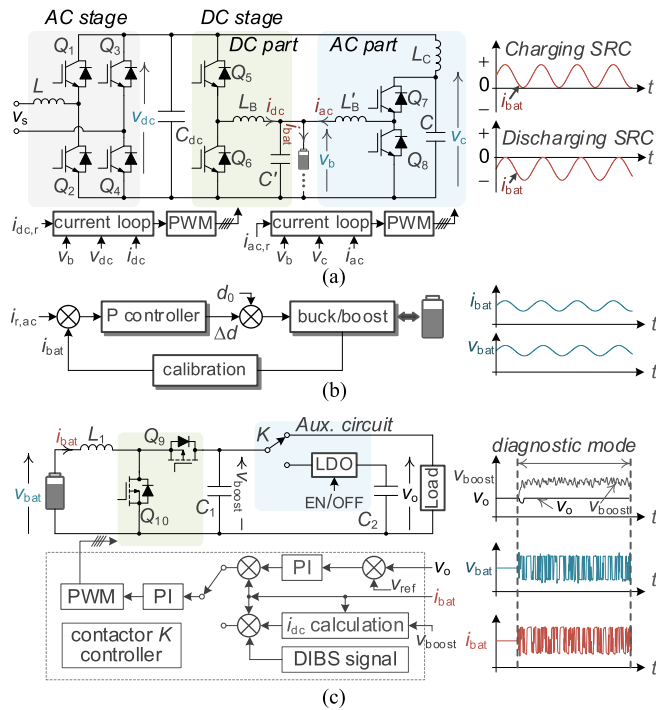


Fig. 23. A4-based schemes. (a) SRC charging–discharging schemes [216]. (b) Modulated current reference during diagnosis modes [232]. (c) Dual-mode circuit-based scheme [233].

By applying an FFT analysis, the broadband impedance can be estimated using (2). Based on [207], the same authors further presented a multifrequency step perturbation scheme [217], which implementation is similar to that in [207]. However, the perturbation waveform is slightly different. Besides the square waveform perturbation, the triangular waveform [218], and multisine signal [219] can also be used for BIM.

Notice that the above schemes' perturbation signals are added into voltage loops. The interface converters are basic buck/boost converters. Generally, the perturbation can also be added to current loops [219], [220], [221], [222], [223], and other types of interface converters are also feasible, such as full-bridge–phase shift–zero-voltage switching (FB-PS-ZVS) converters [222] and interleaved dc/dc converters [223].

c) *Based on method A3:* Generally, method A3 is similar to method A2, but the perturbation signal is added in the duty cycle, as shown in Fig. 22(c). Referring to Fig. 22(c), a sinusoidal perturbation is added to the steady-state duty cycle of a dc/dc converter [208]. Similarly, the square wave [214], multisine [225], [226], and WN [227] signals can also be used, whose implementations are similar to that in Fig. 22(c).

d) *Based on methods A4:* The interface converters operate in normal mode in the abovementioned schemes. Unlike that, the converters operate in open-loop or special operation mode in A4-based schemes.

In [228], a sinusoidal perturbation was added to the open-loop duty cycle of interface converters to generate the perturbation signals on batteries' voltage and current. Here, the interface converters are operated in an open-loop mode. Considering that

the open-loop mode is not popular in actual applications, Choi et al. [229], [230] add a sinusoidal perturbation voltage to the reference voltage of converters after the charge of batteries, i.e., relaxation time. Here, the output current of converters is close to 0, the converters work out of normal operation.

Besides, a dual-mode controlled converter has been widely used for BIM, which includes a normal mode and a diagnosis mode. Referring to the example shown in Fig. 22(d), the current reference is set as sinusoidal when the converter works in diagnostic mode [209]. Although it realizes the BIM without adding dc bias on the excitation current, the converter operates away from the normal working mode (i.e., dc mode). Different from that, the operating points of converters are designed to be close to the normal working statuses in [231]. In [231], an open-loop ac signal superimposed on a dc bias was applied to the PWM modulator of dc/dc converters when the converter operates in diagnosis mode, which results in fuel cells' voltage and current fluctuation. Similarly, the voltage or current reference can be modulated during diagnosis modes [232], as shown in Fig. 23(b). Based on the sampled current i_{bat} and an alternating current reference $i_{r,ac}$, a proportional controller is used to generate the duty cycle perturbation Δd , in order to generate the perturbation on batteries.

Furthermore, a dual-mode circuit-based scheme is used to realize the BIM [233], as shown in Fig. 23(c). In diagnostic mode, the converter output is switched and begins supplying an LDO regulator. Simultaneously, the operating point is instead operating by a DIBS signal superposition dc current. Then, the converter operates near the normal operating point. The corresponding excitation signals on the batteries' voltage and current are shown in the right of Fig. 23(c).

2) *Implementation of BIM Based on Balancing Circuits and Additional Converters:* Although a balancing circuit can be used for BIM, it is not widely used in actual applications. Only a few kinds of literature report the balancing circuits-based BIM schemes. The typical implementation schemes of methods B1 [210], B3 [212], and B4 [213] are shown in Fig. 22.

For method B2, besides the discussed schemes in Fig. 22(f), Gong et al. [234], [235] proposed a linear MOSFET scheme for cell selection-based balancing systems (i.e., scheme 4C in Section IV), as shown in the top of Fig. 24(a). Assuming that one cell is selected to feed energy to loads, the equivalent circuit is shown at the bottom of Fig. 24(a). Here, the cell selection unit equals a MOSFET Q_{shunt} , and the perturbation signal is injected into the system by adjusting the reference of driving voltage v_{pwm} . Notice that the SuperC (C_{sup}) unit reduces the input ripple of dc/dc converters during the measuring stage. The detailed waveforms are shown in Fig. 24(b). Koseoglou et al. [236] proposed a similar scheme, as shown in Fig. 24(c). Here, the parallel-connected MOSFET is controlled as a controllable current source. The perturbation current $i_{EIS,n}$ of the n th cell is added to the battery current $i_{EQ,n}$ to generate perturbation on the battery cell.

Similar to method B, only a few kinds of scheme C are presented in actual applications. For example, in [214] and [237], an additional dc–ac converter is used to generate a sinusoidal disturbance signal on batteries (i.e., method C1), as shown in

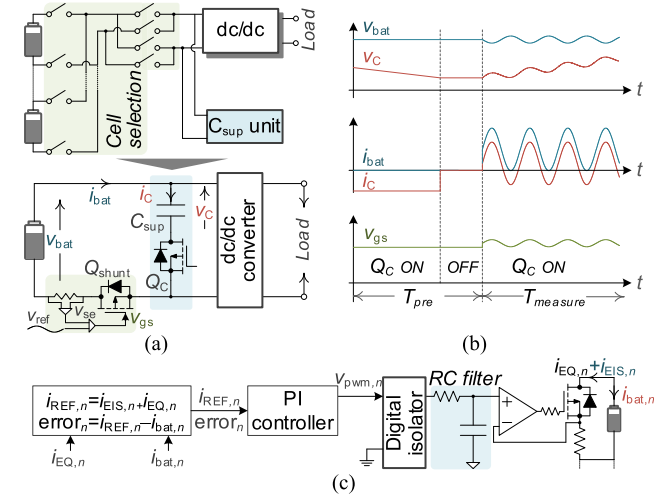


Fig. 24. Balancing circuit-based BIM schemes. (a) Equivalent circuit of cell selection-based balancing systems [234], [235]. (b) BIM waveforms [234], [235]. (c) Dissipative balancing circuit-based scheme [236].

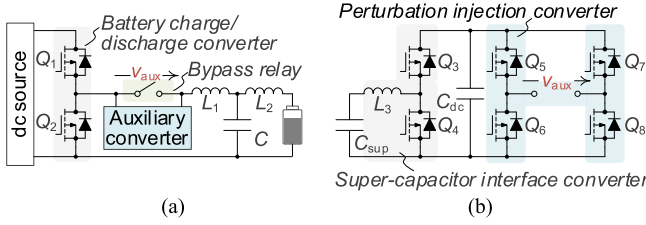


Fig. 25. Auxiliary circuit-based BIM schemes [238]. (a) Schematic diagram. (b) Auxiliary circuit.

Fig. 22(h). Different from that, Dam and John [238] proposed an auxiliary circuit-based scheme, as shown in Fig. 25(a).

An auxiliary converter and a bypass relay are integrated with a conventional charge–discharge converter. The schematic diagram of the auxiliary converter is shown in Fig. 25(b), which includes a PIC and an SIC. The relay is kept open during the BIM stage, and the auxiliary converter is enabled. Then, the SuperC discharges through the SIC, generating an ac perturbation signal from the PIC.

D. Single-Point Impedance-Based Monitoring Techniques

The aforementioned schemes in Sections V-C–V-D are designed for BIM. Besides that, single-point impedance (especially high-frequency impedance) can also be used for the condition monitoring of batteries.

Moral et al. [239] demonstrated that the internal resistance R_{bat} of batteries at a given excitation frequency is approximately linearly correlated with its temperature, as shown in Fig. 26(a). Based on this, a switching harmonics-based battery temperature estimation scheme was presented for buck–boost converter-based battery systems [cf., Fig. 22(b)]. Referring to Fig. 26(b), resistance $R_{bat,n}$ of batteries at the frequency of n th harmonic is obtained based on the calculation of impedance $Z_{bat,n}$. Then, temperature T_{bat} is estimated using the linear

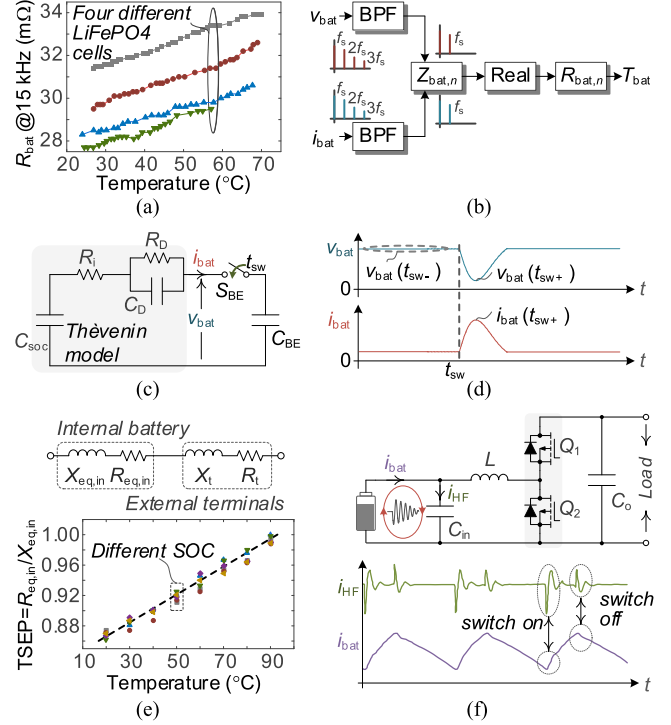


Fig. 26. Single-point impedance-based monitoring schemes. (a) Battery resistance (@ 15 kHz) versus battery temperature [239]. (b) Harmonic-based battery temperature estimation procedure [239]. (c) Equivalent circuit of a switched-capacitor balancing system [240]. (d) Voltage and current waveforms of batteries in an SC system during a switching instant [240]. (e) TSEP characteristic of a battery at an ultra-high frequency [244]. (f) PWM switching oscillation in a battery system [244].

relationship, i.e.,

$$T_{bat} = (R_{bat,n} - R_{bat,n,0}) / (R_{bat,n,0} \alpha_{bat}) + T_0 \quad (4)$$

where $R_{bat,n,0}$ is the measured resistance of $R_{bat,n}$ at the room temperature T_0 and α_{bat} is the temperature coefficient. Generally, $R_{bat,n,0}$ and α_{bat} can be measured during a commissioning process.

Based on (4), Moral et al. [240] further proposed an SC balancing circuit-based temperature monitoring scheme. Fig. 26(c) shows the equivalent circuit of an SC system, where a Thèvenin model represents the battery. R_i represents the total internal resistance of batteries, R_D and C_D are the dynamic performance parameters, C_{SOC} represents the battery capacity, C_{BE} and S_{BE} represent the capacitor and power switch in the SC circuit, respectively, and t_{sw} is the switching instant of S_{BE} . As discussed in [241], [242], and [243], the parameters of an RC circuit can be identified based on the transient response of systems. Similarly, the resistance R_i is calculated as

$$R_i = |v_{bat}(t_{sw-}) - v_{bat}(t_{sw+})| / i_{bat}(t_{sw+}) \quad (5)$$

where $v_{bat}(t_{sw-})$ is the voltage before t_{sw} . $v_{bat}(t_{sw+})$ and $i_{bat}(t_{sw+})$ represent the voltage and current after t_{sw} , respectively.

Similarly, Xiang et al. [244] demonstrated that a battery is equivalent to a series RL circuit at ultra-high frequencies (i.e., 10 kHz–1 MHz), as shown in the top of Fig. 26(e). $X_{eq,in}$ and $R_{eq,in}$ represent the equivalent reactance and resistance

TABLE VI
TYPICAL PATENTS ABOUT ONLINE EIS MEASUREMENT

Scheme	Description	Applicant
Amp.	a pre-amplifier consisting of operation amplifiers is used	Battelle Energy Alliance LLC [246]
A1	pulsed charging for EIS measurement [similar to the sinusoidal charging scheme shown in Fig. 21(a)]	Gbatteries Energy Canada Inc. [247]
A2 or A3	an excitation generation unit is designed for ac/dc or dc/dc converters [similar to A2 and A3 in Table V]	Lithium Balance A/S [248]
A2	ac perturbation is added to the voltage loop of dc/dc converters [similar to the scheme shown in Fig. 20(b)]	Foundation of University-Industry Cooperation [249]
A2	ac perturbation is added to the current loop of dc/dc converters [similar to the scheme shown in Fig. 20(b)]	Bloom Energy Corporation [250]
C3	special designed switching circuits for EIS measurement	Harbin Institute of Technology [251]

of the internal battery, respectively, and X_t and R_t represent the equivalent reactance and resistance of external terminals, respectively. It is found that the battery temperature is linearly related to a thermal-sensitive electric parameter (i.e., $TSEP = R_{eq,in}/X_{eq,in}$) at ultra-high frequencies, as shown in the bottom of Fig. 26(e). Based on this, Xiang et al. proposed a PWM switching oscillations-based scheme for a buck-boost system, as shown in Fig. 26(f). The battery temperature can be estimated by analyzing the high-frequency switching oscillations in the battery-capacitor loop.

E. Typical Commercial and Industrial Solutions for EIS Measurement

Recently, some commercial ICs [245] and patent solutions [246] have been released for EIS measurement. However, they are offline schemes, which are similar to that of industrial instruments. Considering this issue, some patent solutions for online EIS measurement have been presented [247], [248], [249], [251], as summarized in Table VI.

It can be seen that the implementations of these patent solutions comply with the derivation principles in Table V, and A2- and A3-based schemes are popular. For the solutions reported in [247], [248], [249], and [250], similar schemes can be found in Section V-B, which are summarized in Table VI. For the solution reported in [251], the structure of the switching circuit is similar to the CSN in Fig. 12(a). However, the functions are different.

F. Discussion of Online Monitoring Techniques

1) *Comparison and Remarks:* As discussed above, PE-based online monitoring mainly refers to online impedance measurement, including broadband and single-point impedance measurements.

Table VII summarizes the PE-based BIM schemes for LIB systems, where ΔI_m , I_{dc} , ΔV_m , V_{dc} , $\Delta V_m/V_{dc}$, and N_f represent the peak-to-peak value of maximum perturbation current, dc current, nominal battery voltage, ratio of ΔV_m and V_{dc} , number of frequency components. Considering there is a lack of detailed data for patent solutions, Table VII has not summarized them. Brief remarks are given as follows.

- 1) A1-based scheme utilizes the existing ripples, harmonics, and noise to obtain the EIS, which is easily implemented. However, the amplitude and frequency of signals used for EIS are limited by the mission profile and type of converters. The LIB systems with abundant frequency information are suitable, such as motor drives [206] and inverters [215]. Otherwise, a special operation mode of interface converters should be designed [216].
- 2) A2- and A3-based schemes add perturbation to the reference point and duty cycle of interface converters, which are very popular. In [207], [208], [217], [218], [222], [223], and [224], single-frequency sinusoidal, square wave, and triangular perturbation signals are used. Although they can realize the BIM measurement, they are relatively complex by adjusting the perturbation frequency every time. Considering this issue, perturbation signals with multifrequency information are employed in [219], [220], [221], and [227]. However, the relatively small amplitude of the perturbation signal is the main challenge. Additional instrumentation with offset clipping and amplifying circuits is usually required to improve the measurement precision [221].
- 3) Similar to A2- and A3-based schemes, A4-based schemes utilize single-frequency and multifrequency perturbation to realize the BIM. However, the interface converters operate under abnormal conditions, such as open-loop mode [228] and diagnostic mode [209], [231], [232], [233], which reduce these schemes' applicability.
- 4) In [210], the operating waveforms of SC circuits are used to obtain EIS (B1-based scheme). However, it is difficult to realize in actual applications, due to the balancing process being relatively slow and its duration being very long.
- 5) In [211] and [212], additional perturbations are injected into the reference point (B2-based scheme) and controller (B3-based scheme) of balancing circuits, which are similar to those in schemes A2 and A3. In [234], [235], and [236], the MOSFETs in the balancing circuits are linearly controlled during balancing processes, in order to form disturbance in voltage and current. However, the amplitude of perturbation is relatively small, which increases the difficulty of the sampling circuits. Moreover, specially designed drivers are required to realize the linear control of MOSFETs.
- 6) In [213], variable duty cycle signals are used to drive the MOSFETs of balancing circuits (B4-based scheme), in order to form disturbance on battery voltage and current. However, the system operates in an open loop. The applicability is relatively weak.
- 7) Although it is feasible to design a BIM scheme based on additional PE circuits (C1-, C2-, and C3-based schemes), the cost and complexity are relatively high. Few pieces of literature focus on this point [214].

Generally, the single-point impedance-based monitoring techniques [239], [240] are simpler than that of BIM schemes. However, relatively little information on LIBs is reflected by single-point impedance. It should be considered in actual applications.

TABLE VII
SUMMARY OF PE-BASED BIM SCHEMES

	Principle	Converter/ circuit (status)	Signal type	Battery type	Cell parameters	Time	Algo.	$\Delta I_m, I_{dc}$	$\Delta V_m, V_{dc}$	$\frac{\Delta V_m}{V_{dc}}$	Freq. range (N_f)
A1	[206], [215]: Utilizing the noises of 3-phase motor drives [206] and inverters [215]	3-ph inverter (normal operation)	noise [204]	ANR 26650	2.3 Ah, 3.3 V	1 s	N/A	0.13 A, 0.15 A	2 mV, 3.3 V	6.06×10^{-4}	1 Hz–1 kHz (N/A)
	[216]: Designing an SRC charging/discharging converter	specialty designed charger	noise [213]	unavail. (FC)	N/A	20 ms	FFT	1.5 A, 11.5A	8 mV, 0.66 V	0.012	1Hz–4 kHz (N/A)
A2	[207], [217], [218]: Adding step-function [207], [217] and triangular [218] perturbation to voltage loop	boost [207], [217] (in discharge phase)	SF square wave	Tenergy 18650	2.6 Ah, 3.7 V	N/A	FFT,D FT	2 A, 0.52 A	0.2 V, 3.7 V	0.054	200 Hz–1.6 kHz (9)
	[219], [220], [221], [222], [223]: Adding multisine [219], [220], and sinusoidal [221], [222], [223] perturbation to current loop	boost [218] (in discharge phase)	SF triangular	unavail. (FC)	N/A	N/A	FFT	1 A, 2.4 A	2 V, 21 V	0.095	1 Hz–1 kHz (4)
		buck [219] (in charge phase)	Multisine	ICR 18650	2.6 Ah, 3.63 V	20 s	FFT	15 mA, 0.5A	0.02 V, 3.63 V	5.5×10^{-3}	100 Hz–800 Hz (8)
		boost [220] (in discharge phase)	Multisine	lead-acid	7 Ah, 12 V	50 s	FFT	0.05 A, 3A	3 mV, 12 V	2.5×10^{-4}	98 mHz–6.25 Hz (7)
		buck [221] (in charge phase)	chirp wave	Valence 12-XP	40 Ah, 12 V	200 s	FFT	5 A, 10 A	53 mV, 13.6 V	3.9×10^{-3}	0.1 Hz–5 kHz (57)
		FB-PS-ZVS [222] (in charge phase)	SF sine	N/A	N/A	N/A	DQ	2 A, 5 A	20 mV, 13.7 V	1.45×10^{-3}	0.1 Hz–100 Hz (14)
n-ph boost [223] (in discharge phase)	SF sine	unavail. (FC)	N/A	N/A	N/A	4 A, 8 A	1.4 V, +45 V	0.03	1 Hz–2 kHz (11)		
A3	[208], [224], [225], [226], [227]: Adding sinusoidal [208], square wave [224], and WN [227] perturbation to duty cycle	boost [208] (in discharge phase)	SF sine	Tenergy 18650	2.6 Ah, 3.7 V	N/A	N/A	0.75 A, 1.3A	48.9 mV, 3.7 V	0.013	100 Hz–10 kHz (7)
	[228]: Open-loop operation using sinusoidal duty cycle	boost [224] (in discharge phase)	SF square wave	Tenergy 18650	2.6 Ah, 3.7 V	N/A	N/A	1.2 A, 1.3 A	120 mV, 3.7 V	0.032	100 Hz–900 Hz (5)
		boost [227] (in discharge phase)	WN noise	lead-acid	7 Ah, 12 V	N/A	CCT	0.01 A, N/A	0.8 mV, N/A	–	0.3052 Hz–20.4 kHz (N/A)
A4	[228]: Open-loop operation using sinusoidal duty cycle	3-ph buck (open loop)	chirp wave	lead-acid	9 Ah, 12 V	100 s	N/A	0.1 A, N/A	246 mV, 240 V	1×10^{-3}	100 mHz–100 Hz (28)
	[229], [230]: Sinusoidal excitation in relaxation time	buck [229] (after charging phase)	chirp wave	lead-acid	40 Ah, 12 V	200 s	DLIA	1 A, 0 A	N/A, 13.4 V	–	0.1 Hz–1 kHz (N/A)
	[209]: DC converter operates in ac mode	DAB (ac mode)	SF sine	hybrid pack	338.5 V	N/A	N/A	1A, N/A	N/A, N/A	–	0.1 Hz–500 Hz (27)
	[231]: Using sinusoidal duty cycle in diagnostic mode	boost (close to operation point)	Multi sine	unavail. (FC)	N/A	1.2 s	FFT	0.5 A, 3 A	0.03 V, 0.6 V	0.05	0.01 Hz–10 kHz (1024)
	[232]: Using aux. control in diagnostic mode	boost (close to operation point)	SF sine	VLRA AGM	100 Ah, 12 V	N/A	N/A	1 A, 2 A	0.1 V, 12.5 V	8×10^{-3}	0.1 Hz–1 kHz (N/A)
	[233]: Using aux. circuit and control in diagnostic mode	buck (close to operation point)	DIBS	18650	1.2 Ah, 3.7 V	0.8 s	N/A	0.2 A, 0.3 A	25 mV, 3.7 V	6.8×10^{-3}	0.1 Hz–1 kHz (N/A)
B1	[210]: Utilizing the operating waveforms of SC circuit	SC (balancing phase)	ripple	A123	2.5 Ah, 3.2 V	N/A	N/A	2.44 A, 1.59 A	17.7 mV, 86 mV	0.21	1 Hz–1 kHz (N/A)
B2	[211]: Adding perturbation on the reference of SI controller	SI (balancing phase)	SF sine	18650	3.4 Ah, 3.65 V	N/A	LSRA	N/A, N/A	0.03 V, N/A	–	25 mHz–7.66 kHz (4)
	[234], [235]: Linear control of cell selection MOSFETS	CSN (balancing phase)	SF sine	LiNiMn CoO2	N/A	9 s	N/A	30 A, 6 A	N/A, N/A	–	2 Hz–2 kHz (N/A)
	[236]: Linear control of dissipative MOSFETS	mosfets (balancing phase)	chirp sine	LPB042 126H	7.4 Ah, 3.7 V	5.4 min	FFT	1.95 A, 3.5 A	6.5 mV, 3.7–4.2 V	1.8×10^{-3}	20 mHz–2 kHz (46)
B3	[212]: Adding perturbation on the controller of SC	SC (balancing phase)	chirp-like sine	18650	3.4 Ah, 3.7 V	N/A	N/A	0.25 A, 0.1 A	0.06 V, 3.76 V	0.016	15 Hz–20 kHz (15)
B4	[213]: Imposing perturbation on dissipative MOSFETS	dissipative circuit (out of normal operation)	square wave	ICR186 50	N/A	2 ms	FFT	0.05 A, N/A	0.2 V, N/A	–	500 Hz–8 kHz (60)
C1	[214], [237]: A dc/ac inverter is used for current injection	special designed inverter for BIM	SF sine	N/A	N/A	N/A	N/A	10 A, N/A	50 mV, 13.18 V	3.79×10^{-3}	N/A

Notes: peak-to-peak value of maximum perturbation current (ΔI_m), dc current (I_{dc}), nominal battery voltage (V_{dc}), peak-to-peak value of maximum perturbation voltage (ΔV_m), lowest measurement frequency (f_l), highest measurement frequency (f_h), number of frequency components (N_f), fuel cell (FC), sinusoidal ripple current (SRC), single-frequency (SF), fast Fourier transform (FFT), discrete Fourier transform (DFT), digital lock-in amplifier (DLIA), white noise (WN), cross-correlation technique (CCT), discrete-interval binary sequence (DIBS), full-bridge-phase shift-zero-voltage switching (FB-PS-ZVS), switched capacitor (SC), switched inductor (SI), least-square regression analysis (LSRA), cell selection network (CSN).

2) *Suggested Feasible Solutions*: As discussed above, PE-based monitoring schemes mainly refer to online impedance measurement. From complexity perspective, single-point impedance-based monitoring schemes [240], [244] are recommended in actual applications, such as EVs and ESPSs. However, the relationship between single-point impedance and the health status of LIBs should be further investigated.

For BIM, suggested solutions are given in the following.

- 1) Considering abundant frequency information (including ripple, harmonic, and loading profile) in LIBs-feed ASD systems, A1-based schemes are recommended in these applications, such as EVs.
- 2) For the applications without abundant frequency information, such as ESPSs, specially designed chargers are

recommended to realize the functions of charging and BIM. Moreover, A2- and A3-based schemes are also recommended. Here, multisine and chirp waveforms are suggested for perturbation injection, because multifrequency perturbation signal can be sampled during one time of measurement.

VI. LIFETIME IMPROVEMENT TECHNIQUES

Usually, LIBs experience variable loading profiles with different frequencies in actual applications, which mainly include high-frequency ripple caused by PEs and low-frequency fluctuation caused by charging and discharging. The effects of ripples and charging/discharging strategies on the lifetime of batteries,

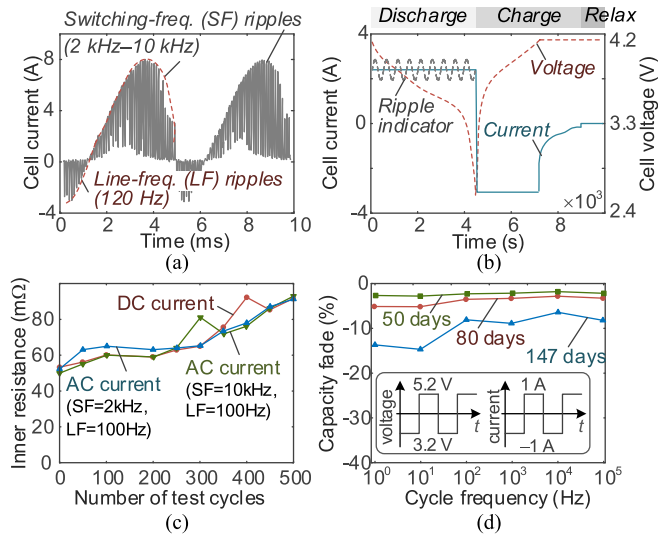


Fig. 27. Effect of an ac ripple on the degradation of batteries. (a) Current ripple of one-battery cell in a cascaded H-bridge system [257]. (b) Current profile of aging experiments in [257]. (c) Inner resistance versus aging time for 18650BD cells [257]. (d) Capacity degradation versus cycle frequency for UF103450P cells [258].

as well as the lifetime improvement techniques are discussed in this section.

A. Effect of Current Ripples on LIB's Lifetime

Generally, the lifetime of batteries is affected by the rms value of current [252]. Many efforts have demonstrated that the high-frequency (greater than 10 Hz) ripples [253], [254], [255] and harmonics [256] caused by PEs almost have no adverse influence on the degradation of LIBs when the rms values of ripples/harmonics equal to a dc current.

However, the ac current at a low frequency (lower than 10 Hz) would accelerate the degradation of batteries [252]. Taking an EV-used cascaded H-bridge system as an example, Fig. 27(a) shows the current ripple of one battery cell [257]. In order to verify the effects of ripples on the degradation of batteries, charge/discharge experiments are taken for Panasonic NCR 18650BD cells. Fig. 27(b) shows the profile of the aging experiment in [257], where the ripple indicator represents the ac current shown in Fig. 27(a). In experiments, all of the tested cells have the same profile during the charging and relaxation stages. However, the tested waveforms during discharging stage are different. Fig. 27(c) shows the aging results for three cells with dc current and ac current stresses respectively, where the inner resistance represents the 200-ms dc resistance at 80% SOC. It can be seen that there is no effect of the switching-frequency ripples on the degradation of batteries. Furthermore, taking square-wave stress as an example, Fig. 27(d) shows the capacity degradation trend versus cycle frequency, where the type of battery is Sanyo UF103450P [258]. It is found that the capacity degradation ratios are significant at frequencies below 10 Hz. The ac ripples have almost no adverse effect on batteries when their frequencies are higher than 100 Hz. Therefore, it

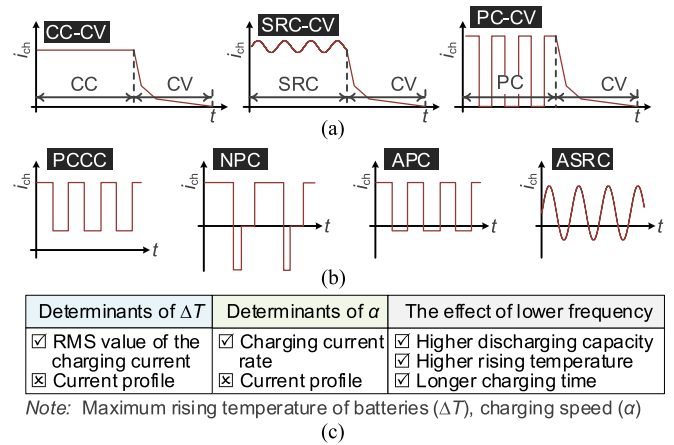


Fig. 28. Different current modes and main conclusions from charging experiments. (a) CC-CV, SRC, and PC-CV modes [266]. (b) PCCC, NPC, APC, and ASRC modes [267]. (c) Main conclusions from charging experiments.

should avoid low frequencies in the design of PEs for battery systems.

B. Effect of Charging Strategies on LIB's Lifetime and Optimization Techniques

1) *Effect of Charging Strategies on Batteries' Performance:* PE converters are widely used for battery charging [259], [260]. Nowadays, various charging strategies have been designed for batteries [261], [262], such as CC-CV charging [263], PC charging [264], and SRC charging [265]. Generally, the lifetime of a battery is affected by the charging strategy. In order to analyze the effect of charging modes on the safety of batteries, Islam and Park [266] investigated the heat loss of the CC-CV strategy, SRC-CV strategy, and pulse current-constant voltage (PC-CV) strategy, as shown in Fig. 28(a). The experimental results demonstrate that the temperature rise of batteries for PC-CV mode is more significant than those of SRC-CV and CC-CV modes. For CC-CV mode, the temperature rise of batteries is the lowest. It is concluded that the temperature rise is mainly dependent on the rms current.

Furthermore, Huang et al. [267] systematically investigated the effect of PC and SRC charging on batteries. Besides the charging profiles shown in Fig. 28(a), the PCCC, NPC, APC, and ASRC modes are considered, as shown in Fig. 28(b). The main conclusions are shown in Fig. 28(c), which are summarized in the following.

- 1) The maximum rising temperature ΔT of batteries is mainly dependent on the rms current, which is not related to the average value of charging profiles.
- 2) The charging speed α is mainly dependent on the charging current rate, which is not related to the shape of charging profiles.
- 3) In the tested frequency band (1 Hz to 10 kHz), a lower frequency of PC and SRC would result in a higher discharging capacity, a higher rising temperature, and a longer charging time.

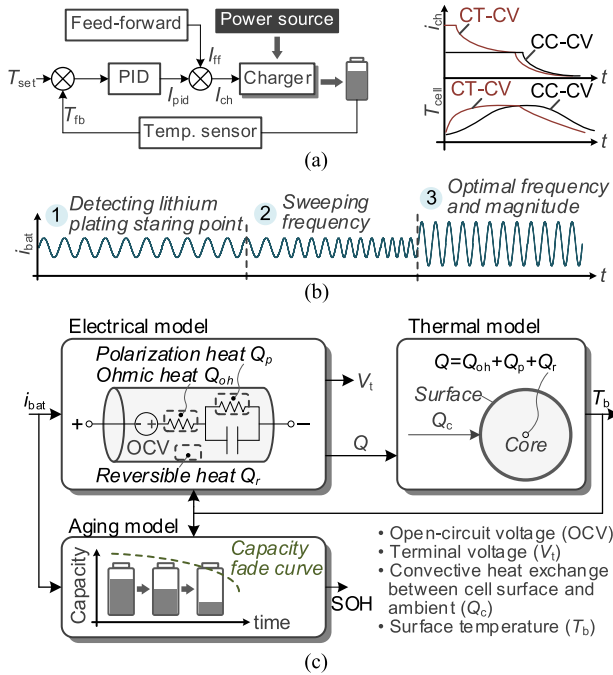


Fig. 29. Charging optimization techniques. (a) CT-CV charging [271]. (b) Electrochemical-based charging [272]. (c) Electrothermal-aging-based charging [273].

From the perspective of safety, it is essential to reduce the temperature rise of batteries, i.e., reducing the rms value of the charging current. However, it may reduce other performances of batteries (e.g., charging speed). Therefore, a tradeoff between safety, speed, etc., should be considered.

2) *Charging Optimization Techniques*: Some efforts have been made to optimize the safety of batteries during charging [262]. From the perspective of dependence on the battery model, there are three main methods.

One is the model-free method (i.e., Type I). Here, the internal physical and electrochemical characteristics of batteries are not considered. The charging strategies were optimized based on experiments. Generally, most of the charging optimization techniques are based on Type I [262], such as optimal-frequency SRC charging [268] and multistage constant-current charging [269]. Although various charging profiles have been designed, the essence is based on the conclusions in Fig. 28(c). Notice that the findings in [267] are drawn by aging experiment of pulsed and sinusoidal current from 1 Hz to 1 kHz. In [270], the same authors further found that the low-frequency pulsed current (less than 1 Hz) can extend the lifetime of batteries. However, the effect of charging speed is not considered. On the other hand, in most of the charging schemes, the temperature of batteries is not controlled. Regarding this issue, Patnaik et al. [271] proposed a CT-CV charging technique, which can control the temperature of batteries, as shown in Fig. 29(a).

Another is based on the electrochemical characteristics, i.e., the electrochemical-based method (i.e., Type II). Lee and Park [272] proposed an electrochemical state-based sinusoidal ripple current charging technique, which includes three stages,

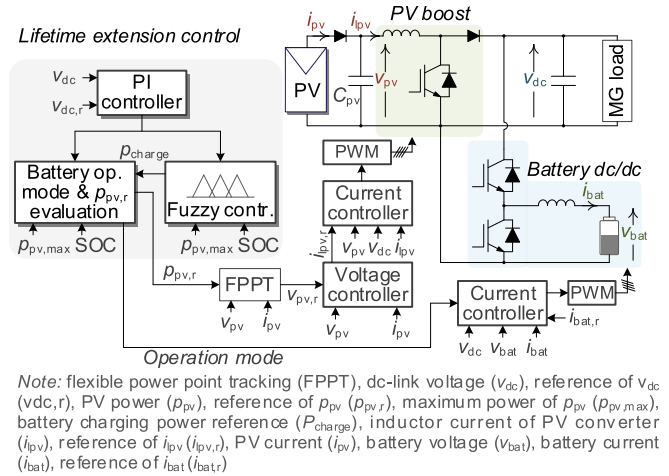


Fig. 30. Battery lifetime extension technique in a DC MG [275].

as shown in Fig. 29(b). In the first stage, the starting point of lithium plating is evaluated by monitoring the real part of the impedance in the first sequence due to lithium plating that may negatively affect a battery's lifetime and charging speed. The optimal ripple magnitude can be obtained based on the starting point of lithium plating. In the second stage, the optimal charging frequency is detected by sweeping the ac current frequency to obtain the minimum ohmic resistance. In the third stage, the optimal magnitude and frequency references are applied to the charging current to obtain an optimal charging performance.

Although electrochemical models can provide internal electrochemical signals of batteries, thermal and aging effects are not considered. Considering this issue, Hu et al. [273] and Liu et al. [274] built an electrothermal-aging coupling model for 18650 Li-ion cells, as shown in Fig. 29(c). Then, optimization algorithms (e.g., particle swarm optimization algorithm [273] and ensemble multiobjective biogeography-based optimization algorithm [274]) are used to find the optimal charging parameters.

In summary, the performance of the electrothermal-aging-based charging strategy is better. However, its complexity is relatively high.

C. Operation Optimization Strategies

Besides designing a particular charging strategy, the current stress of batteries can be adjusted in operating stages, in order to improve the battery lifetime.

Yan et al. [275] proposed a battery lifetime extension scheme for batteries in a stand-alone MG system, as shown in Fig. 30. By employing a fuzzy-logic-based controller, the PV reserve power and battery SOC information are used to adjust the battery charging current, in order to reduce the current stress of batteries during charging. Moreover, the PV system is used primarily, in order to avoid the continuous charging/discharging operation of batteries, further extending the battery lifetime.

TABLE VIII
TYPICAL PATENTS ABOUT LIFETIME IMPROVEMENT

Scheme	Description	Applicant
Charging/ discharging strategy	modulated pulsed charging/discharging based on the voltage/current measurement of each cell	Gbatteries Energy Canada Inc. [276], [277]
	pulsed charging based on online EIS measurement	Gbatteries Energy Canada Inc. [247]
Utilization adjustment	switching network is used to control the configuration of battery packs, so as to control the utilization of cells	Gbatteries Energy Canada Inc. [278], [279]
	each cell in battery packs is individually controlled, so as to adjust the utilization of cells	Beijing Samevolt Co. [280]

D. Typical Commercial and Industrial Solutions for Lifetime Improvement

For lifetime improvement techniques, the schemes discussed in Sections VI-B and IV-C are almost not found in commercial products. Fortunately, some attractive solutions have been presented in patents, as summarized in Table VIII. Generally, two main types of methods are considered. One is to adjust the charging/discharging strategies [276], [277], and the idea is similar to that of Fig. 29. Another is to reduce the utilization of batteries [278], [279], [280], and the idea is similar to that of Fig. 30.

E. Discussions of Lifetime Improvement Schemes

Referring to Sections VI-A–IV-D, brief remarks are given as follows.

- 1) Generally, the high-frequency ripples (greater than 10 Hz) generated by PE devices almost have no adverse effects on LIB's lifetime, without considering the rms current. However, low-frequency ripple (lower than 10 Hz) should be avoided in the design of PE devices for LIB systems.
- 2) From the perspective of charging strategies, electrothermal-aging-based charging [273], [274] strategies have significant advantages when compared with traditional charging schemes. However, some efforts should be made to reduce the complexity.
- 3) From the perspective of operation strategies (mainly including charging and discharging), it is better to reduce the use of LIBs, i.e., the charging and discharging process. However, it is only suitable for some special applications where other power sources exist to replace LIBs, such as PV and battery storage systems. For some applications without an alternative power source, it is better to design an operational strategy to reduce the electrothermal stress of LIBs [273], [274].

VII. CONCLUSION

This article presents an overview of PE-based safety enhancement techniques for LIBs from the battery management perspective. First, feasible PE-based solutions have been summarized, and the discussion of protection techniques is given. Second, the main design principles of BB techniques are summarized. Accordingly, the balancing schemes are derived, and the existing

schemes for LIBs are reviewed and discussed. Third, the basic principles of battery impedance are discussed. Then, the design principles of PE-based impedance measurement for LIBs are summarized. Based on this, the feasible schemes are derived and reviewed. Fourth, the effect of current ripples and charging strategies are discussed. Then, the main charging optimization strategies and operation strategies are discussed.

Based on this literature review, the suggested feasible solutions for industrial applications, future research challenges, and research opportunities are summarized in the following.

A. Suggested Feasible Solutions

The key goal of employing a PE-based safety enhancement technique for LIBs in industrial applications is to maximumly reduce the complexity of software and hardware.

- 1) For battery protection techniques, protection circuits using the state-of-the-art linear FET are recommended [e.g., see Fig. 2(d)], which can realize the functions of disconnect protection and load inrush current protection at the same time.
- 2) For BB techniques, it is recommended to use the dissipative scheme and Principle I-based schemes (1A, 1B, and 1C) for small-scale energy storage applications, such as consumer electronics. For large-scale energy storage applications (e.g., EVs and ESPSs) with several modules/packs and a large number of cells, it is suggested to realize the module-level and pack-level balancing using the existing interface converters (e.g., chargers and converter loads). Moreover, the schemes without complex circuits and control strategies are recommended for cell-level balancing, e.g., the coupling-capacitor scheme [90], and the multiwinding transformer-based scheme [97], [98].
- 3) For online monitoring techniques, it is suggested to utilize the existing frequency information (including ripple, harmonic, and loading profile) of PE circuits to estimate the single-point impedance and broadband impedance. Generally, A1-based schemes are recommended for the applications with abundant frequency information, such as EVs. Specially designed chargers with perturbation signals (A2- and A3-based schemes) are suggested for applications without abundant frequency information, such as ESPSs.
- 4) For lifetime improvement techniques, it is better to develop an electrothermal-aging-based charging strategy and operation strategy, e.g., the schemes reported in [273] and [274].

B. Challenges

Although the safety of LIBs can be enhanced through some PE solutions, the LIBs' intrinsic safety should be further improved using state-of-the-art manufacturing techniques [11]. PEs technology only can improve the safety of LIBs in the application phase. The challenges are given in the following.

- 1) For battery protection and balancing techniques, additional hardware cost and complex control strategies would limit their applications in LIB systems. Moreover, power

loss, heat radiation, and reliability issues caused by additional protection and balancing circuits may threaten the LIB system's security.

- 2) For online monitoring techniques, the relationship between EIS and health indicators of LIBs has not been investigated clearly. Although some numerical relations can be found (e.g., Fig. 21), there is a lack of a representative model for LIBs with different parameters. Moreover, there exists additional hardware costs, software costs, or external interference for EIS measurement.
- 3) For lifetime improvement techniques, the largest challenge is to use complex control strategies in actual applications, as well as to design simple optimal strategies with good performance.

C. Opportunities

From the perspective of PE research, the opportunities can be listed as follows.

- 1) Design of emerging protection and balancing topologies with fewer components and complexity, as well as corresponding control strategies. Emerging wide bandgap devices can be considered as they are efficient [281].
- 2) Design commercial and industrial products with low cost and high reliability for active BB, online EIS measurement, and lifetime improvement.
- 3) Reliability evaluation and optimization for PE devices in LIB systems, such as interface converters, protection, and balancing circuits. Special operation conditions and mission profiles can be considered [282], [283].
- 4) Design of advanced topologies and control strategies for chargers and load converters, in order to minimize the adverse effect of PE devices on LIBs.
- 5) Further research in failure mechanisms of LIBs to obtain an accurate degradation model and failure criteria based on impedance information.
- 6) Design BIM schemes for real industrial applications (working in harsh EMI environments) without additional hardware and software costs [35]. The emerging artificial intelligence technology can be considered.
- 7) Monitoring of LIB's status while monitoring other components in PE converters, such as capacitors and semiconductor switches.
- 8) Design simple control strategies for the lifetime improvement of LIBs, which can be integrated into the BMS.

REFERENCES

- [1] M. Yilmaz and P. T. Krein, "Review of battery charger topologies, charging power levels, and infrastructure for plug-in electric and hybrid vehicles," *IEEE Trans. Power Electron.*, vol. 28, no. 5, pp. 2151–2169, May 2013.
- [2] M. Rouholamini et al., "A review of modeling, management, and applications of grid-connected Li-ion battery storage systems," *IEEE Trans. Smart Grid*, vol. 13, no. 6, pp. 4505–4524, Nov. 2022.
- [3] R. Xiong, R. Yang, Z. Chen, W. Shen, and F. Sun, "Online fault diagnosis of external short circuit for lithium-ion battery pack," *IEEE Trans. Ind. Electron.*, vol. 67, no. 2, pp. 1081–1091, Feb. 2020.
- [4] W. Gao, Y. Zheng, M. Ouyang, J. Li, X. Lai, and X. Hu, "Micro-short-circuit diagnosis for series-connected lithium-ion battery packs using mean-difference model," *IEEE Trans. Ind. Electron.*, vol. 66, no. 3, pp. 2132–2142, Mar. 2019.
- [5] X. Cong, C. Zhang, J. Jiang, W. Zhang, and Y. Jiang, "A hybrid method for the prediction of the remaining useful life of lithium-ion batteries with accelerated capacity degradation," *IEEE Trans. Veh. Technol.*, vol. 69, no. 11, pp. 12775–12785, Nov. 2020.
- [6] T. Foroozan, S. Sharifi-Asl, and R. Shahbazian-Yassar, "Mechanistic understanding of Li dendrites growth by in-situ/operando imaging techniques," *J. Power Sources*, vol. 461, Jun. 2020, Art. no. 228135.
- [7] X. Gao et al., "Thermodynamic understanding of Li-dendrite formation," *Joule*, vol. 4, no. 9, pp. 1864–1879, Sep. 2020.
- [8] Q. Wang, B. Mao, S. Stolarov, and J. Sun, "A review of lithium-ion battery failure mechanisms and fire prevention strategies," *Prog. Energy Combust. Sci.*, vol. 73, pp. 95–131, Jul. 2019.
- [9] P. Sun, R. Bisschop, H. Niu, and X. Huang, "A review of battery fires in electric vehicles," *Fire Technol.*, vol. 56, pp. 1361–1410, Jan. 2020.
- [10] X. Feng, M. Ouyang, X. Liu, L. Lu, Y. Xia, and X. He, "Thermal runaway mechanism of lithium-ion battery for electric vehicles: A review," *Energy Storage Mater.*, vol. 10, pp. 246–267, Jan. 2018.
- [11] K. Liu, Y. Liu, D. Lin, A. Pei, and Y. Cui, "Materials for lithium-ion battery safety," *Sci. Adv.*, vol. 4, Jun. 2018, Art. no. eaas9820.
- [12] Q. Wang, L. Jiang, Y. Yu, and J. Sun, "Progress of enhancing the safety of lithium-ion battery from the electrolyte aspect," *Nano Energy*, vol. 55, pp. 1361–1410, Jan. 2019.
- [13] Q. Wang, B. Jiang, B. Li, and Y. Yan, "A critical review of thermal management models and solutions of lithium-ion batteries for the development of pure electric vehicles," *Renewable Sustain. Energy Rev.*, vol. 64, pp. 106–128, Oct. 2016.
- [14] W. Wu, S. Wang, W. Wu, K. Chen, S. Hong, and Y. Lai, "A critical review of battery thermal performance and liquid based battery thermal management," *Energy Convers. Manag.*, vol. 182, pp. 262–281, Feb. 2019.
- [15] X. Feng, D. Ren, X. He, and M. Ouyang, "Mitigating thermal runaway of lithium-ion batteries," *Joule*, vol. 4, no. 4, pp. 743–770, Apr. 2020.
- [16] P. Chombo and Y. Laoonual, "A review of safety strategies of a Li-ion battery," *J. Power Sources*, vol. 478, 2020, Art. no. 228649.
- [17] Y. Chen et al., "A review of lithium-ion battery safety concerns: The issues, strategies, and testing standards," *J. Energy Chem.*, vol. 59, pp. 83–99, Aug. 2021.
- [18] Y. Qiu and F. Jiang, "A review on passive and active strategies of enhancing the safety of lithium-ion batteries," *Int. J. Heat Mass Transf.*, vol. 184, Mar. 2022, Art. no. 122288.
- [19] J. Duan et al., "Building safe lithium-ion batteries for electric vehicles: A Review," *Electrochem. Energy Rev.*, vol. 3, pp. 1–42, 2020.
- [20] M. A. Hannan, M. H. Lipu, A. Hussain, and A. Mohamed, "A review of lithium-ion battery state of charge estimation and management system in electric vehicle applications: Challenges and recommendations," *Renewable Sustain. Energy Rev.*, vol. 78, pp. 834–854, Oct. 2017.
- [21] J. Meng et al., "An overview and comparison of online implementable SOC estimation methods for lithium-ion battery," *IEEE Trans. Ind. Appl.*, vol. 54, no. 2, pp. 1583–1591, Mar./Apr. 2018.
- [22] R. Xiong, L. Li, and J. Tian, "Towards a smarter battery management system: A critical review on battery state of health monitoring methods," *J. Power Sources*, vol. 405, pp. 18–29, 2018.
- [23] X. Sui, S. He, S. B. Vilsen, J. Meng, R. Teodorescu, and D.-I. Stroe, "A review of non-probabilistic machine learning-based state of health estimation techniques for lithium-ion battery," *Appl. Energy*, vol. 300, 2021, Art. no. 117346.
- [24] Y. Li et al., "Data-driven health estimation and lifetime prediction of lithium-ion batteries: A review," *Renewable Sustain. Energy Rev.*, vol. 113, 2019, Art. no. 109254.
- [25] X. Hu, L. Xu, X. Lin, and M. Pecht, "Battery lifetime prognostics," *Joule*, vol. 4, no. 2, pp. 310–346, 2020.
- [26] X. Hu, F. Feng, K. Liub, L. Zhang, J. Xie, and B. Liu, "State estimation for advanced battery management: Key challenges and future trends," *Renewable Sustain. Energy Rev.*, vol. 114, 2019, Art. no. 109334.
- [27] Y. Wang et al., "A comprehensive review of battery modeling and state estimation approaches for advanced battery management systems," *Renewable Sustain. Energy Rev.*, vol. 131, 2020, Art. no. 110015.
- [28] R. Xiong, Y. Pan, W. Shen, H. Li, and F. Sun, "Lithium-ion battery aging mechanisms and diagnosis method for automotive applications: Recent Advances and perspectives," *Renewable Sustain. Energy Rev.*, vol. 131, Oct. 2020, Art. no. 110048.

- [29] R. Xiong, W. Sun, Q. Yu, and F. Sun, "Research progress, challenges and prospects of fault diagnosis on battery system of electric vehicles," *Appl. Energy*, vol. 279, 2020, Art. no. 115855.
- [30] X. Hu, K. Zhang, K. Liu, X. Lin, S. Dey, and S. Onori, "Advanced fault diagnosis for lithium-ion battery systems: A review of fault mechanisms, fault features, and diagnosis procedures," *IEEE Ind. Electron. Mag.*, vol. 14, no. 3, pp. 65–91, Sep. 2020.
- [31] L. Lu, X. Han, J. Li, J. Hua, and M. Ouyang, "A review on the key issues for lithium-ion battery management in electric vehicles," *J. Power Sources*, vol. 226, pp. 272–288, 2013.
- [32] H. Rahimi-Eichi, U. Ojha, F. Baronti, and M.-Y. Chow, "Battery management system: An overview of its application in the smart grid and electric vehicles," *IEEE Ind. Electron. Mag.*, vol. 7, no. 2, pp. 4–16, Jun. 2013.
- [33] H. Dai, B. Jiang, X. Hu, X. Lin, X. Wei, and M. Pecht, "Advanced battery management strategies for a sustainable energy future: Multilayer design concepts and research trends," *Renewable Sustain. Energy Rev.*, vol. 138, 2021, Art. no. 110480.
- [34] F. Blaabjerg, H. Wang, I. Vernica, B. Liu, and P. Davari, "Reliability of power electronic systems for EV/HEV applications," *Proc. IEEE*, vol. 109, no. 6, pp. 1060–1076, Jun. 2021.
- [35] Z. Zhao, P. Davari, W. Lu, H. Wang, and F. Blaabjerg, "An overview of condition monitoring techniques for capacitors in dc-link applications," *IEEE Trans. Power Electron.*, vol. 36, no. 4, pp. 3692–3716, Apr. 2021.
- [36] A. Turksoy, A. Teke, and A. Alkaya, "A comprehensive overview of the dc-dc converter-based battery charge balancing methods in electric vehicles," *Renewable Sustain. Energy Rev.*, vol. 133, Nov. 2020, Art. no. 110274.
- [37] N. Ghaeminezhad, Q. Ouyang, X. Hu, G. Xu, and Z. Wang, "Active cell equalization topologies analysis for battery packs: A systematic review," *IEEE Trans. Power Electron.*, vol. 36, no. 8, pp. 9119–9135, Aug. 2021.
- [38] M. A. Varnosfaderani and D. Strickland, "A comparison of online electrochemical spectroscopy impedance estimation of batteries," *IEEE Access*, vol. 6, pp. 23668–23677, 2018.
- [39] *Battery Protection Selection Guide*, Infineon, Neubiberg, Germany, 2022.
- [40] *Application of OptiMOS™ Linear FET As Protection Switch in Battery-Powered Motor Drive Applications*, Infineon, Neubiberg, Germany, 2022.
- [41] Z. Zhao, W. Lu, W. Chen, X. Du, and H. H.-C. Lu, "Multi-period frame transient switching control for low-voltage high-current buck converter with a controlled coupled inductor," *IEEE Trans. Power Electron.*, vol. 34, no. 10, pp. 9743–9757, Oct. 2019.
- [42] *BQ297xx Cost-Effective Voltage and Current Protection Integrated Circuit for Single-Cell Li-Ion and Li-Polymer Batteries*, Texas Instruments, Dallas, TX, USA, 2023.
- [43] *Find Your Battery Protector*, Texas Instruments, Dallas, TX, USA. Accessed: Feb. 22, 2023. [Online]. Available: <https://www.ti.com/power-management/battery-management/protectors/overview.html>
- [44] *DS2762—High-Precision Li+ Battery Monitor With Alerts*, Analog Devices, Wilmington, MA, USA, 2023.
- [45] *DS2775/DS2776/DS2777/DS2778—2-Cell, Fuel Gauge With Fuelpack, Protector, and SHA-1 Authentication*, Analog Devices, Wilmington, MA, USA, 2023.
- [46] N. Zhao, N. Schofield, R. Yang, and R. Gu, "Investigation of dc-link voltage and temperature variations on EV traction system design," *IEEE Trans. Ind. Appl.*, vol. 53, no. 4, pp. 3707–3718, Jul./Aug. 2017.
- [47] J. H. Lee, C. Y. Won, B. K. Lee, and H. B. Kim, "IPMSM torque control method considering dc-link voltage variation and friction torque for EV/HEV applications," in *Proc. 2012 IEEE Veh. Power Propulsion Conf.*, 2012, pp. 1063–1069.
- [48] Y. Yao, F. Fassinou, and T. Hu, "Stability and robust regulation of battery-driven boost converter with simple feedback," *IEEE Trans. Power Electron.*, vol. 26, no. 9, pp. 2614–2626, Sep. 2011.
- [49] M. Anun, M. Ordóñez, I. G. Zurbriggen, and G. G. Oggier, "Circular switching surface technique: High-performance constant power load stabilization for electric vehicle systems," *IEEE Trans. Power Electron.*, vol. 30, no. 8, pp. 4560–4572, Aug. 2015.
- [50] W. Song, N. Hou, and M. Wu, "Virtual direct power control scheme of dual active bridge dc-dc converters for fast dynamic response," *IEEE Trans. Power Electron.*, vol. 33, no. 2, pp. 1750–1759, Feb. 2018.
- [51] B. Hredzak, V. G. Agelidis, and M. S. Jang, "A model predictive control for a hybrid battery-ultracapacitor power source," *IEEE Trans. Power Electron.*, vol. 29, no. 3, pp. 1469–1479, Mar. 2014.
- [52] H. Samani and X. Fernando, "Battery current's fluctuations removal in hybrid energy storage system based on optimized control of supercapacitor voltage," *IEEE Embedded Syst. Lett.*, vol. 8, no. 3, pp. 53–56, Sep. 2016.
- [53] O. Aiello, P. S. Crovetto, and F. Fiori, "Susceptibility to EMI of a battery management system IC for electric vehicles," in *Proc. IEEE Int. Symp. Electromagn. Compat.*, Aug. 2015, pp. 749–754.
- [54] *SLUA776—Designing EMI/EMC Safe Battery Pack*, Texas Instruments, Dallas, TX, USA, Jul. 2016.
- [55] N. Lyu, Y. Jin, R. Xiong, S. Miao, and J. Gao, "Real-time overcharge warning and early thermal runaway prediction of Li-ion battery by online impedance measurement," *IEEE Trans. Ind. Electron.*, vol. 69, no. 2, pp. 1929–1936, Feb. 2022.
- [56] Cypress Semiconductor, "Power management - battery charger with cell-balancing and fuel gauge function support," San Jose, CA, USA, Appl. Note AN2344, 2017.
- [57] J. G.-Lozano and E. R. Cadaval, "Battery equalization active methods," *J. Power Sources*, vol. 246, pp. 934–949, Jan. 2014.
- [58] C. Pascual and P. T. Krein, "Switched capacitor system for automatic series battery equalization," in *Proc. IEEE Appl. Power Electron. Conf. Expo.*, 1997, pp. 848–854.
- [59] P. A. Cassani and S. S. Williamson, "Feasibility analysis of a novel cell equalizer topology for plug-in hybrid electric vehicle energy-storage systems," *IEEE Trans. Veh. Technol.*, vol. 58, no. 8, pp. 3938–3946, Oct. 2009.
- [60] N. H. Kutkut, "A modular non dissipative current diverter for EV battery charge equalization," in *Proc. IEEE Appl. Power Electron. Conf.*, vol. 2, 1998, pp. 686–690.
- [61] M. Daowd, M. Antoine, N. Omar, P. Van Den Bossche, and J. Van Mierlo, "Single switched capacitor battery balancing system enhancements," *Energies*, vol. 6, no. 4, pp. 2149–2174, Apr. 2013.
- [62] S. Li, C. C. Mi, and M. Zhang, "A high-efficiency active battery-balancing circuit using multiwinding transformer," *IEEE Trans. Ind. Appl.*, vol. 49, no. 1, pp. 198–207, Jan./Feb. 2013.
- [63] K.-M. Lee, Y.-C. Chung, C.-H. Sung, and B. Kang, "Active cell balancing of Li-ion batteries using LC series resonant circuit," *IEEE Trans. Ind. Electron.*, vol. 62, no. 9, pp. 5491–5501, Sep. 2015.
- [64] M. Einhorn, W. Roessler, and J. Fleig, "Improved performance of serially connected Li-ion batteries with active cell balancing in electric vehicles," *IEEE Trans. Veh. Technol.*, vol. 60, no. 6, pp. 2448–2457, Jul. 2011.
- [65] Y. Wang, C. Zhang, Z. Chen, X. Jing, and X. Zhang, "A novel active equalization method for lithium-ion batteries in electric vehicles," *Appl. Energy*, vol. 145, no. 1, pp. 36–42, May 2015.
- [66] M. Uno and A. Kukita, "Bidirectional PWM converter integrating cell voltage equalizer using series-resonant voltage multiplier for series-connected energy storage cell," *IEEE Trans. Power Electron.*, vol. 30, no. 6, pp. 3017–3090, Jun. 2015.
- [67] Y. Hsieh, T. Liang, and S. Chen, "A novel high-efficiency compact-size low-cost balancing method for series-connected battery applications," *IEEE Trans. Power Electron.*, vol. 28, no. 12, pp. 5927–5939, Dec. 2013.
- [68] W. Huang and J. A. Abu Qahouq, "Energy sharing control scheme for state-of-charge balancing of distributed battery energy storage system," *IEEE Trans. Ind. Electron.*, vol. 62, no. 5, pp. 2764–2776, May 2015.
- [69] Z. Zhang, H. Gui, D. J. Gu, Y. Yang, and X. Ren, "A hierarchical active balancing architecture for lithium-ion batteries," *IEEE Trans. Power Electron.*, vol. 32, no. 4, pp. 2757–2768, Apr. 2017.
- [70] Y. Ye, K. W. E. Cheng, and Y. P. B. Yeung, "Zero-current switching switched-capacitor zero-voltage-gap automatic equalization system for series battery string," *IEEE Trans. Power Electron.*, vol. 27, no. 7, pp. 3234–3242, Jul. 2012.
- [71] A. C. Baughman and M. Ferdowsi, "Double-tiered switched-capacitor battery charge equalization technique," *IEEE Trans. Ind. Electron.*, vol. 55, no. 6, pp. 2277–2285, Jun. 2008.
- [72] M.-Y. Kim, C.-H. Kim, J.-H. Kim, and G.-W. Moon, "A chain structure of switched capacitor for improve cell balancing speed of lithium-ion batteries," *IEEE Trans. Ind. Electron.*, vol. 61, no. 8, pp. 3989–3999, Aug. 2014.
- [73] P. Cassani and S. Williamson, "Design, testing, and validation of a simplified control scheme for a novel plug-in hybrid electric vehicle battery cell equalizer," *IEEE Trans. Ind. Electron.*, vol. 57, no. 12, pp. 3956–3962, Dec. 2010.
- [74] X. Zheng, X. Liu, Y. He, and G. Zeng, "Active vehicle battery equalization scheme in the condition of constant-voltage/current charging and discharging," *IEEE Trans. Veh. Technol.*, vol. 66, no. 5, pp. 3714–3723, May 2017.

- [75] S. Wang, S. Yang, W. Yang, and Y. Wang, "A new kind of balancing circuit with multiple equalization modes for serially connected battery pack," *IEEE Trans. Ind. Electron.*, vol. 68, no. 3, pp. 2142–2150, Mar. 2021.
- [76] X. Cao, Q.-C. Zhong, Y.-C. Qiao, and Z.-Q. Deng, "Multilayer modular balancing strategy for individual cells in a battery pack," *IEEE Trans. Energy Convers.*, vol. 33, no. 2, pp. 526–536, Jun. 2018.
- [77] Y. S. Lee and M. W. Cheng, "Quasi-resonant zero-current-switching bidirectional converter for battery equalization applications," *IEEE Trans. Power Electron.*, vol. 21, no. 5, pp. 1213–1224, Sep. 2006.
- [78] N. Nguyen, S. K. Oruganti, K. Na, and F. Bien, "An adaptive backward control battery equalization system for serially connected lithium-ion battery packs," *IEEE Trans. Veh. Technol.*, vol. 63, no. 8, pp. 3651–3660, Oct. 2014.
- [79] Y.-S. Lee and M. Chen, "Intelligent control battery equalization for series connected lithium-ion battery strings," *IEEE Trans. Ind. Electron.*, vol. 52, no. 5, pp. 1297–1307, Oct. 2005.
- [80] Q. Ouyang, J. Chen, J. Zheng, and Y. Hong, "SOC estimation-based quasi-sliding mode control for cell balancing in lithium-ion battery packs," *IEEE Trans. Ind. Electron.*, vol. 65, no. 4, pp. 3427–3436, Apr. 2018.
- [81] M.-Y. Kim, J.-H. Kim, and G.-W. Moon, "Center-cell concentration structure of a cell-to-cell balancing circuit with a reduced number of switches," *IEEE Trans. Power Electron.*, vol. 29, no. 10, pp. 5285–5297, Oct. 2014.
- [82] F. Peng, H. Wang, and L. Yu, "Analysis and design considerations of efficiency enhanced hierarchical battery equalizer based on bipolar CCM buck-boost units," *IEEE Trans. Ind. Appl.*, vol. 55, no. 4, pp. 4053–4063, Jul./Aug. 2019.
- [83] Y. Ma, P. Duan, Y. Sun, and H. Chen, "Equalization of lithium-ion battery pack based on fuzzy logic control in electric vehicle," *IEEE Trans. Ind. Electron.*, vol. 65, no. 8, pp. 6762–6771, Aug. 2018.
- [84] W. Han, C. Zou, C. Zhou, and L. Zhang, "Estimation of cell SOC evolution and system performance in module-based battery charge equalization systems," *IEEE Trans. Smart Grid*, vol. 10, no. 5, pp. 4717–4728, Sep. 2019.
- [85] Q. Ouyang, W. Han, C. Zou, G. Xu, and Z. Wang, "Cell balancing control for lithium-ion battery packs: A hierarchical optimal approach," *IEEE Trans. Ind. Informat.*, vol. 16, no. 8, pp. 5065–5075, Aug. 2020.
- [86] Y. Ye, K. W. E. Cheng, Y. C. Fong, X. Xue, and J. Lin, "Topology, modeling and design of switched-capacitor-based cell balancing systems and their balancing exploration," *IEEE Trans. Power Electron.*, vol. 32, no. 6, pp. 4444–4454, Jun. 2017.
- [87] Y. Shang, C. Zhang, N. Cui, and C. C. Mi, "A delta-structured switched-capacitor equalizer for series-connected battery strings," *IEEE Trans. Power Electron.*, vol. 34, no. 1, pp. 452–461, Jan. 2019.
- [88] Y. Shang, N. Cui, B. Duan, and C. Zhang, "Analysis and optimization of star-structured switched-capacitor equalizers for series-connected battery strings," *IEEE Trans. Power Electron.*, vol. 33, no. 11, pp. 9631–9646.
- [89] Y. Shang, Q. Zhang, N. Cui, B. Duan, and C. Zhang, "An optimized mesh-structured switched-capacitor equalizer for lithium-ion battery strings," *IEEE Trans. Transp. Electrification*, vol. 5, no. 1, pp. 252–261, Mar. 2019.
- [90] Y. Shang, B. Xia, F. Lu, C. Zhang, N. Cui, and C. C. Mi, "A switched-coupling-capacitor equalizer for series-connected battery strings," *IEEE Trans. Power Electron.*, vol. 32, no. 10, pp. 7694–7706, Oct. 2017.
- [91] Y. Ye and K. W. E. Cheng, "Modeling and analysis of series-parallel switched-capacitor voltage equalizer for battery/supercapacitor strings," *IEEE Trans. Power Electron.*, vol. 3, no. 4, pp. 977–983, Dec. 2015.
- [92] G. Zhou, X. Zhang, K. Gao, Q. Tian, and S. Xu, "Two-mode active balancing circuit based on switched-capacitor and three-resonant-state LC units for series-connected cell strings," *IEEE Trans. Ind. Electron.*, vol. 69, no. 5, pp. 4845–4858, May 2022.
- [93] Y. Ye and K. W. E. Cheng, "Analysis and design of zero-current switching switched-capacitor cell balancing circuit for series-connected battery/supercapacitor," *IEEE Trans. Veh. Technol.*, vol. 67, no. 2, pp. 948–955, Feb. 2018.
- [94] L. Liu, R. Mai, B. Xu, W. Sun, W. Zhou, and Z. He, "Design of parallel resonant switched-capacitor equalizer for series-connected battery strings," *IEEE Trans. Power Electron.*, vol. 36, no. 8, pp. 9160–9169, Aug. 2021.
- [95] Y. Shang, B. Xia, C. Zhang, N. Cui, J. Yang, and C. Mi, "An automatic equalizer based on forward-flyback converter for series-connected battery strings," *IEEE Trans. Ind. Electron.*, vol. 64, no. 7, pp. 5380–5391, Jul. 2017.
- [96] Y. Chen, X. Liu, Y. Cui, J. Zou, and S. Yang, "A multiwinding transformer cell-to-cell active equalization method for lithium-ion batteries with reduced number of driving circuits," *IEEE Trans. Power Electron.*, vol. 31, no. 7, pp. 4916–4929, Jul. 2016.
- [97] Y. Shang, N. Cui, and C. Zhang, "An optimized any-cell-to-any-cell equalizer based on coupled half-bridge converters for series-connected battery strings," *IEEE Trans. Power Electron.*, vol. 34, no. 9, pp. 8831–8841, Sep. 2019.
- [98] R. Zou, F. Liu, Y. Liu, G. Xu, and F. Liu, "An LLC-based battery equalizer with inherent current limitation," *IEEE Trans. Power Electron.*, vol. 37, no. 2, pp. 1828–1840, Feb. 2022.
- [99] S. Park, K. Park, H. Kim, G. Moon, and M. Youn, "Single-magnetic cell-to-cell charge equalization converter with reduced number of transformer windings," *IEEE Trans. Power Electron.*, vol. 27, no. 6, pp. 2900–2911, Jun. 2012.
- [100] Y. Shang, B. Xia, C. Zhang, N. Cui, J. Yang, and C. Mi, "A modularization method for battery equalizers using multiwinding transformers," *IEEE Trans. Veh. Technol.*, vol. 66, no. 10, pp. 8710–8722, Oct. 2017.
- [101] H. Xiong, Y. Fu, and K. Dong, "A novel point-to-point energy transmission voltage equalizer for series-connected supercapacitors," *IEEE Trans. Veh. Technol.*, vol. 65, no. 6, pp. 4669–4675, Jun. 2016.
- [102] V.-L. Pham, V.-T. Duong, and W. Choi, "High-efficiency active cell-to-cell balancing circuit for lithium-ion battery modules using LLC resonant converter," *J. Power Electron.*, vol. 20, no. 4, pp. 1037–1046, 2020.
- [103] Y. Shang, C. Zhang, N. Cui, and J. M. Guerrero, "A cell-to-cell battery equalizer with zero-current switching and zero-voltage gap based on quasi resonant LC converter and boost converter," *IEEE Trans. Power Electron.*, vol. 30, no. 7, pp. 3731–3747, Jul. 2015.
- [104] S. K. Dam and V. John, "Low-frequency selection switch-based cell-to-cell battery voltage equalizer with reduced switch count," *IEEE Trans. Ind. Appl.*, vol. 57, no. 4, pp. 3842–3851, Jul./Aug. 2021.
- [105] S. M. Lambert, V. Pickert, D. J. Atkinson, and H. Zhan, "Transformer-based equalization circuit applied to n-number of high capacitance cells," *IEEE Trans. Power Electron.*, vol. 31, no. 2, pp. 1334–1343, Feb. 2016.
- [106] K. M. Lee, S. W. Lee, Y. G. Choi, and B. Kang, "Active balancing of Li-ion battery cells using transformer as energy carrier," *IEEE Trans. Ind. Electron.*, vol. 64, no. 2, pp. 1251–1257, Feb. 2017.
- [107] S. W. Lee, K. M. Lee, Y. G. Choi, and B. Kang, "Modularized design of active charge equalizer for Li-ion battery pack," *IEEE Trans. Power Electron.*, vol. 65, no. 11, pp. 8697–8706, Nov. 2018.
- [108] S. Yarlagadda, T. T. Hartley, and I. Husain, "A battery management system using an active charge equalization technique based on a dc/dc converter topology," *IEEE Trans. Ind. Appl.*, vol. 49, no. 6, pp. 2720–2729, Nov./Dec. 2013.
- [109] T. Morstyn, M. Momayyezani, B. Hredzak, and V. G. Agelidis, "Distributed control for state-of-charge balancing between the modules of a reconfigurable battery energy storage system," *IEEE Trans. Power Electron.*, vol. 31, no. 11, pp. 7986–7995, Nov. 2016.
- [110] F. Mestrallet, L. Kerachev, J.-C. Crebier, and A. Collet, "Multiphase interleaved converter for lithium battery active balancing," *IEEE Trans. Power Electron.*, vol. 29, no. 6, pp. 2874–2881, Jun. 2014.
- [111] S. K. Dam and V. John, "A modular fast cell-to-cell battery voltage equalizer," *IEEE Trans. Power Electron.*, vol. 35, no. 9, pp. 9443–9461, Sep. 2020.
- [112] Y. Shang, Q. Zhang, N. Cui, B. Duan, Z. Zhou, and C. Zhang, "Multi-cell-to-multi-cell equalizers based on matrix and half-bridge LC converters for series-connected battery strings," *IEEE J. Emerg. Sel. Topics Power Electron.*, vol. 8, no. 2, pp. 1755–1766, Jun. 2020.
- [113] M. Uno and K. Yoshino, "Modular equalization system using dual phase-shift-controlled capacitively isolated dual active bridge converters to equalize cells and modules in series-connected lithium-ion batteries," *IEEE Trans. Power Electron.*, vol. 36, no. 3, pp. 2983–2995, Mar. 2021.
- [114] Y. Shang, S. Zhao, Y. Fu, B. Han, P. Hu, and C. C. Mi, "A lithium-ion battery balancing circuit based on synchronous rectification," *IEEE Trans. Power Electron.*, vol. 35, no. 2, pp. 1637–1648, Feb. 2020.
- [115] H.-S. Park, C.-H. Kim, K.-B. Park, G.-W. Moon, and J.-H. Lee, "Design of a charge equalizer based on battery modularization," *IEEE Trans. Veh. Technol.*, vol. 58, no. 7, pp. 3216–3223, Sep. 2009.
- [116] Y. Li, J. Xu, X. Mei, and J. Wang, "A unitized multiwinding transformer-based equalization method for series-connected battery strings," *IEEE Trans. Power Electron.*, vol. 34, no. 12, pp. 11981–11989, Dec. 2019.

- [117] Y. Shang, N. Cui, B. Duan, and C. Zhang, "A global modular equalizer based on forward conversion for series-connected battery strings," *IEEE J. Emerg. Sel. Topics Power Electron.*, vol. 6, no. 3, pp. 1456–1469, Sep. 2018.
- [118] C.-S. Lim, K.-J. Lee, N.-J. Ku, D.-S. Hyun, and R.-Y. Kim, "A modularized equalization method based on magnetizing energy for a series-connected lithium-ion battery string," *IEEE Trans. Power Electron.*, vol. 29, no. 4, pp. 1791–1799, Apr. 2014.
- [119] M. Liu, Y. Chen, Y. Elasser, and M. Chen, "Dual frequency hierarchical modular multilayer battery balancer architecture," *IEEE Trans. Power Electron.*, vol. 36, no. 3, pp. 3099–3110, Mar. 2021.
- [120] H. Nazi and E. Babaei, "A modularized bidirectional charge equalizer for series-connected cell strings," *IEEE Trans. Ind. Electron.*, vol. 68, no. 8, pp. 6739–6749, Aug. 2021.
- [121] C.-H. Kim, M.-Y. Kim, H.-S. Park, and G.-W. Moon, "A modularized two-stage charge equalizer with cell selection switches for series connected lithium-ion battery string in an HEV," *IEEE Trans. Power Electron.*, vol. 27, no. 8, pp. 3764–3774, Aug. 2012.
- [122] X. Cui, W. Shen, Y. Zhang, C. Hu, and J. Zheng, "Novel active LiFePO₄ battery balancing method based on chargeable and dischargeable capacity," *Comput. Chem. Eng.*, vol. 97, pp. 27–35, Feb. 2017.
- [123] A. M. Imtiaz and F. H. Khan, "'Time shared flyback converter' based regenerative cell balancing technique for series connected Li-ion battery strings," *IEEE Trans. Power Electron.*, vol. 28, no. 12, pp. 5960–5975, Dec. 2013.
- [124] C. Kim, M. Kim, and G. Moon, "A modularized charge equalizer using a battery monitoring IC for series-connected Li-ion battery strings in electric vehicles," *IEEE Trans. Power Electron.*, vol. 28, no. 8, pp. 3779–3787, Aug. 2013.
- [125] M. M. Hoque, M. A. Hannan, and A. Mohamed, "Optimal algorithms for the charge equalization controller of series connected lithium-ion battery cells in electric vehicle applications," *IET Elect. Syst. Transp.*, vol. 7, no. 4, pp. 267–277, Dec. 2017.
- [126] M. A. Hannan, M. M. Hoque, S. E. Peng, and M. N. Uddin, "Lithium-ion battery charge equalization algorithm for electric vehicle applications," *IEEE Trans. Ind. Appl.*, vol. 53, no. 3, pp. 2541–2549, May/Jun. 2017.
- [127] X. Guo, J. Geng, Z. Liu, X. Xu, and W. Cao, "A flyback converter-based hybrid balancing method for series-connected battery pack in electric vehicles," *IEEE Trans. Veh. Technol.*, vol. 70, no. 7, pp. 6626–6635, Jul. 2021.
- [128] Z. Wei, F. Peng, and H. Wang, "An LCC-based string-to-cell battery equalizer with simplified constant current control," *IEEE Trans. Power Electron.*, vol. 37, no. 2, pp. 1816–1827, Feb. 2022.
- [129] Y. Yu, R. Saasaa, A. A. Khan, and W. Eberle, "A series resonant energy storage cell voltage balancing system," *IEEE J. Emerg. Sel. Topics Power Electron.*, vol. 8, no. 3, pp. 3151–3161, Sep. 2020.
- [130] Z. Wei, H. Wang, Y. Lu, D. Shu, G. Ning, and M. Fu, "Bidirectional constant current string-to-cell battery equalizer based on L2C3 resonant topology," *IEEE Trans. Power Electron.*, vol. 38, no. 1, pp. 666–677, Jan. 2023, doi: [10.1109/TPEL.2022.3205440](https://doi.org/10.1109/TPEL.2022.3205440).
- [131] C. Zhang, Y. Shang, Z. Li, and N. Cui, "An interleaved equalization architecture with self-learning fuzzy logic control for series-connected battery strings," *IEEE Trans. Veh. Technol.*, vol. 66, no. 12, pp. 10923–10934, Dec. 2017.
- [132] J. L. Sun, C. B. Zhu, R. G. Lu, K. Song, and G. Wei, "Development of an optimized algorithm for bidirectional equalization in lithium-ion batteries," *J. Power Electron.*, vol. 15, no. 3, pp. 775–785, May 2015.
- [133] J. Lu, Y. Wang, and X. Li, "Isolated bidirectional dc–dc converter with quasi-resonant zero-voltage switching for battery charge equalization," *IEEE Trans. Power Electron.*, vol. 34, no. 5, pp. 4388–4406, May 2019.
- [134] X. Qi, Y. Wang, and M. Fang, "An integrated cascade structure-based isolated bidirectional dc–dc converter for battery charge equalization," *IEEE Trans. Power Electron.*, vol. 35, no. 11, pp. 12003–12021, Nov. 2020.
- [135] X. Qi, Y. Wang, M. Fang, and W. Liu, "A reduced-component-count centralized equalization system for series-connected battery packs based on a novel integrated cascade topology," *IEEE Trans. Ind. Appl.*, vol. 57, no. 6, pp. 6105–6116, Nov./Dec. 2021.
- [136] X. Qi, Y. Wang, Y. Wang, and Z. Chen, "Optimization of centralized equalization systems based on an integrated cascade bidirectional dc–dc converter," *IEEE Trans. Ind. Electron.*, vol. 69, no. 1, pp. 249–259, Jan. 2022.
- [137] X. Qi, Y. Wang, M. Fang, Y. Wang, and Z. Chen, "Principle and topology derivation of integrated cascade bidirectional converters for centralized charge equalization systems," *IEEE Trans. Power Electron.*, vol. 37, no. 2, pp. 1852–1869, Feb. 2022.
- [138] X. Qi, Y. Wang, M. Fang, Y. Wang, and Z. Chen, "Multiport dc–dc converter with integrated cascaded structure for optimizing centralized battery equalization system," *IEEE Trans. Power Electron.*, vol. 37, no. 12, pp. 15111–15126, Dec. 2022.
- [139] G. Dong, F. Yang, K.-L. Tsui, and C. Zou, "Active balancing of lithium-ion batteries using graph theory and A-star search algorithm," *IEEE Trans. Ind. Informat.*, vol. 17, no. 4, pp. 2587–2599, Apr. 2021.
- [140] L. McCurlie, M. Preindl, and A. Emadi, "Fast model predictive control for redistributive lithium-ion battery balancing," *IEEE Trans. Ind. Electron.*, vol. 64, no. 2, pp. 1350–1357, Feb. 2017.
- [141] M. Arias, J. Sebastián, M. M. Hernando, U. Viscarret, and I. Gil, "Practical application of the wave-trap concept in battery–cell equalizers," *IEEE Trans. Power Electron.*, vol. 30, no. 10, pp. 5616–5631, Oct. 2015.
- [142] M. Uno and K. Tanaka, "Single-switch multioutput charger using voltage multiplier for series-connected lithium-ion battery/supercapacitor equalization," *IEEE Trans. Ind. Electron.*, vol. 60, no. 8, pp. 3227–3239, Aug. 2013.
- [143] X. Yang, Y. Qi, J. Liu, Z. Jia, and D. Wang, "Bidirectional converter integrating voltage equalizer based on symmetrical voltage multiplier by sharing a magnetic component for series-connected cells," *IEEE Trans. Transp. Electrification*, vol. 7, no. 3, pp. 1074–1087, Sep. 2021.
- [144] K. Yashiro and M. Uno, "Transformerless bidirectional PWM converter integrating voltage multiplier-based cell voltage equalizer for series-connected electric double-layer capacitors," *IEEE Trans. Power Electron.*, vol. 34, no. 5, pp. 4304–4315, May 2019.
- [145] M. Uno and K. Yashiro, "Tapped-inductor-based single-magnetic bidirectional PWM converter integrating cell voltage equalizer for series-connected supercapacitors," *IEEE Trans. Power Electron.*, vol. 35, no. 12, pp. 13157–13171, Dec. 2020.
- [146] L. Liu et al., "A low-cost multiwinding transformer balancing topology for retired series-connected battery string," *IEEE Trans. Power Electron.*, vol. 36, no. 5, pp. 4931–4936, May 2021.
- [147] R. Mai, B. Xu, Z. Yan, W. Zhou, and L. Liu, "A compact-size multiwinding transformer-based discharge equalizer for electric two-wheelers and three-wheelers vehicles power battery," *IEEE Trans. Veh. Technol.*, vol. 71, no. 5, pp. 4889–4897, May 2022.
- [148] M. Evzelman, M. M. Ur Rehman, K. Hathaway, R. Zane, D. Costinett, and D. Maksimovic, "Active balancing system for electric vehicles with incorporated low-voltage bus," *IEEE Trans. Power Electron.*, vol. 31, no. 11, pp. 7887–7895, Nov. 2016.
- [149] M. Preindl, "A battery balancing auxiliary power module with predictive control for electrified transportation," *IEEE Trans. Ind. Electron.*, vol. 65, no. 8, pp. 6552–6559, Aug. 2018.
- [150] Y.-D. Yang, K.-Y. Hu, and C.-H. Tsai, "Digital battery management design for point-of-load applications with cell balancing," *IEEE Trans. Ind. Electron.*, vol. 67, no. 8, pp. 6365–6375, Aug. 2020.
- [151] J. Qi and D. D.-C. Lu, "A preventive approach for solving battery imbalance issue by using a bidirectional multiple-input Cuk converter working in DCVM," *IEEE Trans. Ind. Electron.*, vol. 64, no. 10, pp. 7780–7789, Oct. 2017.
- [152] C.-M. Young, N.-Y. Chu, L.-R. Chen, Y.-C. Hsiao, and C.-Z. Li, "A single-phase multilevel inverter with battery balancing," *IEEE Trans. Ind. Electron.*, vol. 60, no. 5, pp. 1972–1978, May 2013.
- [153] E. Chatzinikolaou and D. J. Rogers, "Performance evaluation of duty cycle balancing in power electronics enhanced battery packs compared to conventional energy redistribution balancing," *IEEE Trans. Power Electron.*, vol. 33, no. 11, pp. 9142–9153, Nov. 2018.
- [154] F. Baronti, G. Fantechi, R. Roncella, and R. Saletti, "High-efficiency digitally controlled charge equalizer for series-connected cells based on switching converter and super-capacitor," *IEEE Trans. Ind. Informat.*, vol. 9, no. 2, pp. 1139–1147, May 2013.
- [155] F. Baronti, C. Bernardeschi, L. Cassano, A. Domenici, R. Roncella, and R. Saletti, "Design and safety verification of a distributed charge equalizer for modular Li-ion batteries," *IEEE Trans. Ind. Informat.*, vol. 10, no. 2, pp. 1003–1011, May 2014.
- [156] G. Noh, J. Lee, and J.-I. Ha, "Design and analysis of single-inductor power converter for both battery balancing and voltage regulation," *IEEE Trans. Ind. Electron.*, vol. 69, no. 3, pp. 2874–2884, Mar. 2022.
- [157] W. Lujun et al., "Efficient and fast active equalization method for retired battery pack using wide voltage range bidirectional converter and dbscan clustering algorithm," *IEEE Trans. Power Electron.*, vol. 37, no. 11, pp. 13824–13833, Nov. 2022.

- [158] S. Jinlei, L. Wei, T. Chuanyu, W. Tianru, J. Tao, and T. Yong, "A novel active equalization method for series-connected battery packs based on clustering analysis with genetic algorithm," *IEEE Trans. Power Electron.*, vol. 36, no. 7, pp. 7853–7865, Jul. 2021.
- [159] C. Riczu and J. Bauman, "Implementation and system-level modeling of a hardware efficient cell balancing circuit for electric vehicle range extension," *IEEE Trans. Ind. Appl.*, vol. 57, no. 3, pp. 2883–2895, May/June 2021.
- [160] M. Shousha, T. McRae, A. Prodić, V. Marten, and J. Milios, "Design and implementation of high power density assisting step-up converter with integrated battery balancing feature," *IEEE J. Emerg. Sel. Topics Power Electron.*, vol. 5, no. 3, pp. 1068–1077, Sep. 2017.
- [161] M. Shousha, A. Prodić, V. Marten, and J. Milios, "Design and implementation of assisting converter-based integrated battery management system for electromobility applications," *IEEE J. Emerg. Sel. Topics Power Electron.*, vol. 6, no. 2, pp. 825–842, Jun. 2018.
- [162] F. Peng, H. Wang, and Z. Wei, "An LLC-based highly efficient S2M and C2C hybrid hierarchical battery equalizer," *IEEE Trans. Power Electron.*, vol. 35, no. 6, pp. 5928–5937, Jun. 2020.
- [163] M. Uno, K. Yashiro, and K. Hasegawa, "Modularized equalization architecture with voltage multiplier-based cell equalizer and switchless switched capacitor converter-based module equalizer for series-connected electric double-layer capacitors," *IEEE Trans. Power Electron.*, vol. 34, no. 7, pp. 6356–6368, Jul. 2019.
- [164] M. Uno and K. Hasegawa, "Modular equalization system based on star-connected phase-shift switched capacitor converters with inherent constant current characteristics for electric double-layer capacitor modules," *IEEE Trans. Power Electron.*, vol. 35, no. 10, pp. 10271–10284, Oct. 2020.
- [165] K. Liu, Z. Yang, X. Tang, and W. Cao, "Automotive battery equalizers based on joint switched-capacitor and buck-boost converters," *IEEE Trans. Veh. Technol.*, vol. 69, no. 11, pp. 12716–12724, Nov. 2020.
- [166] *Find Your Battery Monitors & Balancers*, Texas Instruments, Dallas, TX, USA. Accessed: Feb. 22, 2023. [Online]. Available: <https://www.ti.com/power-management/battery-management/monitors-balancers/overview.html>
- [167] *Battery Status Monitors*, Analog Devices, Wilmington, MA, USA. Accessed: Feb. 22, 2023. [Online]. Available: <https://www.analog.com/en/parametricsearch/12874#/p270=Cell%20Balancing&andToggle=270>
- [168] *Battery Cell Controllers*, NXP Semiconductors, Eindhoven, Netherlands. Accessed: Feb. 22, 2023. [Online]. Available: <https://www.nxp.com/products/power-management/battery-management/battery-cell-controllers:BATTERY-CELL-CONTROLLERS>
- [169] *LTC3300—High Efficiency Bidirectional Multicell Battery Balancer*, Analog Devices, Wilmington, MA, USA, 2023.
- [170] *LT8584—2.5A Monolithic Active Cell Balancer With Telemetry Interface*, Analog Devices, Wilmington, MA, USA, 2023.
- [171] J. Tanaka and N. Kumagai, "Cell balancing device," U.S. Patent US20220097566A1, Mar. 31, 2022.
- [172] T. Hidaka and H. Kim, "Battery management system," U.S. Patent US11050266B2, Jun. 29, 2021.
- [173] S. Kang, H. Kim, B. Lee, and S. Lee, "Apparatus and method for balancing battery packs connected in parallel," U.S. Patent US20220140620A1, May 5, 2022.
- [174] Y. Li, "Cell balancing device based on capacitor network, cascaded balancing battery pack, and control method thereof," CN Patent App. WO2021244265A1, Dec. 12, 2021.
- [175] T. A. Stuart, "Bilevel equalizer for battery cell charge management," U.S. Patent US10862318B2, Dec. 8, 2020.
- [176] Y. P. Barsukov, Y. Zhang, J. M. Battle, and K. Galburt, "System and method for battery pack management using predictive balancing," U.S. Patent US9979211B2, May 22, 2018.
- [177] C. Zhang, "Battery equalization circuit, method for controlling battery equalization circuit, and uninterruptible power system," U.S. Patent US20210408808A1, Dec. 30, 2021.
- [178] H. Yoon, "Battery balancing apparatus and battery pack including the same," U.S. Patent US20210075067A1, Mar. 11, 2021.
- [179] P. Pognant-Gros and D. Olszewski, "System and method for balancing the charge of a plurality of energy storage modules," U.S. Patent US10186878B2, Jan. 22, 2019.
- [180] D. Xuan, B. Wang, X. Zhao, and J. Chen, "Staggered battery equalization circuit structure based on transformer," CN Patent CN110707780B, Aug. 23, 2022.
- [181] Z. Moussaoui and T. Allen, "System and method for cell balancing and charging using a serially coupled inductor and capacitor," U.S. Patent US10164441B2, Dec. 25, 2018.
- [182] J. Hwan, Y. Moon, C. Kim, and M. Kim, "Charge equalization apparatus for a battery string," U.S. Patent US10680447B2, Jun. 9, 2020.
- [183] T. L. Taylor, N. Ota, and T. Ta, "Systems and methods for series battery charging," U.S. Patent US10680447B2, Feb. 2, 2021.
- [184] C. Sun, C. Chou, and C. Che, "Battery system, control method of cell balance procedure, and calculation method of balance charge capacity," U.S. Patent US20210328441A1, Oct. 21, 2021.
- [185] M. Caspar, T. Eiler, and S. Hohmann, "Systematic comparison of active balancing: A model-based quantitative analysis," *IEEE Trans. Veh. Technol.*, vol. 67, no. 2, pp. 920–934, Feb. 2018.
- [186] F. Qu, Q. Luo, H. Liang, D. Mou, P. Sun, and X. Du, "Systematic overview of active battery equalization structures: Mathematical modeling and performance evaluation," *IEEE Trans. Energy Convers.*, vol. 37, no. 3, pp. 1685–1703, Sep. 2022.
- [187] "Lithium ion NCR18650PF," Panasonic Corp., 2018. [Online]. Available: <https://www.alldatasheet.com/datasheet-pdf/pdf/597041/PANASONICBATTERY/NCR18650.html>
- [188] "LiFePO4 Battery cell 418650-3.2V-1800mAh," Antbatt Co. Ltd., 2019. [Online]. Available: <https://antbatt.com/portfolio-items/lifepo4-battery-cell-18650-3-2v-1800mah/>
- [189] "Tenenergy 18650 2200mAh Li-ion cell," Tenenergy Corp., 2009. [Online]. Available: <https://www.jameco.com/Jameco/Products/ProdDS/2144243.pdf>
- [190] X. Wang et al., "A review of modeling, acquisition, and application of lithium-ion battery impedance for onboard battery management," *eTransportation*, vol. 7, 2021, Art. no. 100093.
- [191] J. Sihvo, D. Stroe, T. Messo, and T. Roinila, "Fast approach for battery impedance identification using pseudo-random sequence signals," *IEEE Trans. Power Electron.*, vol. 35, no. 3, pp. 2548–2557, Mar. 2020.
- [192] A. Waligo and P. Barendse, "A comparison of the different broadband impedance measurement techniques for lithium-ion batteries," in *Proc. IEEE Energy Convers. Congr. Expo.*, 2016, pp. 1–7.
- [193] L. Wang et al., "Research progress of the electrochemical impedance technique applied to the high-capacity lithium-ion battery," *Int. J. Minerals, Metall. Mater.*, vol. 28, no. 4, pp. 538–552, 2021.
- [194] X. Du, J. Meng, J. Peng, Y. Zhang, T. Liu, and R. Teodorescu, "Sensorless temperature estimation of lithium-ion battery based on broadband impedance measurements," *IEEE Trans. Power Electron.*, vol. 37, no. 9, pp. 10101–10105, Sep. 2022.
- [195] P. Iurilli, C. Brivio, and V. Wood, "On the use of electrochemical impedance spectroscopy to characterize and model the aging phenomena of lithium-ion batteries: A Critical review," *J. Power Sources*, vol. 505, 2021, Art. no. 229860.
- [196] D. Andre, M. Meiler, K. Steiner, C. Wimmer, T. Soczka-Guth, and D. U. Sauer, "Characterization of high-power lithium-ion batteries by electrochemical impedance spectroscopy—I: Experimental investigation," *J. Power Sources*, vol. 196, no. 12, pp. 5334–5341, 2011.
- [197] M. Galeotti, L. Cinà, C. Giammanco, S. Cordiner, and A. Di Carlo, "Performance analysis and SOH (state of health) evaluation of lithium polymer batteries through electrochemical impedance spectroscopy," *Energy*, vol. 89, pp. 678–686, 2015.
- [198] Y. Fu, J. Xu, M. Shi, and X. Mei, "A fast impedance calculation-based battery state-of-health estimation method," *IEEE Trans. Ind. Electron.*, vol. 69, no. 7, pp. 7019–7028, Jul. 2022.
- [199] J. Zhu, Z. Sun, X. Wei, and H. Dai, "A new lithium-ion battery internal temperature on-line estimate method based on electrochemical impedance spectroscopy measurement," *J. Power Sources*, vol. 274, pp. 990–1004, 2015.
- [200] C. T. Love and K. Swider-Lyons, "Impedance diagnostic for overcharged lithium-ion batteries," *Electrochem. Solid-State Lett.*, vol. 15, no. 4, pp. A53–A56, 2012.
- [201] X. Kong et al., "Pseudo-two-dimensional model and impedance diagnosis of micro internal short circuit in lithium-ion cells," *J. Energy Storage*, vol. 27, 2020, Art. no. 101085.
- [202] A. Shahrooei, "Comparison of open datasets for lithium-ion battery testing," Dec. 13, 2020. Accessed: Mar. 2023. [Online]. Available: <https://medium.com/batterybits/comparison-of-open-datasets-for-lithium-ion-battery-testing-fd0de091ca2>
- [203] P. Kollmeyer, "Panasonic 18650PF Li-ion battery data," Jun. 21, 2018. Accessed: Mar. 2023. [Online]. Available: <https://data.mendeley.com/datasets/wykht8y7tg/1>

- [204] I. Babaeiyazdi, A. Rezaei-Zare, and S. Shokrzadeh, "State of charge prediction of EV Li-ion batteries using EIS: A machine learning approach," *Energy*, vol. 223, May 2021, Art. no. 120116.
- [205] Y. Zhang, Q. Tang, Y. Zhang, J. Wang, U. Stimming, and A. A. Lee, "Identifying degradation patterns of lithium-ion batteries from impedance spectroscopy using machine learning," *Nature Commun.*, vol. 11, 2020, Art. no. 1706.
- [206] D. A. Howey, P. D. Mitcheson, V. Yufit, G. J. Offer, and N. P. Brandon, "Online measurement of battery impedance using motor controller excitation," *IEEE Trans. Veh. Technol.*, vol. 63, no. 6, pp. 2557–2566, Jun. 2014.
- [207] Z. Xia and J. A. A. Qahouq, "An online battery impedance spectrum measurement method with increased frequency resolution," in *Proc. IEEE Appl. Power Electron. Conf. Expo.*, 2018, pp. 1930–1933.
- [208] W. Huang and J. A. A. Qahouq, "An online battery impedance measurement method using DC–DC power converter control," *IEEE Trans. Ind. Electron.*, vol. 61, no. 11, pp. 5987–5995, Nov. 2014.
- [209] X. Wang, X. Wei, Q. Chen, and H. Dai, "A novel system for measuring alternating current impedance spectra of series-connected Lithium-ion batteries with a high-power dual active bridge converter and distributed sampling units," *IEEE Trans. Ind. Electron.*, vol. 68, no. 8, pp. 7380–7390, Aug. 2021.
- [210] M. A. Varnosfaderani and D. Strickland, "Online impedance spectroscopy estimation of a dc–dc converter connected battery using a switched capacitor-based balancing circuit," *J. Eng.*, vol. 2019, no. 7, pp. 4681–4685, Jul. 2019.
- [211] E. Din, C. Schaef, K. Moffat, and J. T. Stauth, "A scalable active battery management system with embedded real-time electrochemical impedance spectroscopy," *IEEE Trans. Power Electron.*, vol. 32, no. 7, pp. 5688–5698, Jul. 2017.
- [212] C. Schaef, E. Din, and J. T. Stauth, "A hybrid switched-capacitor battery management IC with embedded diagnostics for series-stacked Li-ion arrays," *IEEE J. Solid-State Circuits*, vol. 52, no. 12, pp. 3142–3154, Dec. 2017.
- [213] R. Koch, C. Riebel, and A. Jossen, "On-line electrochemical impedance spectroscopy implementation for telecommunication power supplies," in *Proc. IEEE Int. Telecommun. Energy Conf.*, 2015, pp. 1–6.
- [214] A. Beshatti, S. M. R. Islam, T. Link, S. Park, and S. Park, "Design and control of AC current injector for battery EIS measurement," in *Proc. IEEE Appl. Power Electron. Conf. Expo.*, 2020, pp. 3452–3455.
- [215] G. Dotelli, R. Ferrero, P. G. Stampino, S. Latorrata, and S. Toscani, "Diagnosis of PEM fuel cell drying and flooding based on power converter ripple," *IEEE Trans. Instrum. Meas.*, vol. 63, no. 10, pp. 2341–2348, Oct. 2014.
- [216] M. Bayati, M. Abedi, G. B. Gharehpajian, and M. Farahmandrad, "Sinusoidal-ripple current control in battery charger of electric vehicles," *IEEE Trans. Veh. Technol.*, vol. 69, no. 7, pp. 7201–7210, Jul. 2020.
- [217] J. A. A. Qahouq and Z. Xia, "Single-perturbation-cycle online battery impedance spectrum measurement method with closed-loop control of power converter," *IEEE Trans. Ind. Electron.*, vol. 64, no. 9, pp. 7019–7029, Sep. 2017.
- [218] L. Zhang, Z. Zhou, Q. Chen, R. Long, and S. Quan, "Model predictive control for electrochemical impedance spectroscopy measurement of fuel cells based on neural network optimization," *IEEE Trans. Transp. Electrification*, vol. 5, no. 2, pp. 524–534, Jun. 2019.
- [219] E. Sadeghi, M. H. Zand, M. Hamzeh, M. Saif, and S. M. M. Alavi, "Controllable electrochemical impedance spectroscopy: From circuit design to control and data analysis," *IEEE Trans. Power Electron.*, vol. 35, no. 9, pp. 9933–9942, Sep. 2020.
- [220] R. Ferrero et al., "Low-cost battery monitoring by converter-based electrochemical impedance spectroscopy," in *Proc. IEEE Int. Workshop Appl. Meas. Power Syst.*, 2017, pp. 1–6.
- [221] S. M. R. Islam and S.-Y. Park, "Precise online electrochemical impedance spectroscopy strategies for Li-ion batteries," *IEEE Trans. Ind. Appl.*, vol. 56, no. 2, pp. 1661–1669, Mar./Apr. 2020.
- [222] Y.-D. Lee, S.-Y. Park, and S.-B. Han, "Online embedded impedance measurement using high-power battery charger," *IEEE Trans. Ind. Appl.*, vol. 51, no. 1, pp. 498–508, Jan./Feb. 2015.
- [223] J. Shen, H. Homayouni, and J. Wang, "Converter-based electrochemical impedance spectroscopy for high-power fuel cell stacks with resonant controllers," *IEEE Trans. Ind. Electron.*, vol. 68, no. 9, pp. 8819–8828, Sep. 2021.
- [224] Z. Xia and J. A. A. Qahouq, "Method for online battery AC impedance spectrum measurement using DC–DC power converter duty-cycle control," in *Proc. IEEE Appl. Power Electron. Conf. Expo.*, 2017, pp. 1999–2003.
- [225] J. A. A. Qahouq, "Online battery impedance spectrum measurement method," in *Proc. IEEE Appl. Power Electron. Conf. Expo.*, 2016, pp. 3611–3615.
- [226] O. Alao and P. Barendse, "Online condition monitoring of sealed lead acid & lithium nickel-cobalt-manganese oxide batteries using broadband impedance spectroscopy," in *Proc. IEEE Energy Conver. Congr. Expo.*, 2018, pp. 2026–2032.
- [227] T. N. Gücin and L. Ovacik, "Online impedance measurement of batteries using the cross-correlation technique," *IEEE Trans. Power Electron.*, vol. 35, no. 4, pp. 4365–4375, Apr. 2020.
- [228] S. K. Dam and V. John, "High-resolution converter for battery impedance spectroscopy," *IEEE Trans. Ind. Appl.*, vol. 54, no. 2, pp. 1502–1512, Mar. 2018.
- [229] T. Nguyen, V. Tran, and W. Choi, "Development of the intelligent charger with battery State-of-health estimation using online impedance spectroscopy," in *Proc. IEEE 23rd Int. Symp. Ind. Electron.*, Jun. 2014, pp. 454–458.
- [230] V. T. Doan, V. B. Vu, H. N. Vu, D. H. Tran, and W. Choi, "Intelligent charger with online battery diagnosis function," in *Proc. 9th Int. Conf. Power Electron. ECCE Asia*, 2015, pp. 1644–1649.
- [231] N. Katayama and S. Kogoshi, "Real-time electrochemical impedance diagnosis for fuel cells using a dc–dc converter," *IEEE Energy Convers.*, vol. 30, no. 2, pp. 707–713, Jun. 2015.
- [232] D. Depernet, O. Ba, and A. Berthon, "Online impedance spectroscopy of lead acid batteries for storage management of a standalone power plant," *J. Power Sources*, vol. 219, pp. 65–74, 2012.
- [233] H. H. Abbasali and S. J. Ashtiani, "Online broadband battery impedance spectroscopy using current-mode boost converter," *IEEE Trans. Instrum. Meas.*, vol. 71, 2022, Art. no. 2003908.
- [234] Z. Gong et al., "EV BMS with distributed switch matrix for active balancing, online electrochemical impedance spectroscopy, and auxiliary power supply," in *Proc. 21st Eur. Conf. Power Electron. Appl.*, 2019, pp. P.1–P.10.
- [235] Z. Gong et al., "IC for online EIS in automotive batteries and hybrid architecture for high-current perturbation in low-impedance cells," in *Proc. IEEE Appl. Power Electron. Conf. Expo.*, 2018, pp. 1922–1929.
- [236] M. Koseoglou, E. Tsioumas, D. Papagiannis, and N. Jabbour, and C. Mademlis, "A novel on-board electrochemical impedance spectroscopy system for real-time battery impedance estimation," *IEEE Trans. Power Electron.*, vol. 36, no. 9, pp. 10776–10787, Sep. 2021.
- [237] X. Wei, X. Wang, and H. Dai, "Practical on-board measurement of lithium-ion battery impedance based on distributed voltage and current sampling," *Energies*, vol. 11, no. 1, Jan. 2018, Art. no. 64.
- [238] S. K. Dam and V. John, "High voltage resolution auxiliary power converter for online battery impedance measurement," in *Proc. IEEE Energy Convers. Congr. Expo.*, 2019, pp. 5450–5457.
- [239] C. G. Moral, D. Fernandez, J. M. Guerrero, D. Reigosa, C. R. Pereda, and F. Briz, "Thermal monitoring of lifePO4 batteries using switching harmonics," *IEEE Trans. Ind. Appl.*, vol. 56, no. 4, pp. 4134–4145, Jul./Aug. 2020.
- [240] C. G. Moral et al., "Battery internal resistance estimation using a battery balancing system based on switched capacitors," *IEEE Trans. Ind. Appl.*, vol. 56, no. 5, pp. 5363–5374, Sep./Oct. 2020.
- [241] Z. Zhao, W. Lu, P. Davari, X. Du, H. H. Ju, and F. Blaabjerg, "An online parameters monitoring method for output capacitor of buck converter based on large-signal load transient trajectory analysis," *IEEE J. Emerg. Sel. Topics Power Electron.*, vol. 9, no. 4, pp. 4004–4015, Aug. 2021.
- [242] Z. Zhao, P. Davari, Y. Wang, and F. Blaabjerg, "Online capacitance monitoring for dc/dc boost converters based on low-sampling-rate approach," *IEEE J. Emerg. Sel. Topics Power Electron.*, vol. 10, no. 5, pp. 5192–5204, Oct. 2022.
- [243] Z. Zhao, P. Davari, W. Lu, and F. Blaabjerg, "Online dc-link capacitance monitoring for digital-controlled boost PFC converters without additional sampling devices," *IEEE Trans. Ind. Electron.*, vol. 70, no. 1, pp. 907–920, Jan. 2023.
- [244] D. Xiang, C. Yang, H. Li, Y. Zhou, S. Zhu, and Y. Li, "Online monitoring of lithium-ion battery internal temperature using PWM switching oscillations," *IEEE Trans. Power Electron.*, vol. 38, no. 1, pp. 1166–1177, Jan. 2023.
- [245] *Circuit Note CN-0510*, Analog Devices, Wilmington, MA, USA, 2023.

- [246] J. P. Christophersen, W. H. Morrison, and J. L. Morrison, "Device, system, and method for measuring internal impedance of a test battery using frequency response," U.S. Patent US10345384B2, Jul. 9, 2019.
- [247] O. Tkachenko and M. Sherstyuk, "Battery charging based on real time electrochemical impedance spectroscopy (EIS) measurements," U.S. Patent US10566817B2, Feb. 18, 2020.
- [248] A. E. Christensen and R. Mosbæk, "System for providing an excitation signal to an electrochemical system and method therefor," U.S. Patent US20180203073A1, Jul. 19, 2019.
- [249] "Charger with embedded battery diagnosis and control method thereof," KR Patent KR101511655B1, Apr. 13, 2015.
- [250] A. Ballantine, J. Cronin, and J. Bodkin, "Real-time electrochemical impedance spectroscopy apparatus (EISA) testing," U.S. Patent US20190317152A1, Oct. 17, 2019.
- [251] C. Lv, T. Zhang, and H. Liu, "Electrochemical impedance spectrum on-line measuring device for lithium-ion battery pack," CN Patent CN108663631B, Dec. 25, 2020.
- [252] L. W. Juang, P. J. Kollmeyer, A. E. Anders, T. M. Jahns, R. D. Lorenz, and D. Gao, "Investigation of the influence of superimposed ac current on lithium-ion battery aging using statistical design of experiments," *J. Energy Storage*, vol. 11, pp. 93–103, 2017.
- [253] M. Steintraeter, J. Gandlgruber, J. Everken, and M. Lienkamp, "Influence of pulse width modulated auxiliary consumers on battery aging in electric vehicles," *J. Energy Storage*, vol. 48, Feb. 2022, Art. no. 104009.
- [254] A. Ghassemi, P. C. Banerjee, A. F. Hollenkamp, Z. Zhang, and B. Bahrani, "Effects of alternating current on Li-ion battery performance: Monitoring degradative processes with in-situ characterization techniques," *Appl. Energy*, vol. 284, 2021, Art. no. 116192.
- [255] M. J. Brand, M. H. Hofmann, S. S. Schuster, P. Keil, and A. Jossen, "The influence of current ripples on the lifetime of lithium-ion batteries," *IEEE Trans. Veh. Technol.*, vol. 67, no. 11, pp. 10438–10445, Nov. 2018.
- [256] A. Bessman, R. Soares, O. Wallmark, P. Svens, and G. Lindbergh, "Aging effects of AC harmonics on lithium-ion cells," *J. Energy Storage*, vol. 21, pp. 741–749, Feb. 2019.
- [257] F. Chang, F. Roemer, and M. Lienkamp, "Influence of current ripples in cascaded multilevel topologies on the aging of lithium batteries," *IEEE Trans. Power Electron.*, vol. 35, no. 11, pp. 11879–11890, Nov. 2020.
- [258] M. Uno and K. Tanaka, "Influence of high-frequency charge-discharge cycling induced by cell voltage equalizers on the life performance of lithium-ion cells," *IEEE Trans. Veh. Technol.*, vol. 60, no. 4, pp. 1505–1515, May 2011.
- [259] M. A. H. Rafi and J. Bauman, "A comprehensive review of DC fast-charging stations with energy storage: Architectures, power converters, and analysis," *IEEE Trans. Transp. Electr.*, vol. 7, no. 2, pp. 345–368, Jun. 2021.
- [260] H. Tu, H. Feng, S. Srdic, and S. Lukic, "Extreme fast charging of electric vehicles: A technology overview," *IEEE Trans. Transp. Electr.*, vol. 5, no. 4, pp. 861–878, Dec. 2019.
- [261] A. Tomaszewska et al., "Lithium-ion battery fast charging: A review," *eTransportation*, vol. 1, 2019, Art. no. 100011.
- [262] C. Chen, Z. Wei, and A. C. Knoll, "Charging optimization for Li-ion battery in electric vehicles: A Review," *IEEE Trans. Transp. Electr.*, vol. 8, no. 3, pp. 3068–3089, Sep. 2022.
- [263] S. Lavety, R. K. Keshri, and M. A. Chaudhari, "Multistep constant current-constant voltage charging strategy for a valve regulated lead-acid battery," *IEEE Trans. Ind. Appl.*, vol. 57, no. 6, pp. 6494–6503, Nov./Dec. 2021.
- [264] M. Bayati, M. Abedi, M. Farahmandrad, and G. B. Gharehpetian, "Delivering smooth power to pulse-current battery chargers: Electric vehicles as a case in point," *IEEE Trans. Power Electron.*, vol. 36, no. 2, pp. 1295–1302, Feb. 2021.
- [265] H. Vazini, M. Asadi, M. Karimadini, and H. Hajisadeghian, "A fast charging of Li-ion battery based on Lyapunov function for electrical vehicle," *IET Power Electron.*, vol. 15, no. 1, pp. 23–32, Jan. 2022.
- [266] S. M. R. Islam and S.-Y. Park, "Quantification of heat loss for different charging profiles in a Li-ion battery," *IEEE Trans. Energy Convers.*, vol. 36, no. 3, pp. 1831–1840, Sep. 2021.
- [267] X. Huang, W. Liu, A. B. Acharya, J. Meng, R. Teodorescu, and D.-I. Stroe, "Effect of pulsed current on charging performance of Lithium-Ion batteries," *IEEE Trans. Ind. Electron.*, vol. 69, no. 10, pp. 10144–10153, Oct. 2022.
- [268] L.-R. Chen, S.-L. Wu, D.-T. Shieh, and T.-R. Chen, "Sinusoidal-ripple-current charging strategy and optimal charging frequency study for Li-ion batteries," *IEEE Trans. Ind. Electron.*, vol. 60, no. 1, pp. 88–97, Jan. 2013.
- [269] A. B. Khan and W. Choi, "Optimal charge pattern for the high-performance multistage constant current charge method for the Li-ion batteries," *IEEE Trans. Energy Convers.*, vol. 33, no. 3, pp. 1132–1140, Sep. 2018.
- [270] X. Huang et al., "Lifetime extension of lithium-ion batteries with low-frequency pulsed current charging," *IEEE J. Emerg. Sel. Topics Power Electron.*, vol. 11, no. 1, pp. 57–66, Feb. 2023, doi: [10.1109/JESTPE.2021.3130424](https://doi.org/10.1109/JESTPE.2021.3130424).
- [271] L. Patnaik, A. V. J. S. Praneeth, and S. S. Williamson, "A closed-loop constant-temperature constant-voltage charging technique to reduce charge time of lithium-ion batteries," *IEEE Trans. Ind. Electron.*, vol. 66, no. 2, pp. 1059–1067, Feb. 2019.
- [272] Y.-D. Lee and S.-Y. Park, "Electrochemical state-based sinusoidal ripple current charging control," *IEEE Trans. Power Electron.*, vol. 30, no. 8, pp. 4232–4243, Aug. 2015.
- [273] X. Hu, Y. Zheng, X. Lin, and Y. Xie, "Optimal multistage charging of NCA/graphite lithium-ion batteries based on electrothermal-aging dynamics," *IEEE Trans. Transp. Electr.*, vol. 6, no. 2, pp. 427–438, Jun. 2020.
- [274] K. Liu, C. Zou, K. Li, and T. Wik, "Charging pattern optimization for lithium-ion batteries with an electrothermal-aging model," *IEEE Trans. Ind. Informat.*, vol. 14, no. 12, pp. 5463–5474, Dec. 2018.
- [275] H. Yan et al., "Battery lifetime extension in a stand-alone microgrid with flexible power point tracking of photovoltaic system," *IEEE J. Emerg. Sel. Topics Power Electron.*, vol. 11, no. 2, pp. 2281–2290, Apr. 2023.
- [276] O. Tkachenko and M. Sherstyuk, "Modulated pulse charging and discharging of a reconfigurable battery pack," U.S. Patent US10069313B2, Sep. 4, 2018.
- [277] O. Tkachenko and M. Sherstyuk, "Battery charging with charging parameters sweep," U.S. Patent US10840725B2, Nov. 17, 2020.
- [278] T. Sherstyuk and M. Sherstyuk, "Extended life battery," U.S. Patent US9966780B2, May 8, 2018.
- [279] M. Sherstyuk, T. Sherstyuk, and M. Prokoptsov, "Systems and methods for enhancing the performance and utilization of battery systems," U.S. Patent US11050281B2, Jun. 29, 2021.
- [280] G. Liu, "Smart battery, electric energy allocation bus system, battery charging and discharging method and electric energy allocation method," U.S. Patent US10431996B2, Oct. 1, 2019.
- [281] H. A. Mantooth, M. D. Glover, and P. Shepherd, "Wide bandgap technologies and their implications on miniaturizing power electronic systems," *IEEE J. Emerg. Sel. Topics Power Electron.*, vol. 2, no. 3, pp. 374–385, Mar. 2014.
- [282] Z. Zhao, D. Zhou, P. Davari, J. Fang, and F. Blaabjerg, "Reliability analysis of capacitors in voltage regulator modules with consecutive load transients," *IEEE Trans. Power Electron.*, vol. 36, no. 3, pp. 2481–2487, Mar. 2021.
- [283] Z. Zhao, D. Zhou, H. Wang, P. Davari, and F. Blaabjerg, "Reliability improvement of voltage regulator modules by a virtual series voltage source," *IEEE Trans. Ind. Electron.*, vol. 69, no. 12, pp. 12641–12652, Dec. 2022.

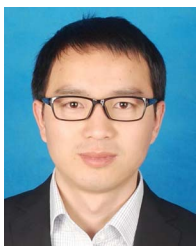


Zhaoyang Zhao (Member, IEEE) received the B.S. and M.S. degrees from Northeast Agricultural University, Harbin, China, in 2014 and 2017, respectively, and the Ph.D. degree from Chongqing University, Chongqing, China, 2020, all in electrical engineering.

From 2019 to 2020, he was a Visiting Ph.D. Student with the Department of Energy Technology, Aalborg University, Aalborg, Denmark. From 2021 to 2022, he was with Zhengzhou University, as an Assistant Professor. In 2022, he joined Southwest Jiaotong University, as Assistant Professor. His research inter-

ests include condition monitoring, safety, and reliability assessment of power electronic converters and battery systems.

Dr. Zhao was the recipient of the Prize Paper Award of the IEEE Journal of Emerging and Selected Topics in Power Electronics in 2021 and the Excellent Doctoral Dissertation of Chongqing City in 2022. He was a Guest Editor-in-Chief for *Microelectronics International* and a Guest Associate Editor for *CPSS Transactions on Power Electronics and Applications*. He is an Associate Editor for *Circuit World*.



Haitao Hu (Senior Member, IEEE) received the B.S. degree from Zhengzhou University, Zhengzhou, China, in 2010, and the Ph.D. degree from Southwest Jiaotong University, Chengdu, China, in 2014, both in electrical engineering.

He is currently a Professor with the School of Electrical Engineering, Southwest Jiaotong University. His main research interests include power quality and stability of the electric traction system.



Zhengyou He (Senior Member, IEEE) received the B.Sc. and M.Sc. degrees in computational mechanics from Chongqing University, Chongqing, China, in 1992 and 1995, respectively, and the Ph.D. degree in electrical engineering from Southwest Jiaotong University, Chengdu, China, in 2001.

He is currently a Professor with the School of Electrical Engineering, Southwest Jiaotong University. His research interests include signal process and information theory applied to power systems, and the application of wavelet transforms in power systems.



Herbert Ho-Ching Iu (Senior Member, IEEE) received the B.Eng. degree (Hons.) in electrical and electronic engineering from The University of Hong Kong, Hong Kong, in 1997, and the Ph.D. degree in electrical engineering from The Hong Kong Polytechnic University, Hong Kong, in 2000.

In 2002, he joined as a Lecturer the School of Engineering, The University of Western Australia, Crawley, WA, Australia, where he is currently a Professor. He has authored or coauthored more than 100 papers in the areas of his research interests, which include power electronics, renewable energy, nonlinear dynamics, current sensing techniques, and memristive systems.

Dr. Iu was the recipient of two IET Premium Awards in 2012 and 2014, the Vice-Chancellor's Mid-Career Research Award in 2014, and the 2019 IEEE Transactions on Very Large Scale Integration (VLSI) Systems Best Paper Award. He is currently an Associate Editor for IEEE TRANSACTIONS ON CIRCUITS AND SYSTEMS— II: EXPRESS BRIEFS, IEEE TRANSACTIONS ON POWER ELECTRONICS, and IEEE TRANSACTIONS ON NETWORK SCIENCE AND ENGINEERING; and an Editor for IEEE TRANSACTIONS ON SMART GRID. He is a Co-Editor of *Control of Chaos in Nonlinear Circuits and Systems* (World Scientific, 2009) and *Development of Memristor Based Circuits* (World Scientific, 2013).



Pooya Davari (Senior Member, IEEE) received the B.Sc. and M.Sc. degrees in electronic engineering in 2004 and 2008, respectively, and the Ph.D. degree in power electronics from the Queensland University of Technology (QUT), Brisbane, QLD, Australia, in 2013.

From 2005 to 2010, he was involved in several electronics and power electronics projects as a Development Engineer. From 2013 to 2014, he was with QUT, as a Lecturer. In 2014, he joined as a Postdoc Aalborg University (AAU), Aalborg, Denmark, where he is

currently an Associate Professor. He has authored or coauthored more than 180 technical papers. He has been focusing on EMI, power quality and harmonic mitigation analysis and control in power electronic systems.

Dr. Davari was a Guest Associate Editor of *IET Journal of Power Electronics*, IEEE ACCESS JOURNAL, *Journal of Electronics*, and *Journal of Applied Sciences*. He is an Associate Editor for *Journal of Power Electronics*, *IET Electronics*, an Editorial Board Member of *Journal of Applied Sciences* and *Journal of Magnetics*. He is Member of the International Scientific Committee (ISC) of EPE (ECCE Europe) and a Member of Joint Working Group six and Working Group eight at the IEC standardization TC77A. He was the recipient of Equinor 2022 Prize and 2020 IEEE EMC Society Young Professional Award for his contribution to EMI and Harmonic Mitigation and Modeling in Power Electronic Applications. He is currently the Editor-in-Chief of *Circuit World Journal*. He is founder and Chair of IEEE EMC Society Chapter Denmark and Leader of EMI/EMC in Power Electronics Research Group at AAU Energy.



Frede Blaabjerg (Fellow, IEEE) received the Ph.D. degree in electrical engineering from Aalborg University, Aalborg, Denmark, in 1995.

From 1987 to 1988, he was with ABB-Scandia, Randers, Denmark. In 1992, he became an Assistant Professor, in 1996 an Associate Professor, and in 1998 a Full Professor of power electronics and drives with Aalborg University, where he became a Villum Investigator in 2017. He is also honoris causa at Universitatea Politehnica Timisoara (UPT), Romania, and the Tallinna University of Technology

(TTU), Tallinn, Estonia. He has authored or coauthored more than 600 journal articles in the fields of power electronics and its applications. He is a coauthor of four monographs and editor of 10 books in power electronics and its applications. His current research interests include power electronics and its applications, such as in wind turbines, PV systems, reliability, harmonics, and adjustable speed drives.

Dr. Blaabjerg was the recipient of 32 IEEE Prize Paper Awards, the IEEE Power Electronics Society (PELS) Distinguished Service Award in 2009, the EPE-PEMC Council Award in 2010, the IEEE William E. Newell Power Electronics Award in 2014, the Villum Kann Rasmussen Research Award in 2014, the Global Energy Prize in 2019, and the 2020 IEEE Edison Medal. He was nominated in 2014–2019 by Thomson Reuters to be between the most 250 cited researchers in engineering in the world. From 2006 to 2012, he was the Editor-in-Chief of IEEE TRANSACTIONS ON POWER ELECTRONICS. He was a Distinguished Lecturer of the IEEE Power Electronics Society from 2005 to 2007, and the IEEE Industry Applications Society from 2010 to 2011 and 2017 to 2018. From 2019 to 2020, he was the President of the IEEE Power Electronics Society. He is also the Vice-President of the Danish Academy of Technical Sciences. He was nominated in 2014–2020 by Thomson Reuters to be between the most 250 cited researchers in Engineering in the world.